2015

Fabrication of stretchable and flexible supercapacitor using nanocarbon based materials

Hyeon Taek Jeong
University of Wollongong

2015

Fabrication of stretchable and flexible supercapacitor using nanocarbon based materials

Hyeon Taek Jeong
University of Wollongong

UNIVERSITY OF WOLLONGONG

FABRICATION OF STRETCHABLE AND FLEXIBLE SUPERCAPACITOR USING NANOCARBON BASED MATERIALS

A thesis submitted in fulfilment of the
requirement for the awards of the degree
Doctor of Philosophy

From

UNIVERSITY OF WOLLONGONG

by

Hyeon Taek Jeong

School of Chemistry

2015

CERTIFICATION

I, Hyeon Taek Jeong, declare that this thesis, submitted in fulfilment of the requirement for the award of Doctor of Philosophy, in the School of Chemistry, University of Wollongong, is wholly my own work unless otherwise referenced or acknowledged. The document has not been submitted for any qualifications at any other academic institution.

Hyeon Taek Jeong

January 2015

ABSTRACT

Stretchable and/or flexible electronic devices have emerged as a new generation technologies for wearable and implantable including high performance sportswear, wearable displays and bio-integrated devices. Stretchable and rechargeable energy storage devices are essential component of fully stretchable and flexible electronic devices. The stretchable and flexible supercapacitors are promising candidates due to their high power density, long life, durability and safety.

In this thesis, we have demonstrated stretchable and flexible supercapacitors base on nanocarbon materials such as, carbon nanotubes (CNTs) and reduced graphene oxide (rGO). Nanocarbon material based supercapacitors have been extensively investigated. However, to date nanocarbon material based supercapacitors have not been investigated for use as stretchable and flexible energy storage devices. Therefore, the theme of this thesis is to successfully design and develop novel nanocarbon material based stretchable and flexible supercapacitors with high durability and performance.

Chapter 1 introduces nanocarbon-based materials such as, carbon nanotubes (CNTs) and graphene with literature review of nanocarbon-based electrode and supercapacitor for investigation of nanocarbon material based energy storage devices.

Chapter 2 also introduces general experimental including chemical, reagents, characterization methodology, instrumentation and fundamental of the electrochemistry.

Chapter 3 investigates the development of stretchable electrode by incorporating acid-treated single-wall nanotubes (SWCNTs) onto latex (natural rubber) substrate using spray coating technique. The use of acid-treated single-wall carbon nanotubes (SWCNTs) improves capacitance due to increased functional groups on the SWCNTs. Electrochemical properties of the electrode are determined using cyclic voltammetry

(CV) and electrochemical impedance spectroscopy (EIS). Galvanostatic charge/discharge tests are also carried out. The impedance and charge/discharge curves of the latex/SWCNTs electrode show good capacitive behaviour even after repetitive stretching to 100% strain. The highest capacitance value obtained for the unstretched SWCNTs electrode is 119 F g^{-1} in 1 M Na_2SO_4 at 5 mV s^{-1}. After 100 stretches approximately 80% of the original capacitance was retained.

In chapter 4, a novel reduced graphene oxide (rGO)/single-wall carbon nanotubes (SWCNTs) composite electrode on stretchable polyurethane substrate was developed. The ratio between rGO and SWCNTs is optimized in order to obtain the best performance. The electrochemical properties of the rGO/SWCNTs composite electrodes were compared to rGO and SWCNTs electrodes. All of the electrodes were characterized by cyclic voltammetry (CV), electrochemical impedance spectroscopy (EIS) and galvanostatic charge/discharge test. The highest capacitance value obtained for the unstretched rGO/SWCNTs electrode is 265 F g^{-1} in 1 M H_2SO_4 at 5 mV s^{-1}. This performance decreased to 219 and 162 F g^{-1} after 50 and 100 stretching cycles, respectively. The rGO/SWCNTs composite electrode maintained 75% of its initial capacitance with an applied strain of 100%. The rGO/SWCNTs composite electrode shows enhanced electrochemical properties in comparison to rGO and SWCNTs electrodes. Approximately 70% of the initial capacitance for the rGO/SWCNTs composite electrode was retained after 100 stretching cycles and through 1000 CV cycles, making the electrodes a potential option for stretchable energy storage.

Chapter 5 extends and develops previous studies (chapter 3 and 4) of a stretchable electrochemical latex and polyurethane (PU) electrode to the highly durable and fully stretchable supercapacitor device with electrochemical behaviour determined as a function of strain (0 to 100%) and stretch/release cycles (up to 100). The stretchable

latex supercapacitor (unstretched) showed a specific capacitance of 61.3 F g^{-1}, which decreased to 41.7 F g^{-1} after 100 stretching cycles at 100% strain. The PU supercapacitor (unstretched) gave a specific capacitance of 42.9 F g^{-1} which decreased to 31.1 F g^{-1} after 100 stretches. The stretchable latex and PU supercapacitor retained 74 % and 89 % of the initial capacitance at 100% elongation, respectively.

In chapter 6, a flexible supercapacitor composed of the rGO/SWCNTs composite electrode on a degradable polycaprolactone (PCL) substrate was developed. All of the electrochemical properties for the PCL supercapacitor were investigated under fixed 180^{o}, 120^{o}, 60^{o} and 30^{o} of bending angle and 0 to 500 bending/releasing cycles using a Shimadzu EZ mechanical tester to assess practical and realistic performance of the biocompatible/flexible PCL supercapacitor. The highest capacitance value obtained for the PCL supercapacitor is 52.5 F g^{-1}. 70% of capacitance value of the PCL supercapacitor was retained after bending 500 times and 10,000.

The high stability, durability and stretchability of these supercapacitors demonstrate that nanocarbon based stretchable energy storage devices as supercapacitors have potential application for wearable and biocompatible devices.

ACKNOWLEDGEMENTS

I would like to thank my patient supervisors Professor Gordon Wallace, A/Prof Michael Higgins and Benny Kim for supporting and guiding me throughout my Ph.D. Without you, I could not have done my Ph.D. Especially, I appreciate the opportunity given to me by Professor Gordon Wallace to work and study at IPRI.

I also would like to give thanks to many people in IPRI for experimental help, Doctors David Harman, Robert Gorkin III and Adrian Gestos for their assistance in the spray coating technique and another fabrication instrument. Thank you to Dr Sanjeev Gambhir for providing me with reduced graphene oxide (rGO). Dr Patricia Hayes, for training me on the FTIR, Raman and discussion about the results. Thank you very much to Tony Romeo for teaching me SEM, sputter coater and other technical support in EMC.

Thank you very much to my friends Danial Sangian, Hongrui Zhang, Kewei Shu, Shazed Aziz , Chen Zhao and all of the people at IPRI for their encouragement and friendship which has made the past four years much more fun and interesting.

Finally, I would like to express gratitude to my family; my Mum and Dad for their unconditional and endless love. Thank you to my wife Miyoung for your patience in Australia - I will always love you. My Son, Tae Weon, you are my everything, I love you so much.

TABLE OF CONTENTS

LIST OF FIGURES

LIST OF TABLES

ABBREVIATIONS

Å	Angstrom : 1 X 10^{-10} m
Ag/AgCl	Silver/silver chloride
Au	Gold
α	Electron transfer coefficient
π	3.142
π	Highest occupied molecular orbital
BOE	Buffered oxide etchant
C*sp*	Specific capacitance
CNTs	Carbon nanotubes
CCG	Chemically converted graphene
CVD	Chemical Vapour Deposition
CV	Cyclic voltammetry
EIS	Electrochemical impedance spectroscopy
ECs	Electrochemical capacitors
EDLC	Electrochemical double layer capacitor
ESR	Equivalent series resistance
FTIR	Fourier transform infrared spectroscopy
F	Farad
FCCVD	Floating catalyst chemical vapour deposition

GO	Graphite oxide
GCD	Galvanostatic charge/discharge
hr	Hours
HiPCO	High-Pressure carbon monoxide process
H_2SO_4	Sulfuric acid
I	Intensity (a.u)
IR	Resistance drop (V)
KOH	Potassium hydroxide
MWCNTs	Multi-wall carbon nanotubes
m	Mass (generally in grams unless otherwise stated)
mg	Milligram
mV	Millivolt
mV s^{-1}	Millivolt per second
min	Minute
NBR	Nitrile-butadiene rubber
Ω	Ohm
OLEDs	Organic light emitting diodes
PTFE	Polytetrafluoroethylene
PCL	Polycaprolactone
PSS	Polystyrene sulfonate

PEDOT	Poly(3,4-ethylenedioxythiophene)
PVA	Polyvinyl alcohol
PU	Polyurethane
PDMS	Polydimethylsiloxane
rGO	Reduced graphene oxide
RBM	Radial breathing mode
S cm^{-1}	Siemens per centimetre
SEM	Scanning electron microscope
SWCNTs	Single-wall carbon nanotubes
t	Time (usually in seconds unless otherwise stated)
θ	Theta
V	Voltage
ν	Scan rate (mV s^{-1} or V s^{-1})
w/w	Weight for weight percent
XPS	X-ray photoelectron spectroscopy
XRD	X-ray diffraction
Z" im	Imaginary part of impedance
Z' Re	Real part of impedance
1D	1-dimensional
2D	2-dimensional

3D	3-dimensional

CHAPTER 1

Introduction and literature review

1. INTRODUCTION

Electrochemical capacitors (ECs) often referred to as supercapacitors, are devices that store charge by electrochemical means. Researchers often aim to develop supercapacitors with high power and energy density. In addition, these devices are potential candidates in wide range of applications due to their high power densities and stability to charge/discharge cycles [1-4]. They are able to produce large power and energy density compared to a conventional capacitor and longer life cycles than battery [5]. The power density requirements, fast charge/discharge cycle, low self-discharging and high electrochemical stability are beneficial feature of the supercapacitors [5, 6]. Table 1.1 summarizes the differences between battery, capacitor and supercapacitor.

	Battery	Capacitor	Supercapacitor
Discharge time	0.3 - 3 hrs	10-3 to 10-6 sec	0.3 - 30 sec
Charge time	1 - 5 hrs	10-3 to 10-6 sec	0.3 - 30 sec
Energy density (Wh/kg)	10 - 100	< 0.1	1 - 10
Power density (W/kg)	50 - 200	> 10,000	1000 - 2000
Charge/discharge efficiency	0.7 – 0.85	≈1	0.85 – 0.98
Cycle life	500 - 2000	> 500,000	> 100,000

Table 1.1 Comparison of the performances for battery, capacitor and supercapacitor [7].

A battery is usually denoted as a high energy density and low power density technology (Figure 1.1). However, a supercapacitor is considered to represent a high power density and low energy density technology (Figure 1.1). The supercapacitor is able to bridge the gap between capacitors and batteries in terms of energy density [5].

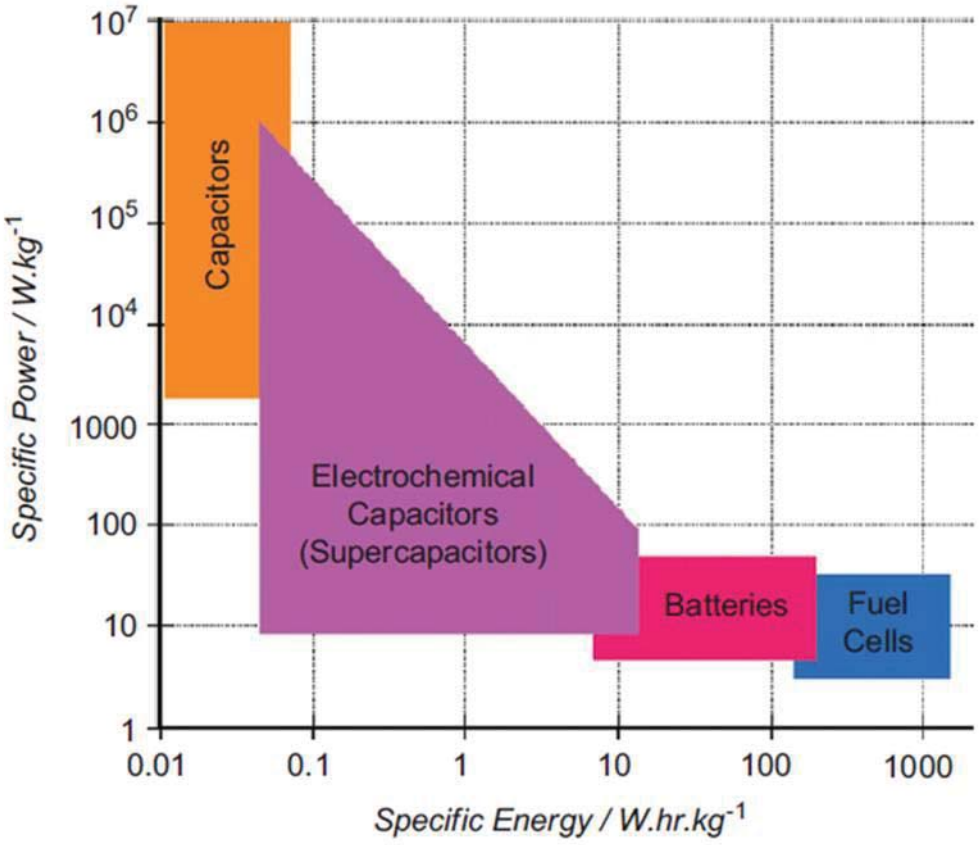

Figure 1.1 The Ragone plot comparing various energy storage systems [5].

Current research and development on supercapacitors conducted globally are listed in Table 1.2. This review covers work directed towards electric/hybrid vehicles, and also medical and consumer electronics applications. Devices using various materials and construction approaches have been fabricated [2].

Country	Company or lab	Funding	Description of technology	Device characteristics	Energy density (Wh/kg)	Power density (W/kg)	Status/availability
Carbon particulate composite							
Japan	Panasonic	Private	Spiral wound, particulate with binder, organic electrolyte	3 V, 800-2000 F	3-4	200-400	Commercial
France/US	Saft/Alcatel	US DOE/private	Spiral wound, particulate with binder, organic electrolyte	3 V, 130 F	3	500	Packaged prototypes
Australia	Cap xx	Private	Spiral wound and monoblock, particulate with binder, organic electrolyte	3 V, 120 F	6	300	Packaged prototypes
Japan	NEC	Private	Monoblock, multi-cell, particulate with binder, aqueous electrolyte	5–11 V, 1–2 F	0.5	5-10	Commercial
Russia (Moscow)	ELIT	Russian Government/private	Bipolar, multi-cell, carbon with sulfuric acid	450 V, 0.5 F	1.0	900–1000> 100,000 cycles	Commercial
Carbon fiber composites							
United States	Maxwell	US DOE/private	Monoblock, carbon cloth on aluminium foil, organic electrolyte	3 V, 1000–2700 F	3–5	400–600	Commercial
Sweden/Ukraine	Superfarad	Private	Monoblock, multi-cell, carbon cloth on aluminum foil, organic electrolyte	40 V, 250 F	5	200–300	Packaged prototypes
Aerogel carbons							
United States	PowerStor	US DOE/private	Spiral wound, aerogel carbon with binder, organic electrolyte	3 V, 7.5 F	0.4	250	Commercial
Conducting polymer films							
United States	Los Alamos National Lab	US DOE	Single-cell, conducting polymer PFPT. On carbon paper, organic electrolyte	2.8 V, 0.8 F	1.2	2000	Laboratory prototype
Mixed metal oxides							
United States	Pinnacle Research Institute	US DOEprivate	Bipolar, multi-cell, ruthenium oxide, on titanium foil, sulfuric acid	15 V, 125 F 100 V, 1 F	0.5–0.6	200	Packaged prototypes
United States	US Army, Fort Monmouth	US DOD	Hydrous ruthenium oxide, bipolar, multi-cell, sulfuric acid	5 V, 1F	1.5	4000	Unpacked lab prototype
Hybrid							
United States	Evans	Private	Double-layerrelectrolytic, single cell, monoblock, ruthenium oxide/tantalum powder dielectric, sulfuric acid	28 V, 0.02 F	0.1	30,000	Packaged prototype
Russia Moscow	ESMA	Russian Government/private	Double-layerrFaradaic, monoblock, multi-cell modules, carbon/nickel oxide/KOH	1.7 V cells/17 V modules/20 A h (50,000 F)	8–10	80–100 (95% discharge effic.) cycle life 10–20 K cycles	Commercial

Table 1.2 World-wide research and development activities on supercapacitor [2].

Two types of capacitor devices have been developed. The first is the electrochemical double layer capacitor (EDLC), which is based on the operating principle of an electric double layer formed at the interface between electrode and an electrolyte. A US patent issued in the 1950s [8, 9] demonstrated the fundamental of electrochemical double layer capacitor (EDLC) and supercapacitor [10]. Based on these initial developments, supercapacitors with aqueous-electrolyte have been developed by NEC (Japan) in 1970s and supercapacitors have been applied to commercial [10-13]. The main components of EDLC are two carbon based electrodes, an electrolyte and a separator (Figure 1.2). EDLC uses the charge formed at the interface between electrolyte and electrode surface. Carbon materials are mostly used for this capacitor as it provide large surface area. The capacitance value of EDLC is dependent on adsorption of the ions, which moves from the electrolyte to the electrode surface. Therefore, charge storage in EDLC is highly reversible with high cycling stabilities [14]. In addition, the performance of the EDLC can be tuned by using different type of electrolytes. EDLC can also operate with either an aqueous or organic electrolyte. Aqueous electrolytes, such as sulfuric acid (H_2SO_4) and potassium hydroxide (KOH) normally exhibit lower equivalent series resistance (ESR) and lower minimum pore size requirement compared to organic electrolyte. However, aqueous electrolytes also have narrow window of voltage ranges. Thus, the trade-off between the capacitance, ESR and window of voltage range should be considered in the use of electrolyte [15-18]. Figure 1.3 illustrates the key technology for the EDLC.

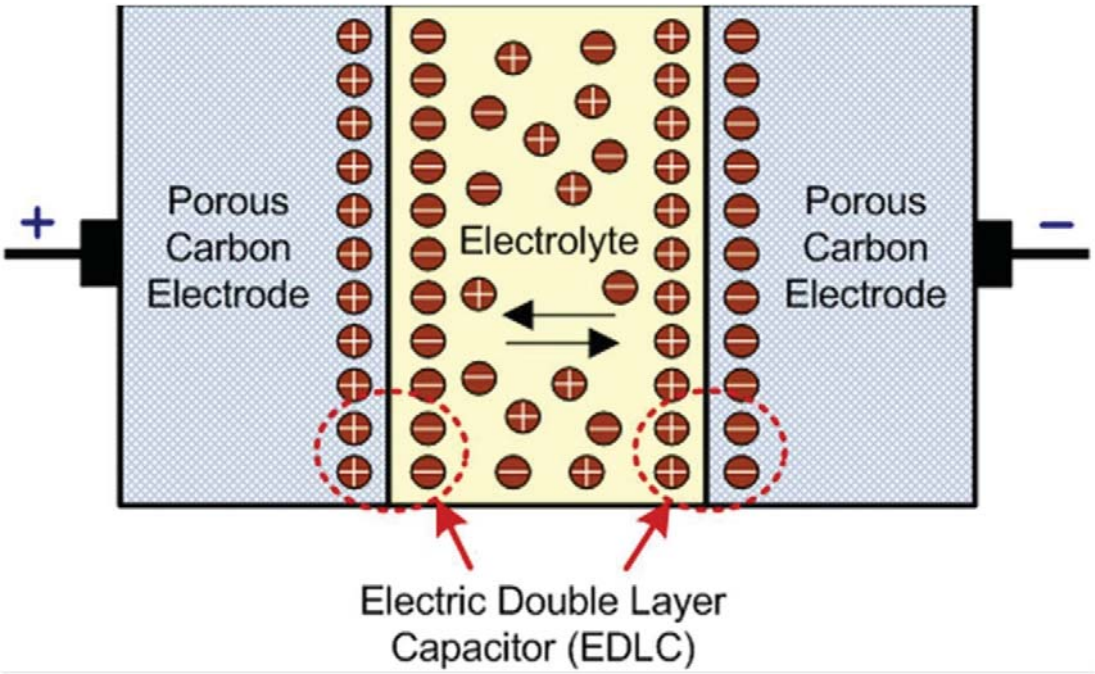

Figure 1.2 Schematic of an Electrochemical Double Layer Capacitor (EDLC) [14].

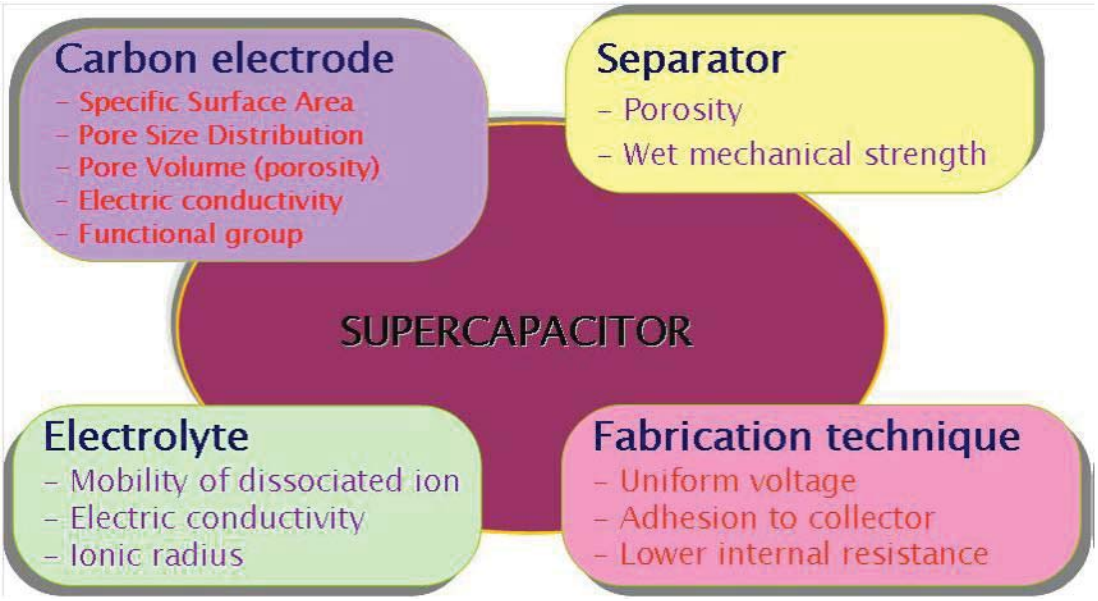

Figure 1.3 Important characteristics for Electrochemical Double Layer Capacitor (EDLC) components [19].

The second type of the devices is based on Faradaic pseudo capacitance (i.e. pseudocapacitor) where charge is transferred at the surface or in the bulk, near the surface of the solid electrode materials. Compared to EDLC that store charge electrostatically, pseudocapacitors store charge faradaically through the transfer of charge between the electrode and electrolyte. This is accomplished through electrosorption, reduction-oxidation reactions and intercalation processes [17, 18, 20, 21]. These Faradaic processes allow pseudocapacitors to achieve greater capacitances and energy densities than EDLC [22-24].

1.1 CARBON NANOTUBES (CNTs)

CNTs are cylindrical nanostructures consisting entirely of carbon. They have attracted a significant interest within the field of nanotechnology due to their unique physical properties including high surface area, low mass density, unique internal structure, high electrical conductivity and remarkable chemical stability [25-30]. CNTs can be categorized into two types with single-wall carbon nanotubes (SWCNTs) and multi-wall carbon nanotubes (MWCNTs). The schematic diagram of SWCNTs and MWCNTs are presented in Figure 1.4.

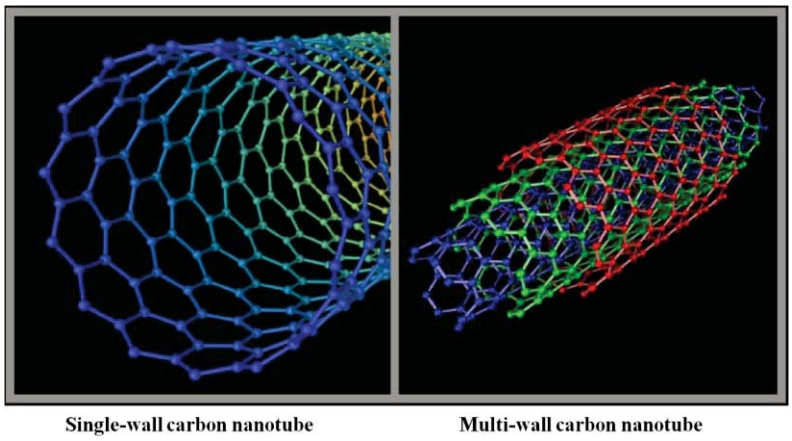

Figure 1.4 Schematic diagram of single-wall carbon nanotubes (SWCNTs) and multi-wall carbon nanotubes (MWCNTs) [28].

SWCNTs have a diameter with a range of 1-2 nm and the length between 0.2 ~ 5 μm depending on the synthesis method [31-33]. The aspect ratios of SWCNTs normally up to 10000, which feature is able to make them an ideal one-dimensional material. Super- long SWCNTs have been constructed with length-to-diameter aspect ratios exceeding 132,000,000:1 [34, 35]. SWCNTs could be compared to "rolled up" one atom thick sheet of graphite based on its structure (Figure 1.5).

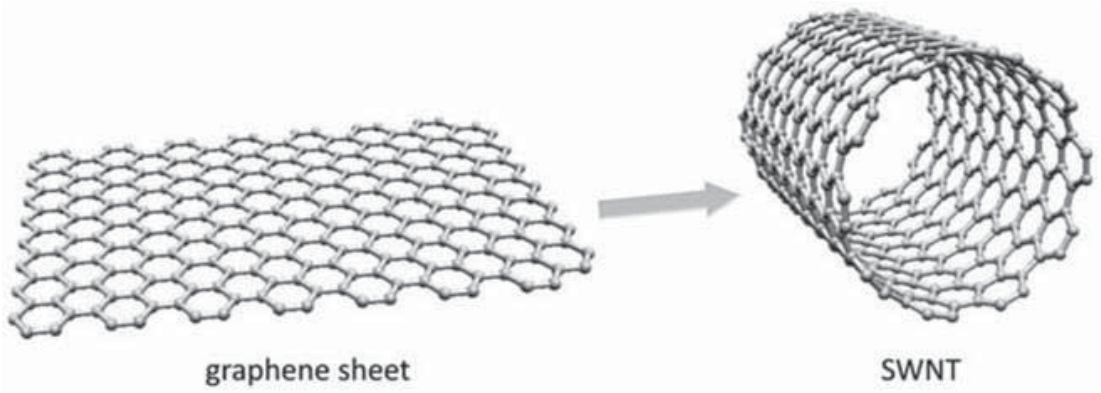

Figure 1.5 Rolling up of graphene sheet to SWCNTs [36]

The way the graphene is wrapped along the honeycomb graphene structure is given by chiral vector $\vec{C}$ which is a result of a pair (*n,m*) of integers that correspond to graphene vectors $\vec{\alpha}_1$ and $\vec{\alpha}_2$ [36, 37]. The construction of the SWCNTs from a graphite sheet along the chiral vector $\vec{C}$ is presented in Figure 1.6 [36]. There are two ways to form a SWCNTs from a graphite sheet according to integers (*n,m*). The (*n,0*) structure is called "zigzag" and $n = m$ (*n,n*) is ‘‘armchair’’ structure. The third non-standard type of SWCNTs construction, which can be characterized by the equation where $n > m > 0$, is called ‘‘chiral’’. The mechanical, electrical, optical and other properties of CNTs are determined by chirality.

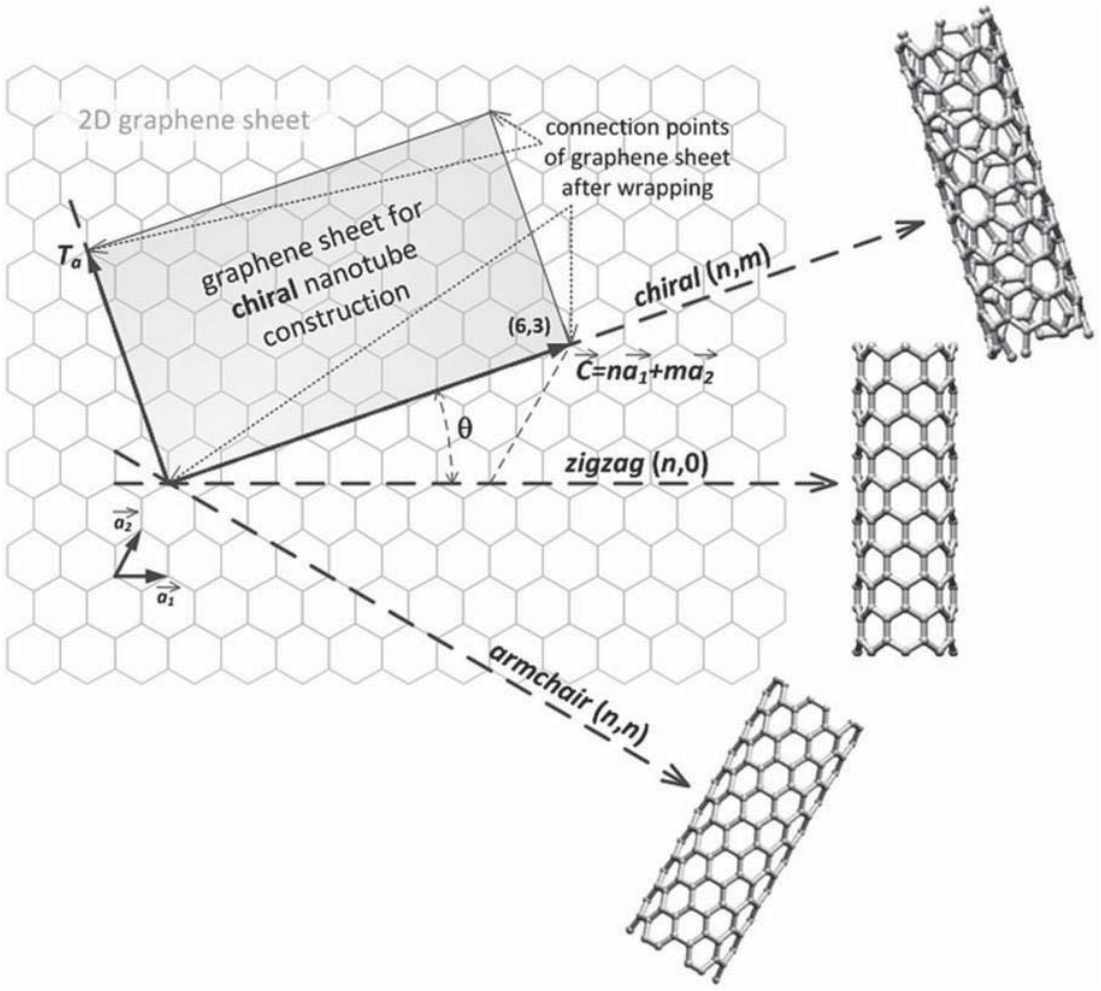

Figure 1.6 The fundamental of SWCNTs construction from the graphite [36].

MWCNTs consist of more than one concentrically rolled layer of graphite with diameters between 2 and 100 nm, [38, 39] which is depending on the number of layers. The interlayer distance of MWCNTs is approximately 0.335 nm, which is close to the distance between graphene layers in graphite [40]. The SWCNTs and MWCNTs could be fabricated by various techniques which are summarized in Figure 1.7 [36]. Each technique has advantages and disadvantages in synthesized CNTs properties including inner diameter, outer diameter and number of walls [41] which is influenced by the specific synthesis method.

Figure 1.7 Various techniques to synthesize CNTs [36].

The diameter of the CNTs affects the solubility and dispersability in solvents. For instance, Duque *et al*. [42] have reported that small diameter of the SWCNTs have enhanced solubility in oleum and surfactant suspensions. Solubility and dispersability are significant factor for SWCNTs processing technique such as thin-film fabrication, material reinforcement and fibre-spinning [42]. Table 1.3 shows the differences in the physical properties of SWCNTs and MWCNTs.

SWCNTs	MWCNTs
Single layer of graphene	Multiple layers of graphene
Catalyst is required for synthesis	Can be produced without catalyst
Bulk synthesis is difficult as require control over growth and atmospheric condition	Bulk synthesis is easy
Poor purity	High purity
Less body aggregation	More body aggregation
Chance of defect is more during functionalization	Chance of defect is less
Owing to simple structure, characterization and evaluation is easy	Due to complex structure characterization and evaluation is difficult
Could be easily twisted and more pliable	These cannot be reformed easily

Properties	SWCNTs	MWCNTs
Thermal conductivity	3×10^3 Wm^{-1} K^{-1}	3×10^3 Wm^{-1} K^{-1}
Specific resistance	5-50 μΩ cm	5-50 μΩ cm
Tensile strength	50-500 GPa	10-60 GPa
Tensile stiffness	~1.4 TPa	~0.3-1 TPa

Table 1.3 Comparison between SWCNTs and MWCNTs [37].

Based on the unique structure of CNTs, they have high electrical and mechanical properties [43-45] that make them potentially useful in high performance nanocomposites for related applications, including semiconductor devices [46], nano-probes [47, 48], energy conversion devices [49], sensors [50], field emission displays [51], radiation sources [52, 53] and drug delivery systems. However, these applications still remain in the "potential" stage. Bulk availability of high quality and

low cost samples, and processing difficulties are the main barriers in extending the technological applications of carbon nanotubes.

1.2 FLEXIBLE ELECTRONICS

Flexible electronics can be bent, twisted, compressed and stretched repeatedly whilst retaining function. They have attracted a great deal of attention due to potential applications in many areas ranging from robotic sensory skins and wearable communication devices to bio-integrated devices [54, 55]. Such applications require electronic materials that can simultaneously exhibit excellent mechanical robustness, electronic functionality and optical transmittance under a high strain [56-60]. The fundamental process for stretchable interconnects is to blend highly conductive materials with soft elastic materials such as polydimethylsiloxane (PDMS) and/or polyurethane (PU). A variety of highly conductive materials such as metal wires, conducting polymer, carbon nanotube or graphene have been used to form stretchable electrodes [61, 62]. Stretchable electrodes were then produced on elastic substrates by various processes such as screen printing, inkjet printing or spray coating. Forming stable dispersions is an important consideration, amenable to these fabrication processes. Modification of nanocarbon materials, including carbon nanotubes and graphene, is often necessary to improve the dispersability, but this modification process may decrease the electrical properties. Thus, the trade-off between the loss of conductivity, capacitance and dispersability should be considered. Sekitani *et al.* [61] have developed an approach to prepare printable elastic conductors comprised of single-walled carbon nanotubes (SWCNTs), which are uniformly dispersed in a fluorinated rubber.

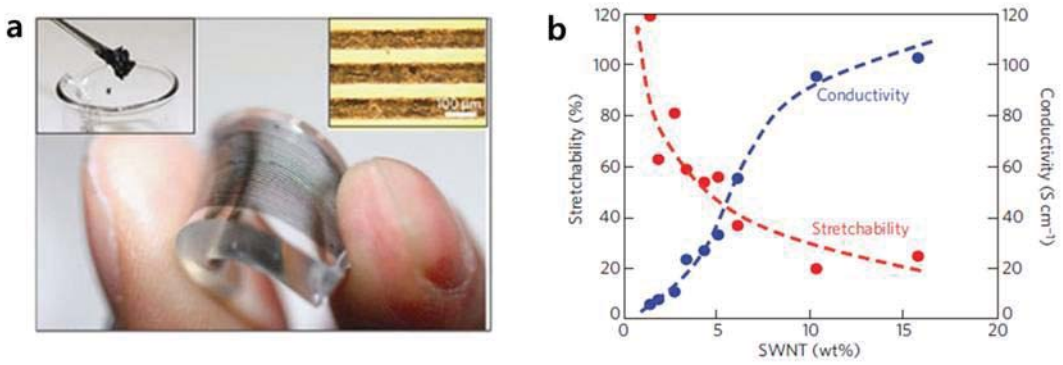

Figure 1.8 Printable elastic conductors. (a) Printed elastic conductors on a PDMS sheet. The printed elastic conductors are patterned by screen printing, and can be stretched by 100% without electrical or mechanical damage. The insets show SWCNTs dispersed in paste and a micrograph of printed elastic conductors with a line width of 100μm (b) Stretchability and conductivity as a function of SWCNTs content (c) SEM image of the surface of printed elastic conductors (d) magnified SEM image of the elastic conductor [61].

They have fabricated a SWCNTs gel by using ionic liquid and then the SWCNTs gel treated by jet-milling to prepare homogeneous SWCNTs paste (Figure 1.8a). In the next stage, the SWCNTs paste was patterned on the PDMS via screen printing through shadow masks (Figure 1.8a). The long and fine SWCNTs bundles can form well-developed conducting networks on the PDMS. The display could be stretched by 30%–50% and used for connecting LEDs over a hemisphere without any loss of mechanical and electrical damage (Figure 1.8b).

On the other hand, Viventi and Kim [62] have demonstrated a technologically challenging feat, in which they have described the integration of an ultrathin and flexible silicon nanomembrane transistor on an electrode array by transferring silicon nano-ribbons onto polyimide using spin coating. Metal was also deposited on top of the transistor arrays as a final layer. This new approach produces dense arrays of thousands of amplified sensors that are connected through fewer wires (Figure 1.9a).

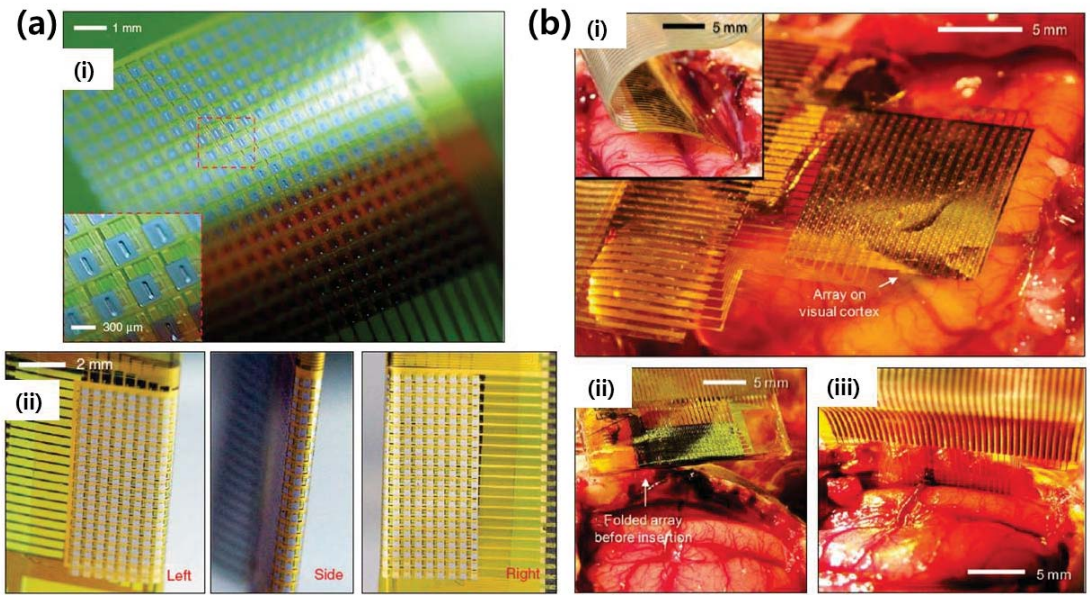

Figure 1.9 (a, i) Photograph of a 360-channel high-density active electrode array. The electrode size and spacing were 300 × 300 µm and 500 µm, respectively. Inset, a closer view showing a few unit cells, (a, ii) Photographs of a folded electrode array around low modulus polydimethylsiloxane (PDMS), (b, i) A flexible, high-density active electrode array was placed on the visual cortex. Inset, the same electrode array was inserted into the interhemispheric fissure, (b, ii) Left, the folded electrode array before insertion into the interhemispheric fissure, (b, iii) The flat electrode array inserted into the interhemispheric fissure [62].

The array was implemented as an electronic device capable of recording spatial properties of a cat's brain activity in vivo, including sleep spindles, single-trial visual evoked responses and electrographic seizures (Figure 1.9b). This development has potential for a new generation of diagnostic and therapeutic brain-machine interface devices.

Kim *et al*. [63] have reported an integrative approach, in which the electrodes, electronics, sensors, power supply, and communication components are all configured together on the sacrificial and water soluble polyvinyl alcohol (PVA). This ultrathin, low-modulus, lightweight, stretchable "skin-like" membrane can be

placed directly on the skin. It is important to note that, in the case of dissolving the PVA in the water, the device is still attached to the skin through van der Waals force alone (Figure 1.10a).

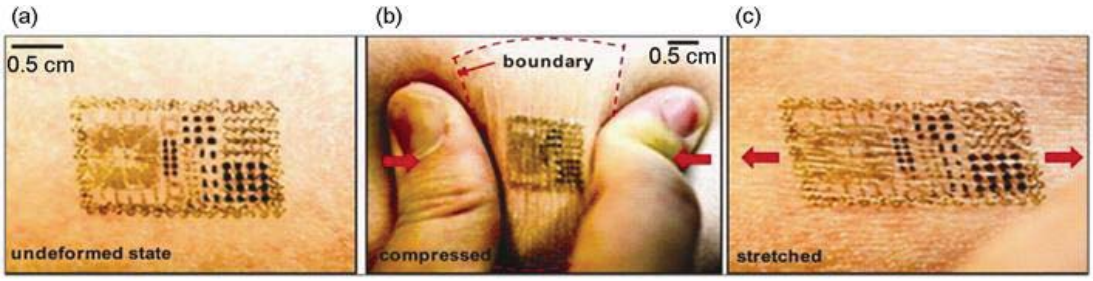

Figure 1.10 Photograph of a multifunctional electronic device temporarily tattooed onto skin. It is able to function in states such as: (a) Undeformed, (b) Compressed, (c) Stretched [63].

The membranes are able to laminate onto the surface of the skin by soft contact, in a manner that is mechanically invisible to the user, much like a temporary transfer tattoo (Figure 1.10). The device was then used to measure electrical activity produced by the heart, brain, and skeletal muscles and the observed results contained sufficient information typical for an unusual type of computer game controller.

Modification of nanocarbon materials, including carbon nanotubes and graphene, is often necessary to improve the dispersability, but this modification process may decrease the electrical properties. Thus, the trade-off between the loss of conductivity, capacitance and dispersability should be considered.

1.3 CARBON NANOTUBES (CNT_S) BASED FLEXIBLE, STRETCHABLE ELECTRODES AND SUPERCAPACITORS

Flexible and stretchable conductors are significant components of electronic and optoelectronic devices that facilitate human interaction and compatibility, such as implantable medical devices [64], interactive electronics [65], robotic devices with human-like sensing capabilities [66]. The availability of conducting thin films is able to the development of skin-like sensors [67] that stretch reversibly, sense pressure, bend into hairpin turns, integrate with collapsible, stretchable and mechanically robust displays [68], supercapacitor [69-73], solar cells [74] and also wrap around non-planar and biological [75-77] surfaces such as skin [62] and organs [78], without wrinkling.

Carbon nanotubes (CNTs) are suitable for flexible and stretchable electrode due to their remarkable properties such as high electrical conductivity, thermal and chemical stability and a large surface area [79-81]. Especially, SWCNTs possess high flexibility, low mass density, and large aspect ratio (typically >1000) enabling them to maintain conductive pathways by bridging cracked regions under large strain [28, 82, 83].

There are some approaches for fabrication of flexible and stretchable electrode or supercapacitor based on carbon nanotubes. Yu *et al*. [84] have reported a stretchable supercapacitor based on buckled single-wall carbon nanotubes (SWCNTs) macrofilms (Figure 1.11).

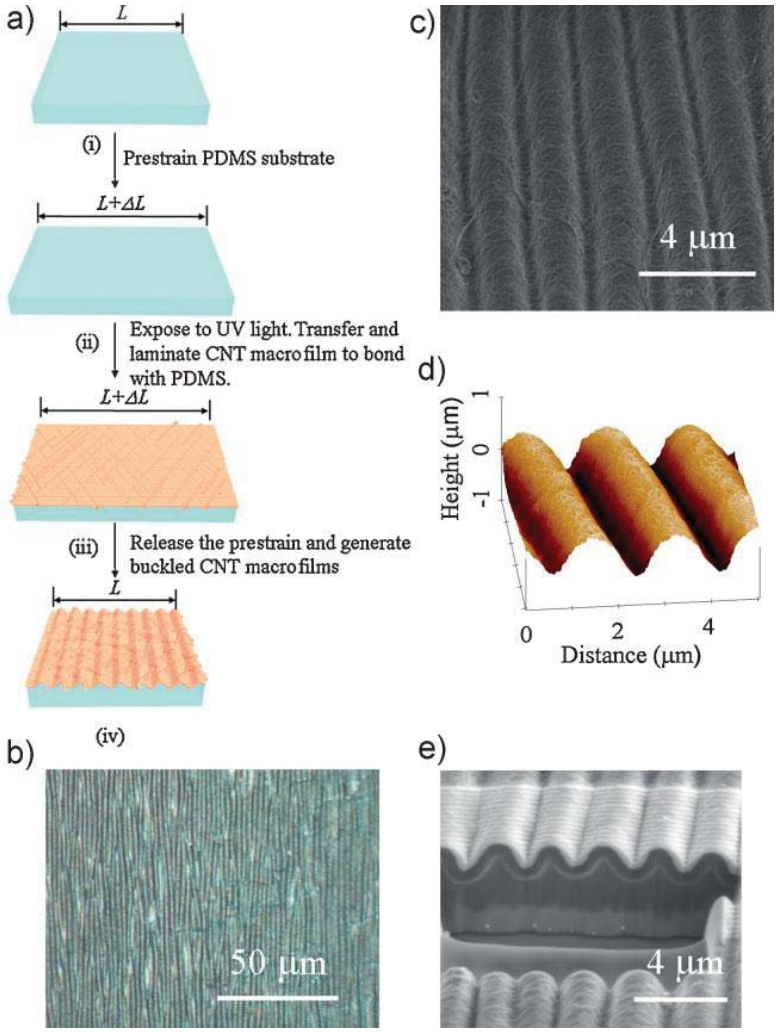

Figure 1.11 Fabrication steps of a buckled SWCNTs macrofilms on an elastomeric PDMS substrate. a) Illustration of the fabrication flow comprising surface treatment, transfer, and relaxation of the pre-strained PDMS substrate. b) Optical microscopy image of a 50-nm-thick buckled SWCNTs macrofilms on a PDMS substrate with 30% pre-strain, where the well-defined periodic buckling structure is shown. c) SEM image of a buckled SWCNTs macrofilms. The buckling wavelength is 2mm. d) AFM image of the buckling profile of the SWCNTs macrofilms. The buckling amplitude is 0.4mm. e) SEM image of the buckled SWCNTs macrofilms/PDMS substrate interface, where the top white layer is a very thin layer of platinum that was sputtered onto the SWCNTs macrofilms in advance to prevent the SWCNTs macrofilms from damage during ion milling [84].

The purified SWCNTs macrofilms with extensive hydroxyl groups were laminated and aligned along the direction of a pre-strained and UV-treated PDMS substrate to form covalent bonds (—C—O—Si—). The periodically buckled patterns were formed by relaxing the pre-strained PDMS substrate occurred due to mechanical competition between the relatively stiff SWCNTs macrofilms and compliant PDMS substrate. The buckled SWCNTs macrofilms based stretchable supercapacitor presented a maximum specific capacitance of 54 F g^{-1} and a power density of 0.5 KW kg^{-1} at 4.2 Wh kg^{-1} energy density. It was also shown that the buckled SWNT films could stretch up to 30%.

Hu *et al*. [85] have studied transparent and conductive SWCNTs films on a commercial 3M VHB 4905 substrate as a stretchable electrode that maintains high conductivity up to 700% strain (Figure 1.12a). The SWCNTs thin film was coated on the 3M VHB 4905 substrate by spray coating technique. As a substrate, the 3M VHB 4905 film is highly viscoelastic and enables the stretching properties of the SWNT thin films to be investigated. Figure 1.12a shows the change in resistance with strain. The resistance of the SWCNTs film increases linearly with strain and stretched SWCNTs films show white large areas indicative of a loss of conductivity (Figure 1.12d and e).

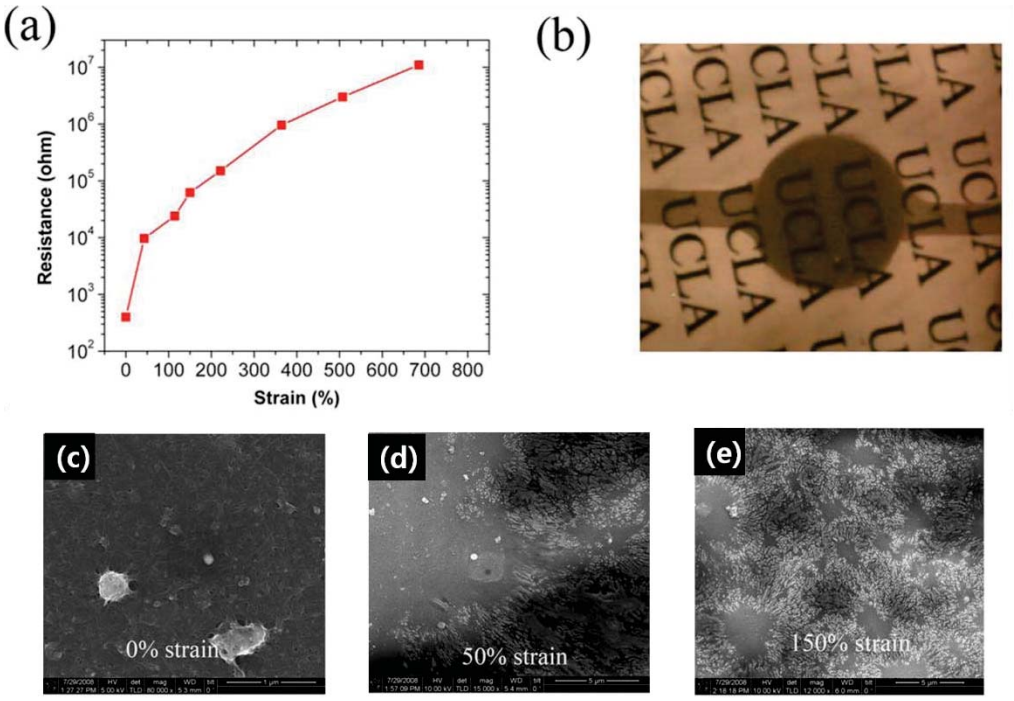

Figure 1.12 (a) Resistance of the transparent and stretchable SWCNTs film as a function of strain under unidirectional stretching. (b) Set up for tropically stretching of SWCNTs thin film with layered structures. (c) SEM image of sprayed SWCNTs film on the 3M VHB 4905 substrate. (d) SEM image of SWCNTs film under 50% strain. (e) SEM image of SWCNTs film under 150% strain [85].

Flexible and stretchable SWCNTs film could also be incorporated into clothing or attached directly to the body.

Yamada *et al*. [86] have developed a class of wearable and stretchable devices fabricated from thin films of aligned SWCNTs. The stretchable human motion detector prepared by connecting SWCNTs electrodes to the film and assembling them on bandage and clothing (Figure 1.13 a-d).

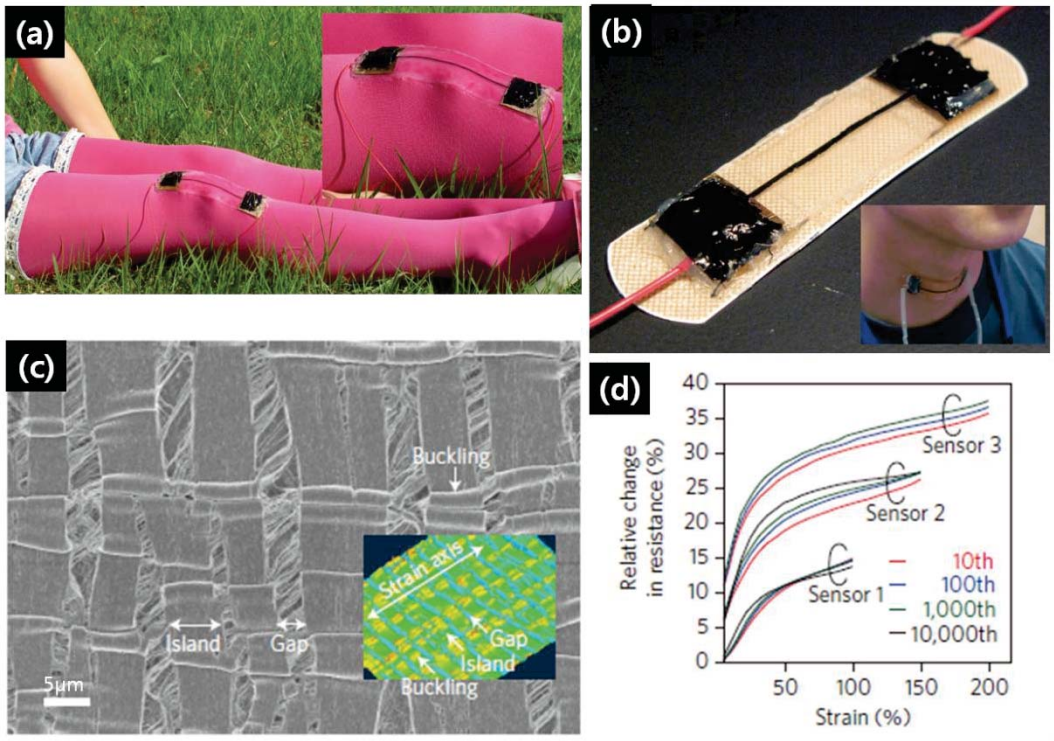

Figure 1.13 Photographs of the SWCNTs based bandage strain sensor (a) Fixed to a stocking, (b) Adhered to the throat, (c) SEM image of the fractural structure of the SWCNTs film at 100% strain, (d) Relative change in resistance versus strain for multiple-cycle tests [86].

The SWCNTs conductive paste was fabricated by dispersing elastic fluorinated copolymer rubber into a SWCNTs gel and used to avoid mechanical failure at the junction between SWCNTs film and rigid electrode. The stretchable sensor exhibited durability and stability even at high strain levels (100, 150 and 200%). The electrical response of the SWCNTs based sensor was maintained at 100 and 150% strain (Figure 1.13d).

Another approach for fabricating the flexible and stretchable electrode is by embedding aligned SWCNTs layers on polydimethylsiloxane (PDMS). Liu *et al*. [87] have reported flexible and stretchable SWCNTs conductive film on the PDMS as a substrate.

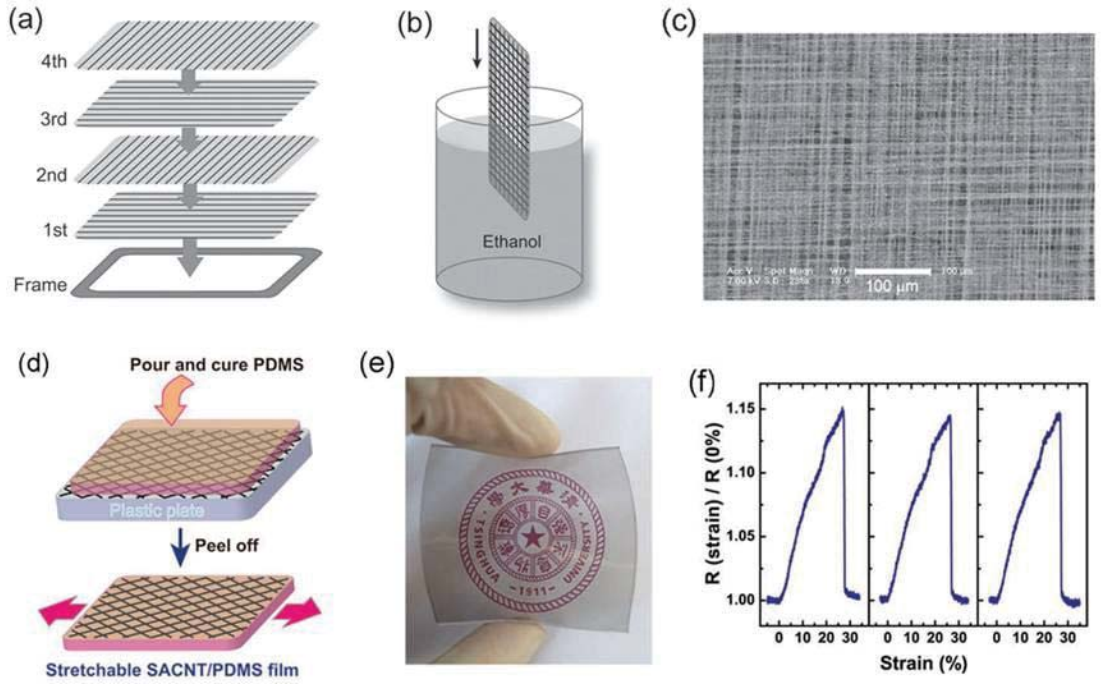

Figure 1.14 Fabrication of flexible and stretchable PDMS electrode using cross-stacked SWCNTs. (a) Stacking aligned SWCNTs layers in sequence on a square frame, (b) Densifying the cross-stacked SWCNTs layers by dipping them in ethanol, (c) SEM image of the cross-stacked SWCNTs film, (d) Fabrication process of the cross-stacked SWCNTs/PDMS electrode, (e) As-prepared flexible and stretchable SWCNTs/PDMS electrode, (f) Change of resistance of the SWCNTs/PDMS electrode during three sequential stretch processes after the first stretch process [87].

In order to preserve the morphology of the aligned SWCNTs film from being destroyed, they have used cross-stacking and densifying processes (Figure 1.14a, b and c). The flexible and stretchable SWCNTs/PDMS electrode was fabricated by embedding the aligned SWCNTs film into the PDMS (Figure 1.14d and e). The SWCNTs/PDMS electrode showed stretchable and reversible electrical behaviours even at the 30% strain (Figure 1.14f). The flexible and stretchable SWCNTs/PDMS electrode can be applied for stretchable energy storage or conversion devices such as

solar cell, strain sensor, implanted conductor and supercapacitor.

Hu *et al*. [88] have developed the acid treated SWCNTs based flexible supercapacitor using a non-woven 100% cotton paper and PVA (polyvinyl alcohol)/H_3PO_4 (phosphoric acid) electrolyte. Figure 1.15 illustrates the procedure for producing SWCNTs coated cotton supercapacitor. The acid treated SWCNTs were coated on the paper by simple dip-coating method and the SWCNTs coated cotton showed 9 ~ 10 Ω/sq sheet resistance. The SWCNTs coated cotton electrodes were soaked into the PVA/H_3PO_4 electrolyte for 10 minutes then dried at room temperature for 12 hours to remove residual excessive water. The dried two SWCNTs coated cotton electrodes were assembled together, face to face, to form a sandwich configuration. The SWCNTs coated cotton supercapacitor gave 13.15 F g^{-1} of specific capacitance with 5.54 Wh kg^{-1} of specific energy density. The performances of the SWCNTs coated cotton supercapacitor were competitive with two commercial supercapacitor (EPCOS, B49410B-2506Q000 and ESMA, EC303) [88]. They have also reported that PVA plays two significant roles in the fabrication process. It functioned as a binder to hold assembled two electrodes in a sandwich conformation. It also acted as a separator to avoid electrode shorting.

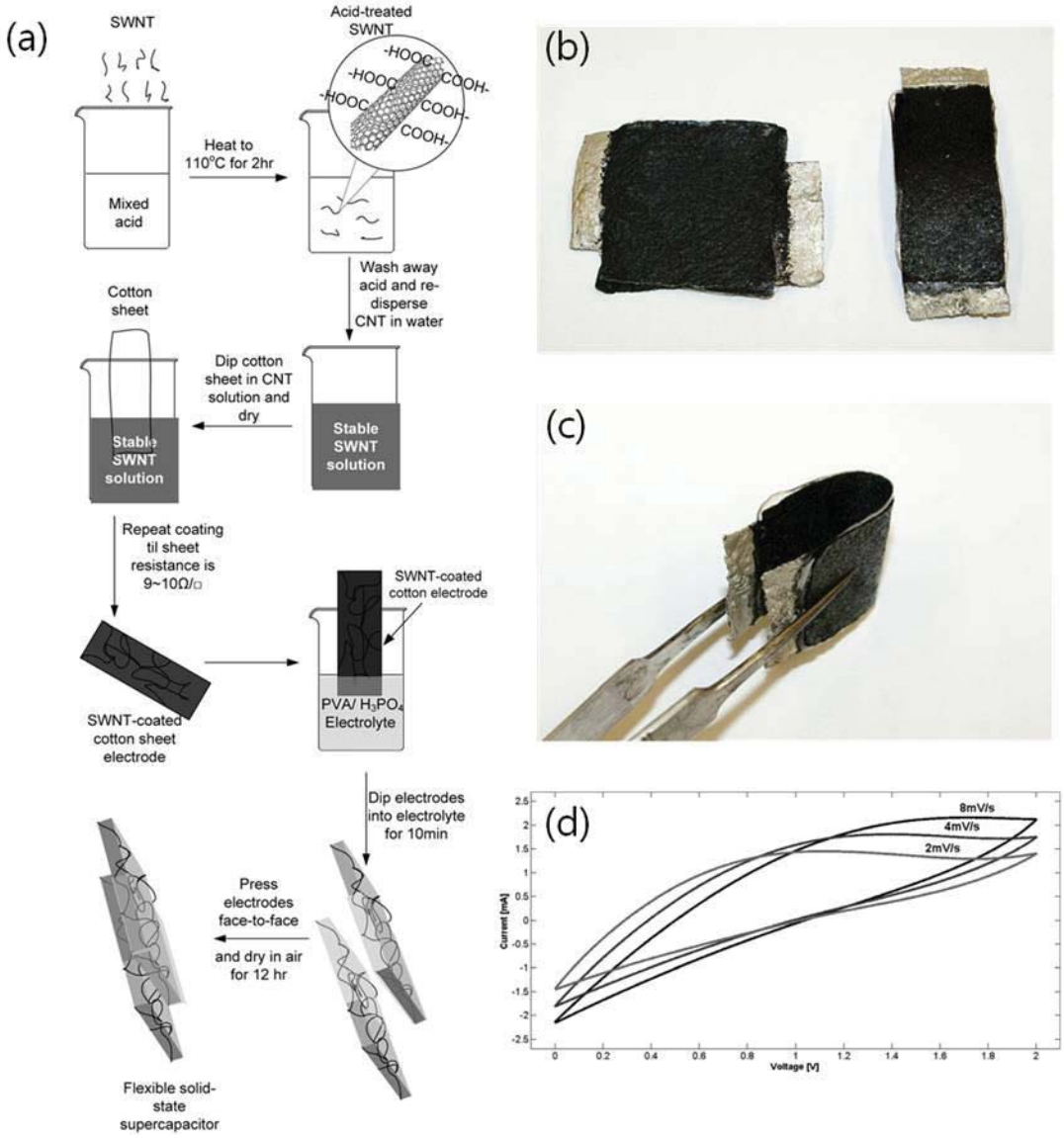

Figure 1.15 (a) Fabrication procedure of SWCNTs coated cotton based flexible, and solid-state supercapacitor, (b) and (c) Photos of the SWCNTs coated cotton based supercapacitor, (d) Cyclic voltammetry of the SWCNTs coated cotton based supercapacitor [88].

Chen *et al*. [89] have reported stretchable and transparent supercapacitor based on highly aligned multi-wall carbon nanotubes (MWCNTs) sheet with excellent transmittance and stretchability. Figure 1.16a illustrates the fabrication process for the aligned MWCNTs based stretchable supercapacitor.

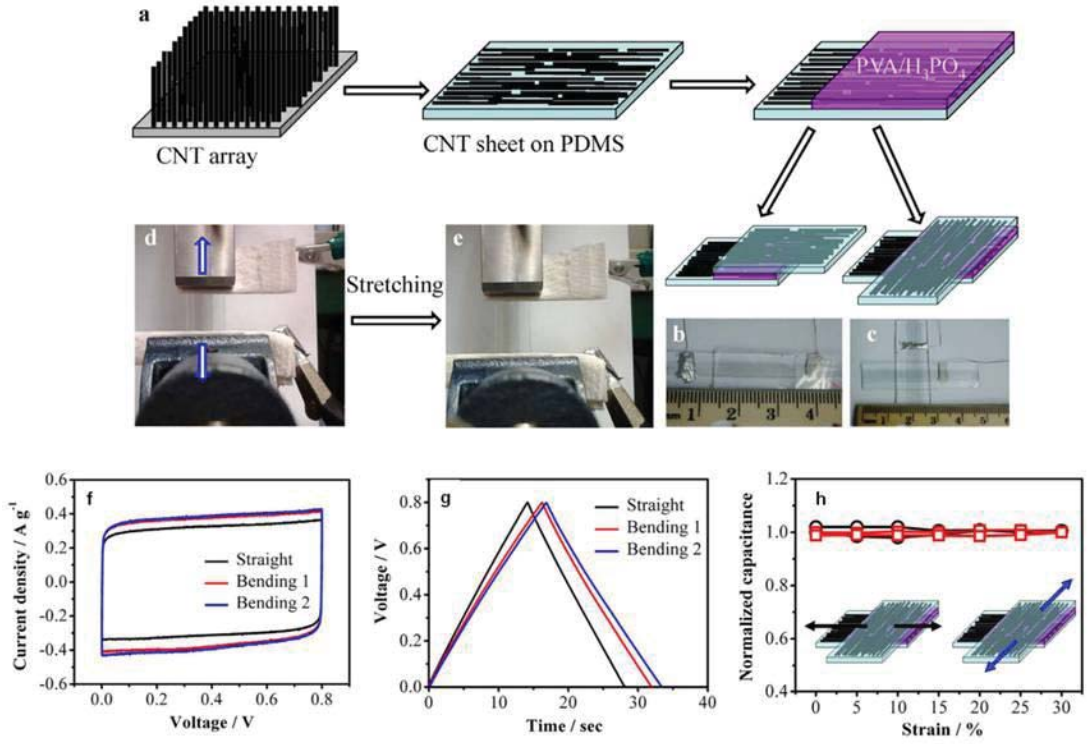

Figure 1.16 Fabrication procedure for MWCNTs based stretchable supercapacitors and optical images. (a) Schematic demonstration of the process for stretchable supercapacitor, (b, c) Photographs of the assembled supercapacitor in the parallel and cross configurations, (d, e) Photographs of the supercapacitor before and after stretching, (f) CV curves of the stretchable supercapacitor under different state, (g) Charge/discharge test of the stretchable supercapacitor under different state, (h) Normalized specific capacitance of the supercapacitor with cross assembly as a function of strain and biaxial stretched [89].

The MWCNTs forest for supercapacitor was synthesized by Chemical Vapour Deposition (CVD) method on a Fe/Al_2O_3 coated silicon wafer. The synthesized MWCNTs forest was drawn onto PDMS substrate in order to create stretchable MWCNTs sheet, then coated with PVA (polyvinyl alcohol)/H_3PO_4 electrolyte on the MWCNTs sheet. The two MWCNTs sheet electrodes assembled together in either parallel (Figure 1.16b) or cross configuration (Figure 1.16c). The MWCNTs based stretchable supercapacitor showed specific capacitance of 7.3 F g^{-1} and could be

stretched to 30% strain without any decrease in electrochemical properties (Figure 1.16h).

Niu *et al*. [90] have focused on a highly stretchable supercapacitor based on single-wall carbon nanotubes (SWCNTs) film. The freestanding and highly conductive SWCNTs films were fabricated by improving the floating catalyst chemical vapour deposition (FCCVD) technique [91]. Figure 1.17 shows the schematic procedure for stretchable SWCNTs film based supercapacitor. The synthesized SWCNTs films were spread out on the pre-strained and UV-treated PDMS and then, ethanol was dripped down on the SWCNTs film to remove the wrinkles on the SWCNTs film. The buckled SWCNTs film on the PDMS was created by releasing pre-strained PDMS (Figure 1.17).

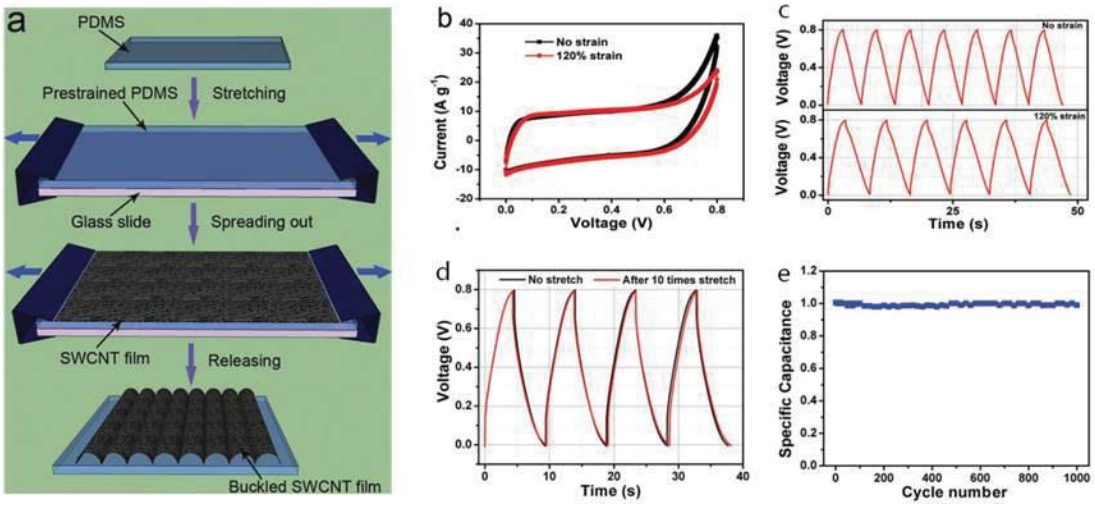

Figure 1.17 (a) Schematic procedure for fabrication of buckled SWCNTs based stretchable supercapacitor. (b) CV curves of the representative stretchable supercapacitor with and without 120% strain at a scan rate of 200 mV s^{-1}. (c) Charge/discharge test of the stretchable supercapacitor before and after 10 stretching. (d) Charge/discharge curves of the stretchable supercapacitor with and without 120% strain at a constant current of 10 A g^{-1}. (e) Normalized specific capacitance on the function of cycle number [90].

A buckled SWCNTs based stretchable supercapacitor was fabricated by assembling two stretchable electrodes face to face to form a sandwich conformation using the PVA/H_2SO_4 gel electrolyte. The cyclic voltammetry of the stretchable supercapacitor with application of 120% strain showed only very small deviation at the high potential in the cyclic voltammetry (CV) graph (Figure 1.17b) and also, the stretchable supercapacitor was stable in the charge/discharge test under 120% strain (Figure 1.17c). The specific capacitance of the stretchable supercapacitor was unchanged, even after 1000 charge/discharge cycles, indicating an excellent electrochemical stability of the buckled SWCNTs based stretchable supercapacitor (Figure 1.17 d and e).

1.4 GRAPHENE

A two dimensional material known as graphene has been attracting interest in the scientific community. The graphene also is a mother for graphitic materials of all other dimensionalities (Figure 1.18). It consists of a single layer of carbon atoms bonded in a hexagonal lattice and possess intriguing mechanical and electrical properties. The attractive characteristics of graphene for electrochemical applications are its charge carrier mobility of 200,000 cm^2/V-s and specific surface area of 2,630 m^2/g [92, 93].

The first graphene was produced from graphite by using a technique known as micromechanical cleavage [94]. This approach allowed easy production of high-quality graphene crystallites and further led to enormous experimental activities. Although the graphene obtained from this method is defect free, the yield and throughput is very low. In order to facilitate large scale production of graphene, exfoliation of graphite in the liquid phase (via chemical conversion or

surfactant/solvent stabilization) was developed [95].

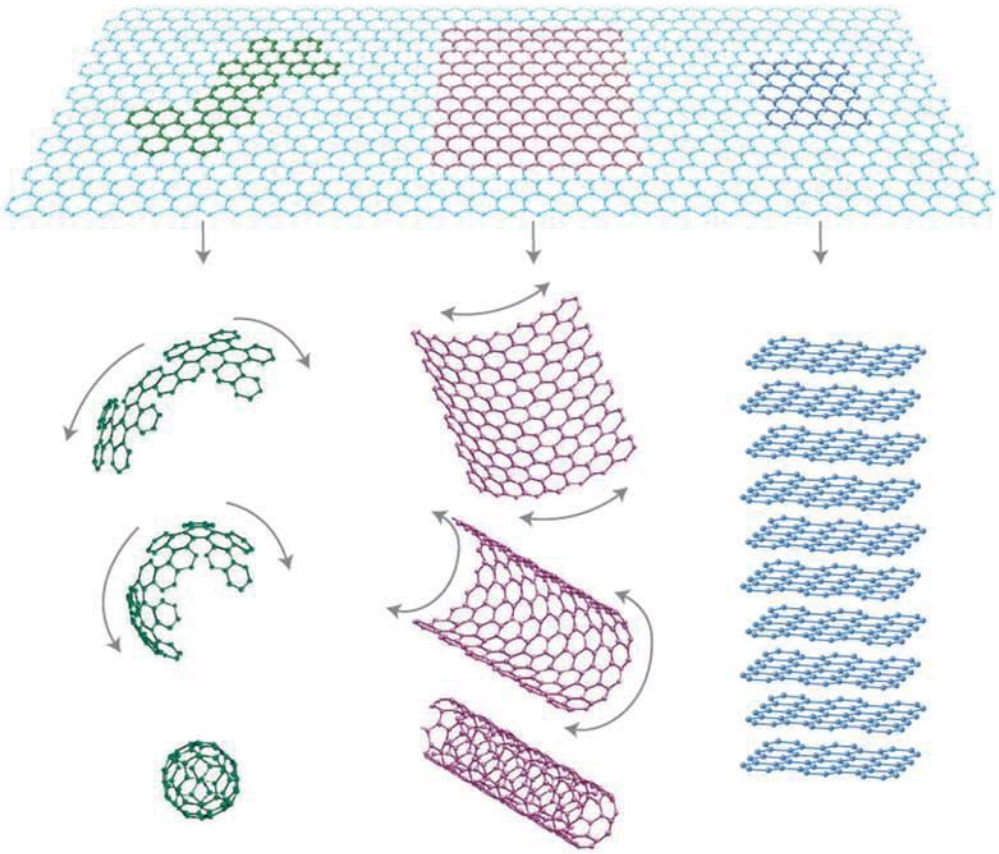

Figure 1.18 Mother of all graphitic forms. Graphene is a 2D building material for carbon materials of all other dimensionalities. It can be wrapped up into 0D bucky balls, rolled into 1D nanotubes or stacked into 3D graphite [96].

Chemical conversion of graphene involves two main steps. Firstly, the graphite is oxidized in the presence of strong acids and oxidants, resulting in a material called graphite oxide (GO). The introduction of oxygen to the graphite stack results in hydroxyl, epoxy, ether, diol, and ketone groups on the basal planes and edges. These functional groups make GO hydrophilic by virtue of their polar nature allowing intercalation of water molecules into the GO layers [97]. This makes exfoliation of GO in aqueous media very easy to carry out. Suitable ultrasonic treatment can produce dispersions of very thin graphene oxide sheets [97, 98]. Secondly, the

functional groups that stabilize GO in water also make it electrically insulating by disrupting the graphitic network [99], hence this material is converted back to graphene by chemical or thermal reduction to recover its conductivity. Figure 1.19 illustrates the process for chemically converted graphene (CCG) by reduction of graphene oxide.

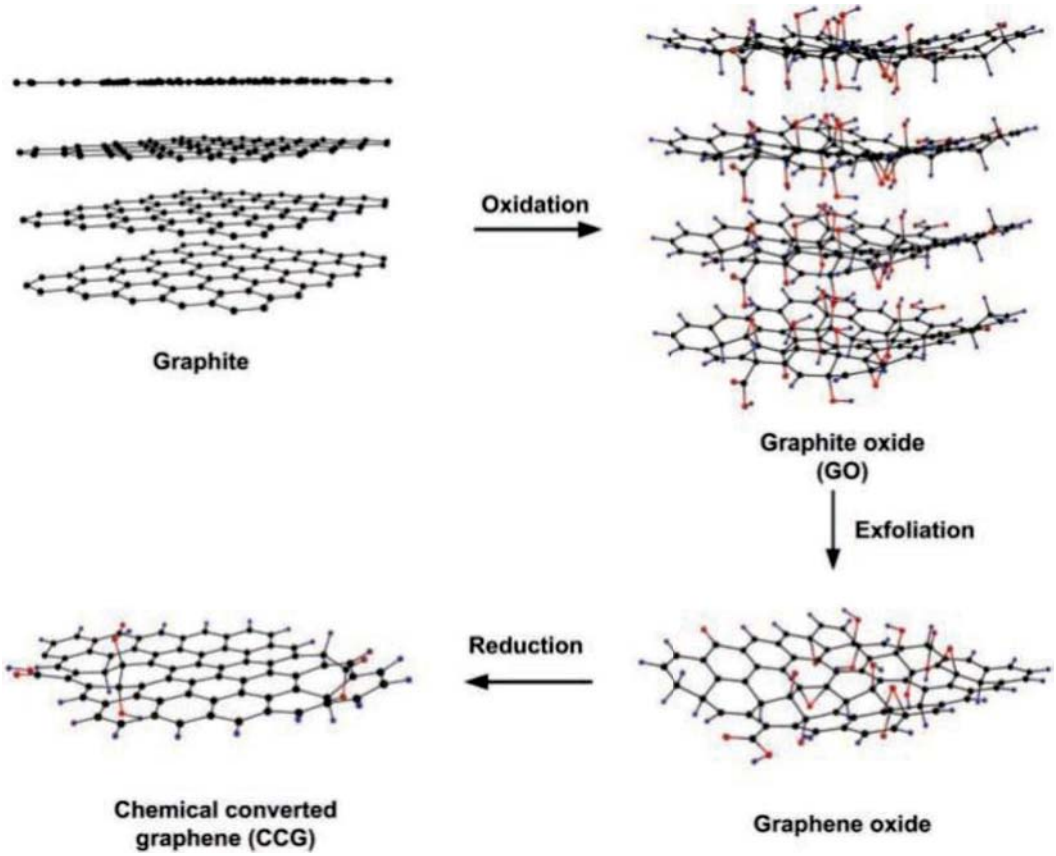

Figure 1.19 Schematic diagram for Preparation of chemically converted graphene (CCG) by reduction of graphene oxide [100, 101].

Elemental analysis of chemically converted graphene (CCG) reveals that the atomic C/O ratio is around 10 [101]. This implies that a considerable amount of oxygen is present after the reduction step and that CCG is not the same as pristine graphene. An enhancement in the restoration of the sp^2 carbon network is observed after thermal annealing of CCG [99, 100].

1.5 GRAPHENE BASED FLEXIBLE, STRETCHABLE ELECTRODES AND SUPERCAPACITORS

The extraordinary electrical, mechanical, chemical properties, large surface area and high carrier mobility of graphene make it a potential candidate for application in flexible and stretchable electrode or supercapacitor [102, 103]. Theoretically, graphene based electrochemical double layer capacitor (EDLC) is able to reach a capacitance up to 550 F g^{-1} which is the highest value of intrinsic capacitance among all carbon-based electrodes [104].

Recently, such uses of graphene have been studied by many research groups for development of flexible and stretchable electrode or supercapacitor. Kim *et al*. [105] have developed a technique to grow a few layers of graphene films using chemical vapour deposition (CVD) and then transfer the graphene films to polydimethylsiloxane (PDMS) substrate, without mechanical and chemical treatments, to preserve the crystalline quality of the graphene films (Figure 1.20).

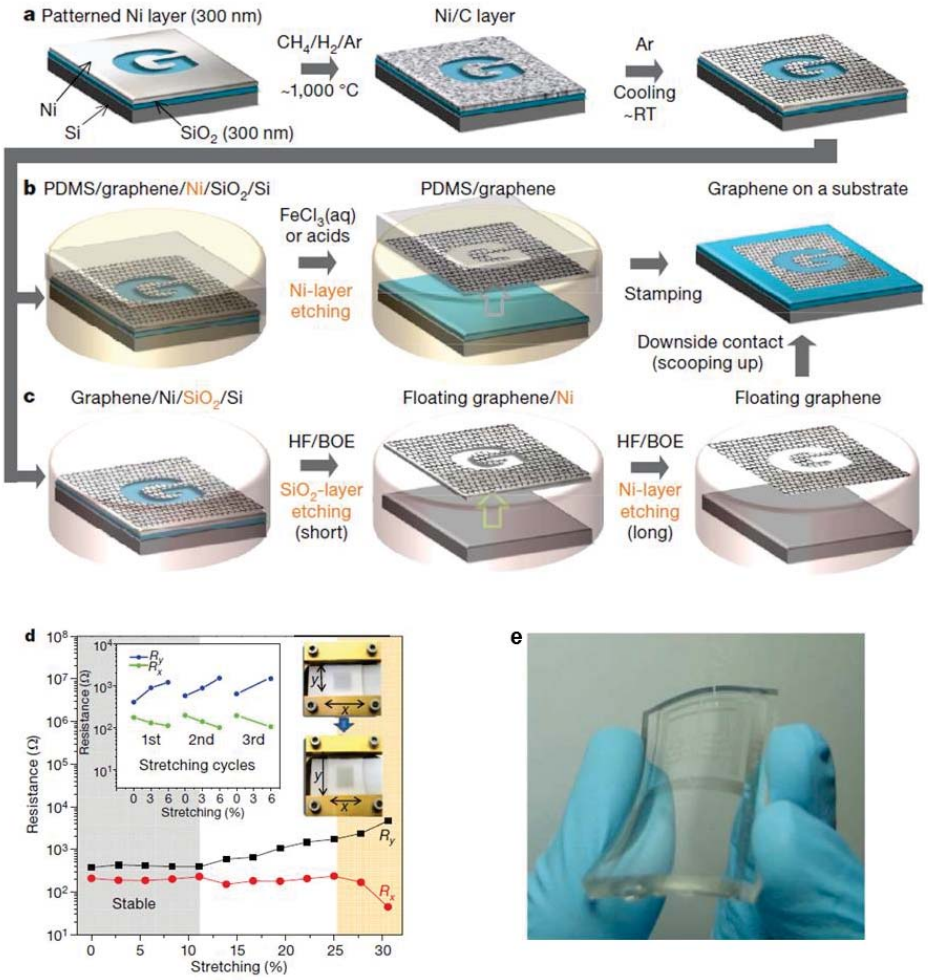

Figure 1.20 Synthesis, etching and transfer process for the large scale and patterned graphene films. (a) Synthesis of patterned graphene films on thin nickel layers. (b) Etching using $FeCl_3$ (or acids) and transfer of graphene films using a PDMS stamp. (c) Etching using buffered oxide etchant (BOE) or hydrogen fluoride (HF) solution and transfer of graphene films at room temperature (25 ^{o}C). (d) Resistance of the graphene film transferred to the PDMS substrate isotropically stretched by ~12%. The left inset shows the case in which the graphene film is transferred to an unstretched PDMS substrate. The right inset shows the movement of holding stages and the consequent change in shape of the graphene film. (e) Graphene film on the PDMS substrate is transparent and flexible [105].

This graphene film has excellent electromechanical properties when used to fabricate flexible and stretchable electrode and their resistance on the pre-strained and unstrained PDMS were measured with respect uniaxial strain ranging from 0 to 30% (Figure 1.20d). The graphene film on the unstrained PDMS recovers its original resistance after stretching by ~6%. However, further stretching results in mechanical failure. To overcome this, the films were transferred to pre-strained PDMS to improve the electromechanical stability by making buckled shape.

Kaner *et al* [106]. have recently developed graphene based flexible supercapacitors with 276 F g^{-1} of high specific capacitance, 20 W cm^{-3} of power density (20 times higher than activated carbon counterpart) and 1.36 mWh cm^{-3} of energy density (2 times higher activated carbon counterpart). The schematic procedure for graphene based flexible supercapacitor is presented in Figure 1.22 A ~ F [106]. The graphene based flexible supercapacitor also has an excellent stability during bending from 0^{o} to 180^{o} (Figure 1.21 G ~ I). The device has been developed by using a standard Light Scribe DVD optical drive to directly reduce graphene oxide films to graphene electrodes.

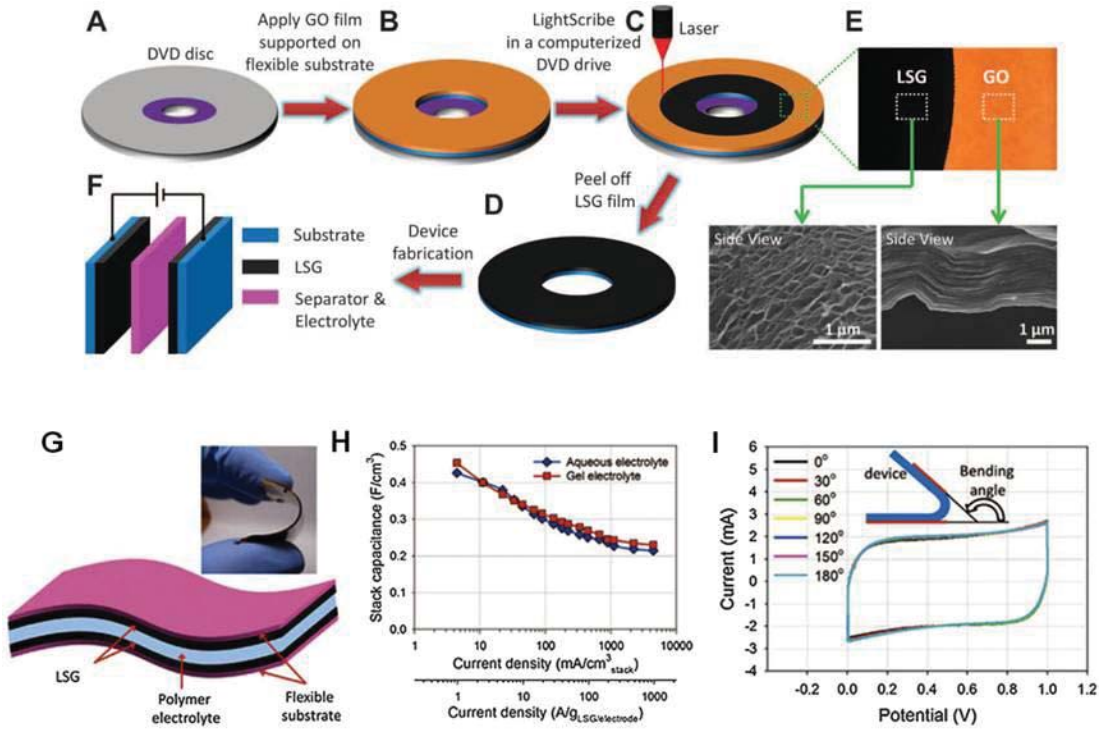

Figure 1.21 Schematic diagram and electrochemical properties of the laser-scribed graphene-based flexible supercapacitor. (A to D) A GO film supported on a flexible substrate is placed on top of a LightScribe-enabled DVD media disc and a computer image is then laser-irradiated on the GO film in a computerized LightScribe DVD drive. (E) The low-power infrared laser changes the stacked GO sheets immediately into well-exfoliated few-layered LSG film, as shown in the cross-sectional SEM images. (F) A symmetric supercapacitor is constructed from two identical graphene based electrodes, ion-porous separator, and electrolyte. (G) Illustration of assembled graphene based supercapacitor; inset is showing the flexibility of the device. (H) A comparison between performances of the supercapacitor using gelled versus aqueous electrolytes. (I) Flexibility of the supercapacitor: CV measurements were carried out at a scan rate of 1000 mV s^{-1} [106].

Yu and co-worker [107] have studied the ultrathin and transparent graphene film for use in flexible supercapacitor application. The graphene produced by modified Hummers method [108] and using a vacuum filtration for preparing 25, 50, 75, and 100 nm thick ultrathin graphene films (Figure 1.22). The ultrathin graphene film

based supercapacitor showed the highest capacitance value of 135 F g^{-1} for 25nm film thickness with high power density of 7200 W kg^{-1} in 2 M potassium chloride (KCl) electrolyte.

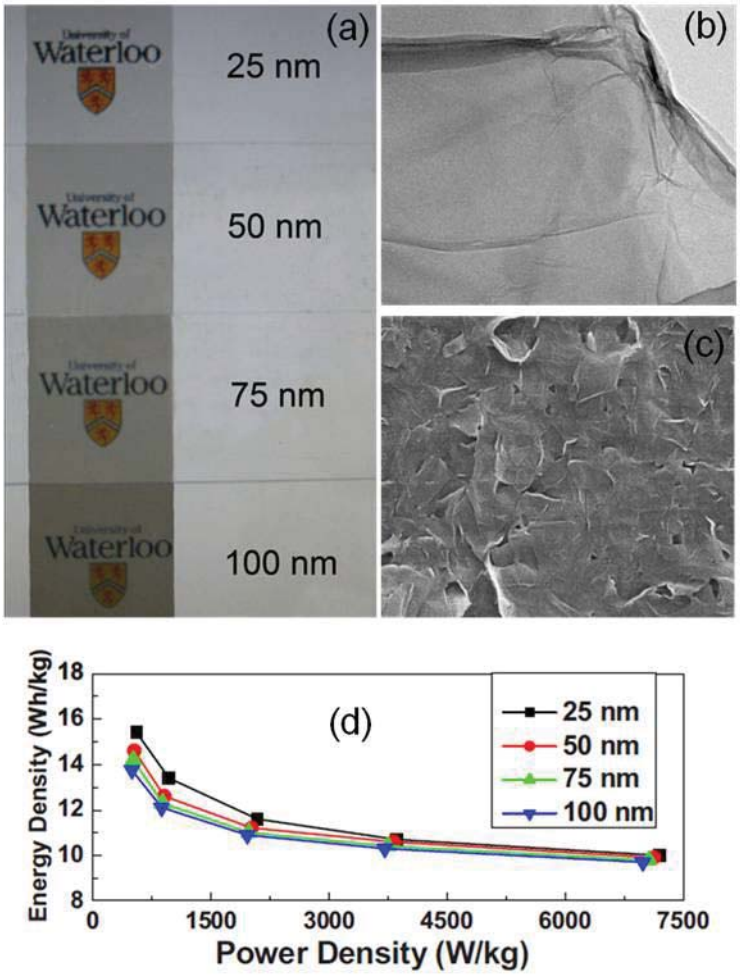

Figure 1.22 (a) Photographs of transparent thin graphene films with various thicknesses on slide glass. (b) TEM image of graphene collected from dispersion before filtration. (c) SEM image of 100 nm graphene film on slide glass [107].

In addition, graphene based transparent and stretchable electrode can be applicable to strain sensors. Bae and co-workers [109] have constructed a graphene based strain sensor capable of monitoring the motion of body parts. The CVD-grown graphene

based sensor was fabricated onto stretchable PDMS substrate using a micro-fabrication process (Figure 1.23 a).

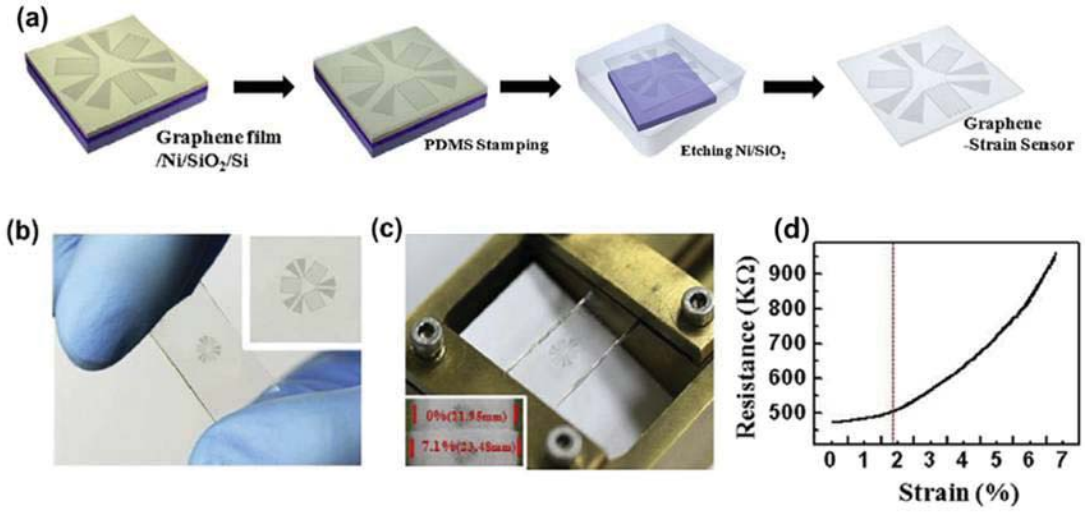

Figure 1.23 (a) Schematic representation of various steps in fabrication process. (b) Photograph of transparent graphene strain sensor. (c) Photograph of graphene strain sensor fixed in motion controller under stretching test. Inset shows the initial distance (~0%) and final distance (~7.1%) between two fixed points. (d) Variation of resistance with respect to stretching up to ~7.1% for graphene strain sensor [109].

The graphene based strain sensor showed variation in normalized resistance as the strain was increased linearly before fracture of the graphene strain sensor. This resistance varied with a tensile strain of up to 7.1%. When the applied strain was more than 7.1%, the strain sensor exhibited an unexpected increase in the resistance; this indicates that the sensor failed above this strain value due to mechanical fracture.

Lee *et al.* [110] have fabricated stretchable, printable, and transparent transistors based on graphene films on polydimethylsiloxane (PDMS). Briefly, the graphene electrodes and graphene semiconducting channels could be transferred onto the PDMS substrate with a supporting layer. After transfer, the supporting layer was

etched with acetone. The ion gel gate dielectric and PEDOT (Poly(3,4-ethylenedioxythiophene) : PSS (Polystyrene sulfonate) gate electrodes were subsequently printed using commercial aerosol jet printing techniques (Figure 1.24A).

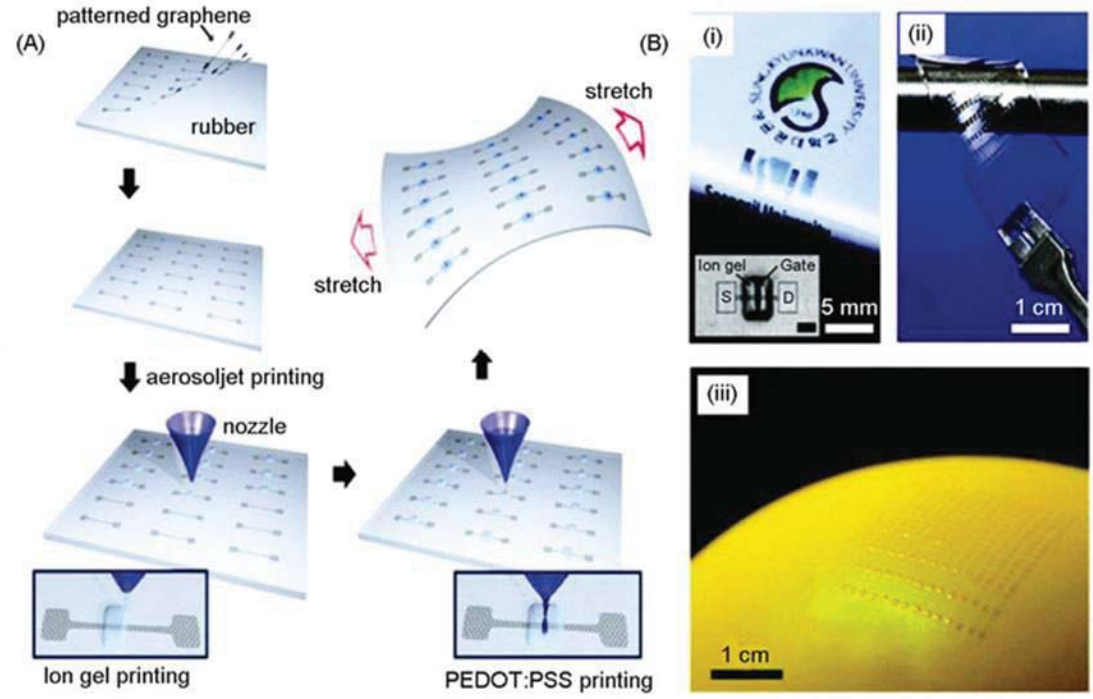

Figure 1.24 (A) A schematic of the fabrication approach for arrays of graphene FETs on the stretchable PDMS substrate. The inset shows the microscopy image of monolayer graphene FETs on PET (scale bar, 300 µm) (B) Various photographic images of the ion gel-gated graphene FETs on different substrates (i) polyethylene terephthalate (PET), (ii) PDMS and (iii) balloon [110].

This material exhibited excellent mechanical, electrical, and optical properties, and was also applicable for semiconducting channels as well as the source/drain electrodes (Figure 1.24B). Such graphene transistors showed hole and electron mobility of 1188 ± 136 and 422 ± 52 cm^2 (V s), respectively, with stable operation at stretching of up to 5% even after 1000 cycles. Nanocarbon materials such as, CNTs and graphene is a potential and applicable material that is widely used in electronic

devices such as supercapacitor, sensor, stretchable and flexible electrode. Table 1.4 summarized specific capacitance values of different nanocarbon based materials for stretchable and flexible supercapacitor application. It is important to note that the application of nanocarbon materials for stretchable and flexible energy storage devices are still under developed.

It is clear that there are considerable numbers of research and development of CNTs and graphene to use as electrode materials for stretchable and flexible energy storage applications. At the current stage, the potential of nano structured nanocarbon material based supercapacitors has not been fully developed. For future nanocarbon based supercapacitors, there are different develop requirement, except for the common goal to achieve a higher energy, power density and longer life cycle [111]. The conventional supercapacitors are too heavy and bulky to apply for potable and wearable electronics. In order to overcome these challenges, there are few stretchable, flexible and transparent supercapacitors have been developed based on limited electrode materials. CNTs and graphene film with high flexibility , stretchability and charge mobility are promising electrode materials for flexible and stretchable supercapacitors, although it is still in the initial research stage. We believe that research efforts in this thesis can lead to a prosperous area of stretchable and flexible supercapacitor technologies.

Active material	Electrolyte	Capacitance	Reference
SWCNTs	1 M of tetraethylammonium tetrafluoroborate in propylene carbonate	54 F g^{-1} (52 F g^{-1}=at the 30% strain)	[84]
SWCNTs	PVA-H_3PO_4	13.15 F g^{-1}	[88]
SWCNTs	PVA-H_2SO_4	10 F g^{-1} (it was retained after 1000 charge/discharge)	[80]
MWCNTs	PVA-KOH	25.4 F cm^{-1}	[73]
MWCNTs	EMI-TFSI based ionogel	430 uF cm^{-1} (90% capacitance retention after 1000 bending cycle)	[35]
MWCNTs	PVA-H_3PO_4	7.3 F g^{-1}	[89]
Graphene	PVA-H_3PO_4	276 F g^{-1}	[106]
Graphene	PVA-H_2SO_4	78.9 uF cm^{-1}	[103]
Graphene	2 M KCl	135 F g^{-1} (with 70% transmittance)	[107]

Table 1.4 Specific capacitance values of different nanocarbon based materials for stretchable and/or flexible supercapacitors.

1.6 THESIS AIMS

The development of stretchable and flexible energy storage devices is highly important for applications in the rapidly growing field of flexible and wearable electronics [50, 112, 113]. Among the various energy storage devices, the supercapacitor is considered to be very attractive due to its high power density, long cycle life time, low environmental impact and safety [114, 115]. It is believed that supercapacitors may find new applications in the biomedical industry, particularly for the powering of implantable electrodes in the body. In addition, research in the field of supercapacitor over the last decade has manifested that nanocarbon based materials such as carbon nanotube and graphene are potentially attractive as electrode materials for supercapacitor due to their extraordinary properties. The overall goal of the thesis is to design and fabricate novel biocompatible and stretchable supercapacitor with excellent endurability and high stability in various environments using carbon nanomaterials such as carbon nanotubes and graphene. The aim is to incorporate some biological entities into the capacitor to improve or enhance the biocompatibility of the device. The initial objectives of the project are the:

1. Characterization and optimization of carbon-based materials, including Single-wall carbon nanotubes (SWNT), graphene oxide (GO) and reduced graphene Oxide (rGO), that will be employed for the fabrication of nanostructure energy storage devices.

One consideration in the thesis is that these nanomaterials display large attractive van der Waals forces. As such, as-produced SWNT or graphite samples are acquired in bundled form which is extremely difficult to individualize. To improve their

performance, the carbon-based materials should be de-bundled and exfoliated well in a suitable solvent. The project will implement established approaches for dispersing these carbon nanomaterials and implement various characterization techniques such as FT-IR, Raman, XPS, XRD and Scanning electron microscope (SEM) to systematically monitor their preparation prior to incorporation into the devices.

2. Preparation of stretchable and biocompatible polymers substrates to develop nanocarbon based energy storage devices.

Recent inventions such as high performance sportswear, wearable displays and embedded health monitoring devices are demanding power systems with not only high capacitance, but which are flexible and stretchable. A variety of stretchable materials such as silicone rubber, latex, polychloroprene rubber, polyurethane and cotton have been employed as a matrix to investigate a stretchable electrode. Latex and polyurethane is the most suitable materials for stretchable electrode and supercapacitor construction. Latex and polyurethane is an elastomeric material that is cheap, non-toxic, eco friendly, highly stretchable and easily processed. Most work to date on conductive, stretchable, composites electrodes has mainly focused on sensors and actuators, while their capacitive behaviour has been investigated to a lesser extent. In this thesis , we aim to identify the most suitable flexible polymer both in terms of its material properties but also its ability to integrate with other components (e.g. CNT, graphene, biomolecules, electrolyte) to be incorporated into the capacitor.

3. Development of coating technique to prepare the nanocarbon based stretchable and biocompatible electrode.

There are many types of methods to fabricate an electrode coating of nanocarbon materials. In this thesis, we would like to explore various approaches including layer-by-layer, spin-coating, dip-coating and spray-coating methods. Spray-coating is particularly suitable for deposition of nanocarbon materials due to its low equipment cost, short runs time and applicability to industrial scales. This work will investigate the ability to control the properties of the thin films coatings and, importantly, assess the fabrication techniques to determine the best for producing nanostructured films with ideal capacitive properties. In this part of the thesis, the biocompatible and stretchable latex and polyurethane substrate will firstly be cast and then the nanocarbon materials deposition or coating on substrate will be conducted.

4. Development of the polymer electrolyte for stretchable energy storage devices.

In order to produce the stretchable supercapacitors, modification and development of stretchable polymer electrolyte with high ionic conductivity is required. Currently, there are only a few stretchable polymer electrolytes reported including graft copolymer poly[(oxyethylene)$_9$ methacrylate]-g-poly(dimethylsiloxane) doped with $LiCF_3SO_3$, [116] poly(methyl methacrylate) networks solvated by the ionic liquid 1-ethy-3-methylimidazolium bis(trifluoromethanesulfonyl) imide (EMI.TFSI) [117].

The preparation of these electrolytes involves complex chemical reaction/polymerization, and their conductivities are low (10^{-5}-10^{-4} S cm^{-1}). H_3PO_4-PVA or H_2SO_4-PVA is a commonly used gel electrolyte in flexible energy devices [118, 119]. In this thesis, the stretchable solid electrolyte is investigate to establish

fully stretchable supercapacitor device, and are attracting intense interests in the field of electrochemistry [111, 114] and analytical electrochemistry.

5. Characterisation of final stretchable devices.

The stretchable and biocompatible full device as supercapacitor will be prepared and subsequently, the investigation on the capacitive properties of those electrodes will be carried out as a function of the strain and stress of nanocarbon materials coated on the biocompatible elastomer. For example, cyclic voltammetry (CV), electrochemical impedance spectroscopy (EIS), charge/discharge and stability test will be performed to assess their electrochemical properties. In order to do so, the electrochemical performance of those electrodes should be considered using stretchable solid electrolyte.

1.7 REFERENCES

[1] W.-C. Fang, O. Chyan, C.-L. Sun, C.-T. Wu, C.-P. Chen, K.-H. Chen, L.-C. Chen, and J.-H. Huang, "Arrayed CNx NT–RuO2 nanocomposites directly grown on Ti-buffered Si substrate for supercapacitor applications," *Electrochemistry Communications,* vol. 9, pp. 239-244, 2007.

[2] A. Burke, "Ultracapacitors: why, how, and where is the technology," *Journal of Power Sources,* vol. 91, pp. 37-50, 2000.

[3] H. Kim and B. N. Popov, "Characterization of hydrous ruthenium oxide/carbon nanocomposite supercapacitors prepared by a colloidal method," *Journal of Power Sources,* vol. 104, pp. 52-61, 2002.

[4] K.-H. Chang and C.-C. Hu, "Oxidative Synthesis of $RuO_x \cdot nH_2O$ with Ideal Capacitive Characteristics for Supercapacitors," *Journal of The Electrochemical Society,* vol. 151, pp. A958-A964, July 1, 2004 2004.

[5] P. J. Hall and E. J. Bain, "Energy-storage technologies and electricity generation," *Energy Policy,* vol. 36, pp. 4352-4355, 2008.

[6] A. Shukla, S. Sampath, and K. Vijayamohanan, "Electrochemical supercapacitors: Energy storage beyond batteries," *Current science,* vol. 79, pp. 1656-1661, 2000.

[7] S. Bose, T. Kuila, A. K. Mishra, R. Rajasekar, N. H. Kim, and J. H. Lee, "Carbon-based nanostructured materials and their composites as supercapacitor electrodes," *Journal of Materials Chemistry,* vol. 22, pp. 767-784, 2012.

[8] P. Soudan, J. Gaudet, D. Guay, D. Bélanger, and R. Schulz, "Electrochemical Properties of Ruthenium-Based Nanocrystalline Materials as Electrodes for Supercapacitors," *Chemistry of Materials,* vol. 14, pp. 1210-1215, 2002/03/01 2002.

[9] T. A. Skotheim and J. Reynolds, *Conjugated polymers: processing and applications*: CRC press, 2006.

[10] B. Y. Choi, I. J. Chung, J. H. Chun, and J. M. Ko, "Electrochemical characteristics of dodecylbenzene sulfonic acid-doped polyaniline in aqueous solutions," *Synthetic Metals,* vol. 99, pp. 253-256, 1999.

[11] J. C. LaCroix and A. F. Diaz, "Electrolyte Effects on the Switching Reaction of Polyaniline," *Journal of The Electrochemical Society,* vol. 135, pp. 1457-1463, June 1, 1988 1988.

[12] Y. G. Wang, H. Q. Li, and Y. Y. Xia, "Ordered Whiskerlike Polyaniline Grown on the Surface of Mesoporous Carbon and Its Electrochemical Capacitance Performance," *Advanced Materials,* vol. 18, pp. 2619-2623, 2006.

[13] J. Maier, "Nanoionics: ion transport and electrochemical storage in confined systems," *Nature materials,* vol. 4, pp. 805-815, 2005.

[14] L.-Z. Fan and J. Maier, "High-performance polypyrrole electrode materials for redox supercapacitors," *Electrochemistry Communications,* vol. 8, pp. 937-940, 2006.

[15] D. Yu and L. Dai, "Self-assembled graphene/carbon nanotube hybrid films for supercapacitors," *The Journal of Physical Chemistry Letters,* vol. 1, pp. 467-470, 2009.

[16] H. R. Byon, S. W. Lee, S. Chen, P. T. Hammond, and Y. Shao-Horn, "Thin films of carbon nanotubes and chemically reduced graphenes for electrochemical micro-capacitors," *Carbon,* vol. 49, pp. 457-467, 2011.

[17] N. Vassal, E. Salmon, and J. F. Fauvarque, "Electrochemical properties of an alkaline solid polymer electrolyte based on P(ECH-co-EO)," *Electrochimica Acta,* vol. 45, pp. 1527-1532, 2000.

[18] A. Lewandowski, K. Skorupska, and J. Malinska, "Novel poly(vinyl alcohol)–KOH–H2O alkaline polymer electrolyte," *Solid State Ionics,* vol. 133, pp. 265-271, 2000.

[19] A. Lewandowski, M. Zajder, E. Frąckowiak, and F. Béguin, "Supercapacitor based on activated carbon and polyethylene oxide–KOH–H2O polymer electrolyte," *Electrochimica Acta,* vol. 46, pp. 2777-2780, 2001.

[20] S. Nohara, H. Wada, N. Furukawa, H. Inoue, M. Morita, and C. Iwakura, "Electrochemical characterization of new electric double layer capacitor with polymer hydrogel electrolyte," *Electrochimica Acta,* vol. 48, pp. 749-753, 2003.

[21] X. Zhu, H. Yang, Y. Cao, and X. Ai, "Preparation and electrochemical characterization of the alkaline polymer gel electrolyte polymerized from acrylic acid and KOH solution," *Electrochimica Acta,* vol. 49, pp. 2533-2539, 2004.

[22] H. Wada, S. Nohara, N. Furukawa, H. Inoue, N. Sugoh, H. Iwasaki, M. Morita, and C. Iwakura, "Electrochemical characteristics of electric double layer capacitor using sulfonated polypropylene separator impregnated with polymer hydrogel electrolyte," *Electrochimica Acta,* vol. 49, pp. 4871-4875, 2004.

[23] H. Wada, K. Yoshikawa, S. Nohara, N. Furukawa, H. Inoue, N. Sugoh, H. Iwasaki, and C. Iwakura, "Electrochemical characteristics of new electric

double layer capacitor with acidic polymer hydrogel electrolyte," *Journal of Power Sources,* vol. 159, pp. 1464-1467, 2006.

[24] N. A. Choudhury, A. K. Shukla, S. Sampath, and S. Pitchumani, "Cross-Linked Polymer Hydrogel Electrolytes for Electrochemical Capacitors," *Journal of The Electrochemical Society,* vol. 153, pp. A614-A620, March 1, 2006 2006.

[25] S. Iijima, "Helical microtubules of graphitic carbon," *Nature,* vol. 354, pp. 56-58, 1991.

[26] R. Saito, G. Dresselhaus, and M. S. Dresselhaus, "Electronic structure of double-layer graphene tubules," *Journal of Applied Physics,* vol. 73, pp. 494-500, 1993.

[27] M. S. Dresselhaus, G. Dresselhaus, and R. Saito, "C60-related tubules," *Solid State Communications,* vol. 84, pp. 201-205, 1992.

[28] J. P. Issi, L. Langer, J. Heremans, and C. H. Olk, "Electronic properties of carbon nanotubes: Experimental results," *Carbon,* vol. 33, pp. 941-948, 1995.

[29] T. Ebbesen, H. Lezec, H. Hiura, J. Bennett, H. Ghaemi, and T. Thio, "Electrical conductivity of individual carbon nanotubes," 1996.

[30] E. Frackowiak, K. Jurewicz, S. Delpeux, and F. Béguin, "Nanotubular materials for supercapacitors," *Journal of Power Sources,* vol. 97–98, pp. 822-825, 2001.

[31] A. Kotwal and C. E. Schmidt, "Electrical stimulation alters protein adsorption and nerve cell interactions with electrically conducting biomaterials," *Biomaterials,* vol. 22, pp. 1055-1064, 2001.

[32] N. K. Guimard, N. Gomez, and C. E. Schmidt, "Conducting polymers in biomedical engineering," *Progress in Polymer Science,* vol. 32, pp. 876-921, 2007.

[33] Z. Niu, W. Zhou, J. Chen, G. Feng, H. Li, W. Ma, J. Li, H. Dong, Y. Ren, and D. Zhao, "Compact-designed supercapacitors using free-standing single-walled carbon nanotube films," *Energy & Environmental Science,* vol. 4, pp. 1440-1446, 2011.

[34] A.-D. Bendrea, L. Cianga, and I. Cianga, "Review paper: progress in the field of conducting polymers for tissue engineering applications," *Journal of biomaterials applications,* vol. 26, pp. 3-84, 2011.

[35] B. Hsia, J. Marschewski, S. Wang, J. B. In, C. Carraro, D. Poulikakos, C. P. Grigoropoulos, and R. Maboudian, "Highly flexible, all solid-state micro-supercapacitors from vertically aligned carbon nanotubes," *Nanotechnology,* vol. 25, p. 055401, 2014.

[36] J. Prasek, J. Drbohlavova, J. Chomoucka, J. Hubalek, O. Jasek, V. Adam, and R. Kizek, "Methods for carbon nanotubes synthesis—review," *Journal of Materials Chemistry,* vol. 21, pp. 15872-15884, 2011.

[37] R. Osmani, A. Kulkarni, N. Aloorkar, R. Bhosale, P. Ghodake, and B. Harkare, "Carbon Nanotubes: An Impending Carter in Therapeutics."

[38] R. Williams and P. Doherty, "A preliminary assessment of poly (pyrrole) in nerve guide studies," *Journal of materials science: materials in medicine,* vol. 5, pp. 429-433, 1994.

[39] L. J. del Valle, D. Aradilla, R. Oliver, F. Sepulcre, A. Gamez, E. Armelin, C. Alemán, and F. Estrany, "Cellular adhesion and proliferation on poly(3,4-ethylenedioxythiophene): Benefits in the electroactivity of the conducting polymer," *European Polymer Journal,* vol. 43, pp. 2342-2349, 2007.

[40] E. S. Takeuchi and R. A. Leising, "Lithium batteries for biomedical applications," *MRS bulletin,* vol. 27, pp. 624-627, 2002.

[41] C. Laurent, E. Flahaut, and A. Peigney, "The weight and density of carbon nanotubes versus the number of walls and diameter," *Carbon,* vol. 48, pp. 2994-2996, 2010.

[42] J. G. Duque, A. N. G. Parra-Vasquez, N. Behabtu, M. J. Green, A. L. Higginbotham, B. K. Price, A. D. Leonard, H. K. Schmidt, B. Lounis, J. M. Tour, S. K. Doorn, L. Cognet, and M. Pasquali, "Diameter-Dependent Solubility of Single-Walled Carbon Nanotubes," *ACS Nano,* vol. 4, pp. 3063-3072, 2010/06/22 2010.

[43] A. T. Yahiro, S. M. Lee, and D. O. Kimble, "Bioelectrochemistry: I. Enzyme utilizing bio-fuel cell studies," *Biochimica et Biophysica Acta (BBA) - Specialized Section on Biophysical Subjects,* vol. 88, pp. 375-383, 1964.

[44] R. A. Bullen, T. C. Arnot, J. B. Lakeman, and F. C. Walsh, "Biofuel cells and their development," *Biosensors and Bioelectronics,* vol. 21, pp. 2015-2045, 2006.

[45] L. Hu, J. W. Choi, Y. Yang, S. Jeong, F. La Mantia, L.-F. Cui, and Y. Cui, "Highly conductive paper for energy-storage devices," *Proceedings of the National Academy of Sciences,* vol. 106, pp. 21490-21494, December 22, 2009 2009.

[46] J. Kim, H. Jia, and P. Wang, "Challenges in biocatalysis for enzyme-based biofuel cells," *Biotechnology advances,* vol. 24, pp. 296-308, 2006.

[47] S. Calabrese Barton, J. Gallaway, and P. Atanassov, "Enzymatic biofuel cells for implantable and microscale devices," *Chemical Reviews,* vol. 104, pp. 4867-4886, 2004.

[48] J.-J. Sun, H.-Z. Zhao, Q.-Z. Yang, J. Song, and A. Xue, "A novel layer-by-layer self-assembled carbon nanotube-based anode: Preparation, characterization, and application in microbial fuel cell," *Electrochimica Acta,* vol. 55, pp. 3041-3047, 2010.

[49] K. H. An, W. S. Kim, Y. S. Park, J. M. Moon, D. J. Bae, S. C. Lim, Y. S. Lee, and Y. H. Lee, "Electrochemical Properties of High-Power Supercapacitors Using Single-Walled Carbon Nanotube Electrodes," *Advanced Functional Materials,* vol. 11, pp. 387-392, 2001.

[50] V. L. Pushparaj, M. M. Shaijumon, A. Kumar, S. Murugesan, L. Ci, R. Vajtai, R. J. Linhardt, O. Nalamasu, and P. M. Ajayan, "Flexible energy storage devices based on nanocomposite paper," *Proceedings of the National Academy of Sciences,* vol. 104, pp. 13574-13577, August 21, 2007 2007.

[51] Y.-k. Zhou, B.-l. He, W.-j. Zhou, and H.-l. Li, "Preparation and Electrochemistry of SWNT/PANI Composite Films for Electrochemical Capacitors," *Journal of The Electrochemical Society,* vol. 151, pp. A1052-A1057, July 1, 2004 2004.

[52] C. Liu, S. Alwarappan, Z. Chen, X. Kong, and C.-Z. Li, "Membraneless enzymatic biofuel cells based on graphene nanosheets," *Biosensors and Bioelectronics,* vol. 25, pp. 1829-1833, 2010.

[53] W. Shin, J. Lee, Y. Kim, H. Steinfink, and A. Heller, "Ionic Conduction in Zn3 (PO4) 2⊙ 4H2O Enables Efficient Discharge of the Zinc Anode in Serum," *Journal of the American Chemical Society,* vol. 127, pp. 14590-14591, 2005.

[54] T. Someya, Y. Kato, T. Sekitani, S. Iba, Y. Noguchi, Y. Murase, H. Kawaguchi, and T. Sakurai, "Conformable, flexible, large-area networks of pressure and thermal sensors with organic transistor active matrixes," *Proceedings of the National Academy of Sciences of the United States of America,* vol. 102, pp. 12321-12325, August 30, 2005 2005.

[55] R. Carta, P. Jourand, B. Hermans, J. Thoné, D. Brosteaux, T. Vervust, F. Bossuyt, F. Axisa, J. Vanfleteren, and R. Puers, "Design and implementation of advanced systems in a flexible-stretchable technology for biomedical applications," *Sensors and Actuators A: Physical,* vol. 156, pp. 79-87, 2009.

[56] J. A. Rogers, T. Someya, and Y. Huang, "Materials and Mechanics for Stretchable Electronics," *Science,* vol. 327, pp. 1603-1607, March 26, 2010 2010.

[57] S. P. Lacour, J. Jones, S. Wagner, T. Li, and Z. Suo, "Stretchable interconnects for elastic electronic surfaces," *Proceedings of the IEEE,* vol. 93, pp. 1459-1467, 2005.

[58] A. C. Siegel, D. A. Bruzewicz, D. B. Weibel, and G. M. Whitesides, "Microsolidics: Fabrication of Three-Dimensional Metallic Microstructures in Poly (dimethylsiloxane)," *Advanced Materials,* vol. 19, pp. 727-733, 2007.

[59] E. Smela, "Conjugated Polymer Actuators for Biomedical Applications," *Advanced Materials,* vol. 15, pp. 481-494, 2003.

[60] J. A. Fan, W.-H. Yeo, Y. Su, Y. Hattori, W. Lee, S.-Y. Jung, Y. Zhang, Z. Liu, H. Cheng, and L. Falgout, "Fractal design concepts for stretchable electronics," *Nature communications,* vol. 5, 2014.

[61] T. Sekitani, Y. Noguchi, K. Hata, T. Fukushima, T. Aida, and T. Someya, "A rubberlike stretchable active matrix using elastic conductors," *Science,* vol. 321, pp. 1468-1472, 2008.

[62] J. Viventi, D.-H. Kim, L. Vigeland, E. S. Frechette, J. A. Blanco, Y.-S. Kim, A. E. Avrin, V. R. Tiruvadi, S.-W. Hwang, and A. C. Vanleer, "Flexible, foldable, actively multiplexed, high-density electrode array for mapping brain activity in vivo," *Nature neuroscience,* vol. 14, pp. 1599-1605, 2011.

[63] D.-H. Kim, N. Lu, R. Ma, Y.-S. Kim, R.-H. Kim, S. Wang, J. Wu, S. M. Won, H. Tao, A. Islam, K. J. Yu, T.-i. Kim, R. Chowdhury, M. Ying, L. Xu, M. Li, H.-J. Chung, H. Keum, M. McCormick, P. Liu, Y.-W. Zhang, F. G. Omenetto, Y. Huang, T. Coleman, and J. A. Rogers, "Epidermal Electronics," *Science,* vol. 333, pp. 838-843, August 12, 2011 2011.

[64] A. Heller, "Potentially implantable miniature batteries," *Analytical and bioanalytical chemistry,* vol. 385, pp. 469-473, 2006.

[65] B. Winther-Jensen, M. Gaadingwe, D. R. Macfarlane, and M. Forsyth, "Control of magnesium interfacial reactions in aqueous electrolytes towards a biocompatible battery," *Electrochimica Acta,* vol. 53, pp. 5881-5884, 2008.

[66] M. P. Staiger, A. M. Pietak, J. Huadmai, and G. Dias, "Magnesium and its alloys as orthopedic biomaterials: A review," *Biomaterials,* vol. 27, pp. 1728-1734, 2006.

[67] D. J. Lipomi, M. Vosgueritchian, B. C. Tee, S. L. Hellstrom, J. A. Lee, C. H. Fox, and Z. Bao, "Skin-like pressure and strain sensors based on transparent elastic films of carbon nanotubes," *Nature nanotechnology,* vol. 6, pp. 788-792, 2011.

[68] F. I. Wolf and A. Cittadini, "Chemistry and biochemistry of magnesium," *Molecular Aspects of Medicine,* vol. 24, pp. 3-9, 2003.

[69] X. Li, T. Gu, and B. Wei, "Dynamic and galvanic stability of stretchable supercapacitors," *Nano Letters,* vol. 12, pp. 6366-6371, 2012.

[70] J. Smithyman and R. Liang, "Flexible supercapacitor yarns with coaxial carbon nanotube network electrodes," *Materials Science and Engineering: B,* vol. 184, pp. 34-43, 2014.

[71] P. Xu, T. Gu, Z. Cao, B. Wei, J. Yu, F. Li, J.-H. Byun, W. Lu, Q. Li, and T.-W. Chou, "Carbon Nanotube Fiber Based Stretchable Wire-Shaped Supercapacitors," *Advanced Energy Materials,* vol. 4, pp. n/a-n/a, 2014.

[72] X. Zhao, B. T. Chu, B. Ballesteros, W. Wang, C. Johnston, J. M. Sykes, and P. S. Grant, "Spray deposition of steam treated and functionalized single-walled and multi-walled carbon nanotube films for supercapacitors," *Nanotechnology,* vol. 20, p. 065605, 2009.

[73] C. Choi, J. A. Lee, A. Y. Choi, Y. T. Kim, X. Lepró, M. D. Lima, R. H. Baughman, and S. J. Kim, "Flexible Supercapacitor Made of Carbon Nanotube Yarn with Internal Pores," *Advanced Materials,* vol. 26, pp. 2059-2065, 2014.

[74] A. Hartwig, "Role of magnesium in genomic stability," *Mutation Research/Fundamental and Molecular Mechanisms of Mutagenesis,* vol. 475, pp. 113-121, 2001.

[75] J. Vormann, "Magnesium: nutrition and metabolism," *Molecular Aspects of Medicine,* vol. 24, pp. 27-37, 2003.

[76] W. Sun, R. Gao, and K. Jiao, "Electrochemistry and Electrocatalysis of Hemoglobin in Nafion/nano-CaCO3 Film on a New Ionic Liquid BPPF6 Modified Carbon Paste Electrode," *The Journal of Physical Chemistry B,* vol. 111, pp. 4560-4567, 2007/05/01 2007.

[77] L. Cooper, H. Amano, M. Hiraide, S. Houkyou, I. Y. Jang, Y. J. Kim, H. Muramatsu, J. H. Kim, T. Hayashi, Y. A. Kim, M. Endo, and M. S. Dresselhaus, "Freestanding, bendable thin film for supercapacitors using DNA-dispersed double walled carbon nanotubes," *Applied Physics Letters,* vol. 95, pp. -, 2009.

[78] V. T. Truong, P. K. Lai, B. T. Moore, R. F. Muscat, and M. S. Russo, "Corrosion protection of magnesium by electroactive polypyrrole/paint coatings," *Synthetic Metals,* vol. 110, pp. 7-15, 2000.

[79] M. Kaempgen, C. K. Chan, J. Ma, Y. Cui, and G. Gruner, "Printable Thin Film Supercapacitors Using Single-Walled Carbon Nanotubes," *Nano Letters,* vol. 9, pp. 1872-1876, 2009/05/13 2009.

[80] J. Kalupson, D. Ma, C. A. Randall, R. Rajagopalan, and K. Adu, "Ultrahigh-Power Flexible Electrochemical Capacitors Using Binder-Free Single-Walled Carbon Nanotube Electrodes and Hydrogel Membranes," *The Journal of Physical Chemistry C,* vol. 118, pp. 2943-2952, 2014/02/13 2014.

[81] K. Kinoshita, "Carbon: electrochemical and physicochemical properties," 1988.

[82] J. H. Kim, K.-W. Nam, S. B. Ma, and K. B. Kim, "Fabrication and electrochemical properties of carbon nanotube film electrodes," *Carbon,* vol. 44, pp. 1963-1968, 2006.

[83] S. W. Lee, B.-S. Kim, S. Chen, Y. Shao-Horn, and P. T. Hammond, "Layer-by-layer assembly of all carbon nanotube ultrathin films for electrochemical applications," *Journal of the American Chemical Society,* vol. 131, pp. 671-679, 2008.

[84] C. Yu, C. Masarapu, J. Rong, B. Wei, and H. Jiang, "Stretchable Supercapacitors Based on Buckled Single-Walled Carbon-Nanotube Macrofilms," *Advanced Materials,* vol. 21, pp. 4793-4797, 2009.

[85] L. Hu, W. Yuan, P. Brochu, G. Gruner, and Q. Pei, "Highly stretchable, conductive, and transparent nanotube thin films," *Applied Physics Letters,* vol. 94, p. 161108, 2009.

[86] T. Yamada, Y. Hayamizu, Y. Yamamoto, Y. Yomogida, A. Izadi-Najafabadi, D. N. Futaba, and K. Hata, "A stretchable carbon nanotube strain sensor for human-motion detection," *Nature nanotechnology,* vol. 6, pp. 296-301, 2011.

[87] K. Liu, Y. Sun, P. Liu, X. Lin, S. Fan, and K. Jiang, "Cross-Stacked Superaligned Carbon Nanotube Films for Transparent and Stretchable Conductors," *Advanced Functional Materials,* vol. 21, pp. 2721-2728, 2011.

[88] S. Hu, R. Rajamani, and X. Yu, "Flexible solid-state paper based carbon nanotube supercapacitor," *Applied Physics Letters,* vol. 100, pp. -, 2012.

[89] T. Chen, H. Peng, M. Durstock, and L. Dai, "High-performance transparent and stretchable all-solid supercapacitors based on highly aligned carbon nanotube sheets," *Scientific reports,* vol. 4, 2014.

[90] Z. Niu, H. Dong, B. Zhu, J. Li, H. H. Hng, W. Zhou, X. Chen, and S. Xie, "Highly Stretchable, Integrated Supercapacitors Based on Single-Walled Carbon Nanotube Films with Continuous Reticulate Architecture," *Advanced Materials,* vol. 25, pp. 1058-1064, 2013.

[91] W. Ma, L. Song, R. Yang, T. Zhang, Y. Zhao, L. Sun, Y. Ren, D. Liu, L. Liu, J. Shen, Z. Zhang, Y. Xiang, W. Zhou, and S. Xie, "Directly Synthesized Strong, Highly Conducting, Transparent Single-Walled Carbon Nanotube Films," *Nano Letters,* vol. 7, pp. 2307-2311, 2007/08/01 2007.

[92] L. Qiu, X. Yang, X. Gou, W. Yang, Z.-F. Ma, G. G. Wallace, and D. Li, "Dispersing Carbon Nanotubes with Graphene Oxide in Water and Synergistic Effects between Graphene Derivatives," *Chemistry – A European Journal,* vol. 16, pp. 10653-10658, 2010.

[93] L. Huang, C. Li, and G. Shi, "High-performance and flexible electrochemical capacitors based on graphene/polymer composite films," *Journal of Materials Chemistry A,* vol. 2, pp. 968-974, 2014.

[94] M. Zhou, Y. Wang, Y. Zhai, J. Zhai, W. Ren, F. Wang, and S. Dong, "Controlled Synthesis of Large-Area and Patterned Electrochemically Reduced Graphene Oxide Films," *Chemistry – A European Journal,* vol. 15, pp. 6116-6120, 2009.

[95] P. Yu, Y. Lin, L. Xiang, L. Su, J. Zhang, and L. Mao, "Molecular Films of Water-Miscible Ionic Liquids Formed on Glassy Carbon Electrodes: Characterization and Electrochemical Applications," *Langmuir,* vol. 21, pp. 9000-9006, 2005/09/01 2005.

[96] A. K. Geim and K. S. Novoselov, "The rise of graphene," *Nature materials,* vol. 6, pp. 183-191, 2007.

[97] M. Kosmulski, R. A. Osteryoung, and M. Ciszkowska, "Diffusion Coefficients of Ferrocene in Composite Materials Containing Ambient Temperature Ionic Liquids," *Journal of The Electrochemical Society,* vol. 147, pp. 1454-1458, April 1, 2000 2000.

[98] J. N. Barisci, G. G. Wallace, D. R. MacFarlane, and R. H. Baughman, "Investigation of ionic liquids as electrolytes for carbon nanotube electrodes," *Electrochemistry Communications,* vol. 6, pp. 22-27, 2004.

[99] J. R. Miller, R. A. Outlaw, and B. C. Holloway, "Graphene Double-Layer Capacitor with ac Line-Filtering Performance," *Science,* vol. 329, pp. 1637-1639, September 24, 2010 2010.

[100] P. L. Taberna, P. Simon, and J. F. Fauvarque "Electrochemical Characteristics and Impedance Spectroscopy Studies of Carbon-Carbon Supercapacitors," *Journal of The Electrochemical Society,* vol. 150, pp. A292-A300, March 1, 2003 2003.

[101] X. Zhao, H. Tian, M. Zhu, K. Tian, J. J. Wang, F. Kang, and R. A. Outlaw, "Carbon nanosheets as the electrode material in supercapacitors," *Journal of Power Sources,* vol. 194, pp. 1208-1212, 2009.

[102] W. Lu, L. Qu, K. Henry, and L. Dai, "High performance electrochemical capacitors from aligned carbon nanotube electrodes and ionic liquid electrolytes," *Journal of Power Sources,* vol. 189, pp. 1270-1277, 2009.

[103] Z. S. Wu, K. Parvez, X. Feng, and K. Müllen, "Graphene-based in-plane micro-supercapacitors with high power and energy densities," *Nature communications,* vol. 4, 2013.

[104] M. D. Stoller, S. Park, Y. Zhu, J. An, and R. S. Ruoff, "Graphene-Based Ultracapacitors," *Nano Letters,* vol. 8, pp. 3498-3502, 2008/10/08 2008.

[105] K. S. Kim, Y. Zhao, H. Jang, S. Y. Lee, J. M. Kim, K. S. Kim, J.-H. Ahn, P. Kim, J.-Y. Choi, and B. H. Hong, "Large-scale pattern growth of graphene films for stretchable transparent electrodes," *Nature,* vol. 457, pp. 706-710, 2009.

[106] M. F. El-Kady, V. Strong, S. Dubin, and R. B. Kaner, "Laser Scribing of High-Performance and Flexible Graphene-Based Electrochemical Capacitors," *Science,* vol. 335, pp. 1326-1330, March 16, 2012 2012.

[107] A. Yu, I. Roes, A. Davies, and Z. Chen, "Ultrathin, transparent, and flexible graphene films for supercapacitor application," *Applied Physics Letters,* vol. 96, pp. -, 2010.

[108] W. S. Hummers and R. E. Offeman, "Preparation of Graphitic Oxide," *Journal of the American Chemical Society,* vol. 80, pp. 1339-1339, 1958/03/01 1958.

[109] S.-H. Bae, Y. Lee, B. K. Sharma, H.-J. Lee, J.-H. Kim, and J.-H. Ahn, "Graphene-based transparent strain sensor," *Carbon,* vol. 51, pp. 236-242, 2013.

[110] S.-K. Lee, B. J. Kim, H. Jang, S. C. Yoon, C. Lee, B. H. Hong, J. A. Rogers, J. H. Cho, and J.-H. Ahn, "Stretchable Graphene Transistors with Printed Dielectrics and Gate Electrodes," *Nano Letters,* vol. 11, pp. 4642-4646, 2011/11/09 2011.

[111] X. Li and B. Wei, "Supercapacitors based on nanostructured carbon," *Nano Energy,* vol. 2, pp. 159-173, 2013.

[112] H. Nishide and K. Oyaizu, "Toward Flexible Batteries," *Science,* vol. 319, pp. 737-738, February 8, 2008 2008.

[113] A. S. Aricò, P. Bruce, B. Scrosati, J.-M. Tarascon, and W. Van Schalkwijk, "Nanostructured materials for advanced energy conversion and storage devices," *Nature materials,* vol. 4, pp. 366-377, 2005.

[114] R. Kötz and M. Carlen, "Principles and applications of electrochemical capacitors," *Electrochimica Acta,* vol. 45, pp. 2483-2498, 2000.

[115] B. E. Conway, "Electrochemical supercapacitors," 1999.

[116] P. E. Trapa, Y.-Y. Won, S. C. Mui, E. A. Olivetti, B. Huang, D. R. Sadoway, A. M. Mayes, and S. Dallek, "Rubbery Graft Copolymer Electrolytes for Solid-State, Thin-Film Lithium Batteries," *Journal of The Electrochemical Society,* vol. 152, pp. A1-A5, January 1, 2005 2005.

[117] S. Saricilar, D. Antiohos, K. Shu, P. G. Whitten, K. Wagner, C. Wang, and G. G. Wallace, "High strain stretchable solid electrolytes," *Electrochemistry Communications,* vol. 32, pp. 47-50, 2013.

[118] L. Yuan, X.-H. Lu, X. Xiao, T. Zhai, J. Dai, F. Zhang, B. Hu, X. Wang, L. Gong, J. Chen, C. Hu, Y. Tong, J. Zhou, and Z. L. Wang, "Flexible Solid-State Supercapacitors Based on Carbon Nanoparticles/MnO2 Nanorods Hybrid Structure," *ACS Nano,* vol. 6, pp. 656-661, 2012/01/24 2011.

[119] C. Meng, C. Liu, L. Chen, C. Hu, and S. Fan, "Highly Flexible and All-Solid-State Paperlike Polymer Supercapacitors," *Nano Letters,* vol. 10, pp. 4025-4031, 2010/10/13 2010.

CHAPTER 2

GENERAL EXPERIMENTAL

2 INRODUCTION

General experimental techniques, materials and instrumental details used in this thesis are described in this chapter. The specific experimental procedure is presented in the experimental section of each chapter. All of the measurements are carried out at room temperature.

2.1 CHEMICAL AND REAGENTS

HiPCO Single-wall carbon nanotubes (SWCNTs) were purchased from Carbon Nanotechnologies, Inc (Houston, TX). N, N-Dimethylformamide (DMF) (AR grade), concentrated nitric acid (70%) and sodium sulfate (Na_2SO_4) (AR grade) were obtained from Sigma- Aldrich and used as received. The liquid latex was purchased from AA Rubber and Seals. Pty, Ltd (Belmore, NSW, Australia). Graphite powder was obtained from Bay Carbon. Milli-Q water with a resistivity of 18.2 $m\Omega\ cm^{-1}$ was used in all preparations. Potassium permanganate, phosphorous pentaoxide, hydrazine hydrate, triethylamine were sourced from Sigma-Aldrich. Ammonia solution in water (28%) was sourced from Labtech and used as received. Medical grade polyurethane (PU) was purchased from Advan Source Biomaterials Corp. and used as a stretchable substrate. 1M Sulfuric acid (H_2SO_4) (Sigma- Aldrich) was used as electrolyte to measure the electrochemical properties of the stretchable electrode. Polycaprolactone (M_W = 80,000) was sourced from Sigma-Aldrich and used as received. Polyvinyl alcohol (PVA) (M_W = 124,000-186,000 g mol^{-1}) was obtained from Sigma-Aldrich.

Orthophosphoric acid (85%) and acetonitrile were purchased from Ajax Fine chemicals.

2.2 PHYSICL CHARACTERIZATION AND INSTRUMENTATION

The characterization techniques and employed instrumentation are depicted in this chapter. Physical characterization of synthesized materials is studied by Raman spectroscopy, scanning electron microscopy (SEM), x-ray photo-electron spectroscopy (XPS), x-ray diffraction (XRD), fourier transform infrared spectroscopy (FTIR), sputter coater, ultra-sonication and four-point probe. Raman spectroscopy is used to evaluate the vibrational, rotational and low frequency mode of diverse prepared materials. XPS is able to assess quantity of the oxygen and carbon component before and after reduction. XRD is used to realize the crystallinity of the structure. FTIR is employed in order to obtain an infrared spectrum of absorption, emission and photoconductivity of the synthesized materials. Sputter coater is used to create current collector on the substrate by coating with gold. Probe type ultra-sonication is employed to maximize dispersability of the rGO, SWCNTs and rGO/SWCNTs dispersion.

2.2.1 Raman spectroscopy

Raman spectroscopy is a powerful tool to obtain quantitative and qualitative information of SWCNTs or graphene regarding electronic structure, purity, crystallinity, diameter, metallic and semiconducting property [1]. Raman spectroscopy is the most widely used technique to investigate vibrational, rotational and other low frequency modes in a sample. The sample in an exposing monochromatic light with an electron which makes a real transition to the higher

energy level, where the electrons interact with phonon in advance of electronic ground state [2] Raman spectroscopy also is based on the inelastic scattering of photons by the samples (Figure 2.1).

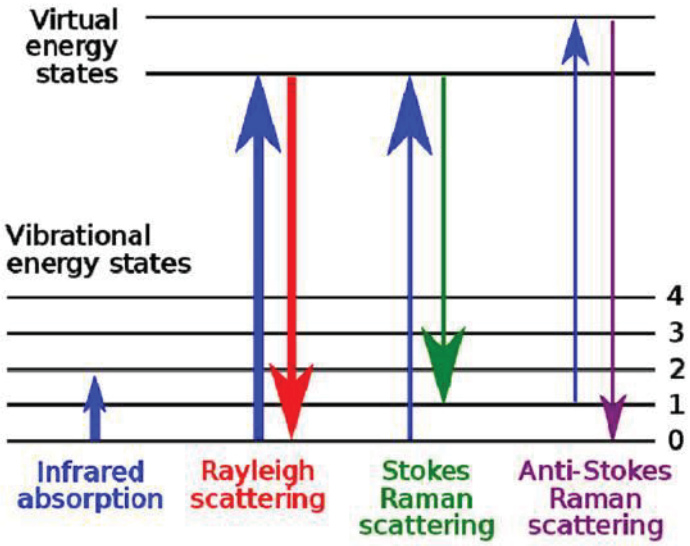

Figure 2.1 Schematic of the vibrational energy level diagram in the Raman spectroscopy [2].

In this thesis, the Raman spectroscopy was carried out using a Jobin-Yvon Horbia 800 Raman spectrometer equipped with a visible Raman microscope as Olympus BX41 and CCD detector. The excitation wavelength was 632.81 nm and spectra are obtained over 30 s at 1.0 cm^{-1} resolution.

2.2.2 Scanning electron microscopy (SEM)

Scanning electron microscopy is a type of electron microscope, which can provide information on elemental composition, electronic structure with sensitive single atom and surface topography. The SEM works by generating a focused beam of electrons from a probe which is scanned over the conducting specimen with collecting a signal to form an image. A constant current is retained by a feedback system while scanning

the specimen [3]. The various signals are detected by electrons interaction between the specimen and probe.

In this thesis, all of the rGO and SWCNTs based materials have enough conductivity to avoid electrostatic charge accumulation while probe scan. All the surface morphologies of the samples studied without metal coating on the surface. SEM images were obtained by a JEOL-7500FA field emission SEM with 5.0 kV accelerating voltage and 10 μA emission current.

2.2.3 X-ray photo-electron spectroscopy (XPS)

X-ray photo-electron spectroscopy (XPS) is a type of quantitative surface analysis technique used for elemental analysis of samples. The photoelectrons are emitted from the surface of the sample by irradiation with mono-energetic x-ray (Figure 2.2).

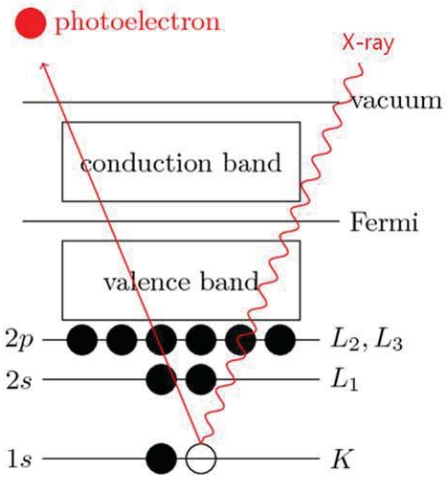

Figure 2.2 Principle of the X-ray photo-electron spectroscopy (XPS) [4].

An electron energy analyzer detects the binding energy of the photoelectrons. The binding energy of the peaks is characteristic of each element. The peaks can be used

to determine elemental identity, chemical state and composition of the materials surface. The XPS technique has been widely used in many industrial fields such as corrosion, polymer surface modification, dielectric material, electronics packaging, semiconductor, thin film coating and magnetic media [4].

The XPS is carried out using a PHOIBOS 100 hemispherical energy analyzer from SPECS with Al, Kα radiation (1486.6 eV) on fixed analyzer transmission mode.

2.2.4 X-ray diffraction (XRD)

The X-ray is a useful to study in structure determination of crystalline materials. X-ray is an electromagnetic radiation which has a wavelength in the range from 0.01 to 10 nanometers. In XRD, the x-ray beam is incident on a surface of a crystalline material, interacting with the atomic planes of a crystal [5]. The diffracted x-ray beam by the interaction with the crystalline structure is defined 2θ angle to the incident beam as presented in Figure 2.3a [5]. The unique diffraction patterns are figured out from the element, which is able to be assessed structure of the different materials. XRD was performed on a GBC MMA XRD using a Cu x-rays. Spectra were obtained in a range of $5^{o} \sim 40^{o}$ angles with 1^{o}/min of scan rate.

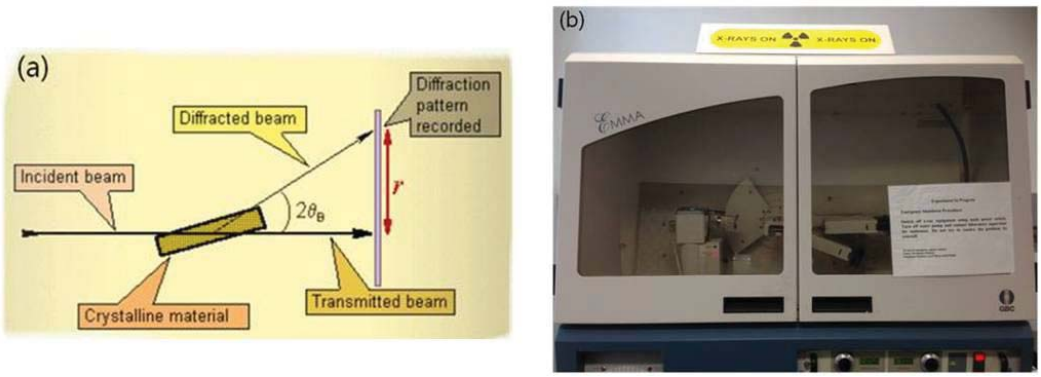

Figure 2.3 (a) Illustration of the X-ray diffraction by a crystalline material [5], (b) Photograph of the GBC MMA XRD instrumental.

2.2.5 Fourier Transform Infrared spectroscopy (FTIR)

Fourier Transform Infrared spectroscopy (FTIR) is concerned with the interaction between light and vibrational motion of the covalent bonding of molecules and lattice vibrations of ionic crystals. FTIR has been widely used to investigate qualitative and quantitative information on the nature of chemical bonding and chemical lattice from transmitted, reflected or scattered Infrared (IR) radiation [6]. The interaction energy corresponds to the IR light which has wavelength ranging 10 to 15,000 cm^{-1}. In the FTIR system, IR radiation is introduced to a scanning interferometer and the output radiation intensity on the function of time is decoded to frequency and intensity information by Fourier transformation. The fundamental design of the interferometer is presented in Figure 2.4.

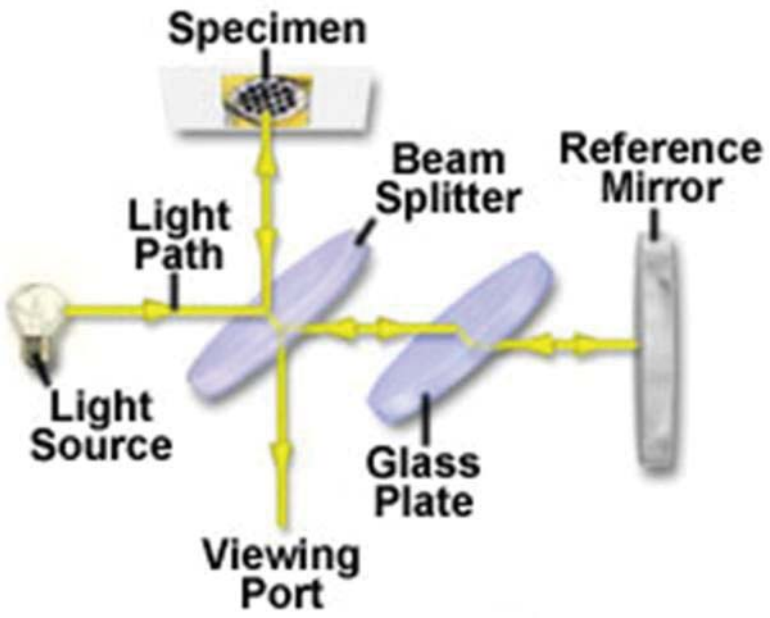

Figure 2.4 Principle of the interferometer [6].

A beam emitted from the light source is divided into two beams of equal intensity by a beam splitter, the transmitted beam and reflected beam. The two beams reflected by reference mirror and specimen surface, respectively. The light produced by reflection of the two beams is then made to interfere. The interference between the image of the reference mirror and specimen surface observed on the viewing port. Since the light waves reflected by the specimen and reference mirror derive from the splitting of a beam by the light source, these waves are mutually coherent and thus a two-beam interference pattern is obtained [6]. The FTIR spectroscopy was carried out using a Shimadzu IR Prestige-21 FTIR spectrophotometer with single reflection HATR accessories (Miracle, Pike Technologies). The scanning range of the experiment was 1000 – 4000 cm^{-1} on transmittance mode with 30 scans and 8.0 resolutions.

2.2.6 Sputter coater

Sputter coating is conducted using a Edwards Sputter Coater AUTO306. The sputter coating of gold (Au) onto stretchable substrate as latex, polyurethane (PU) and polycaprolactone (PCL) was carried out to minimize equivalent series resistance (ESR) between active material and substrate, while improvement of charge storage and current collecting capability.

2.2.7 Probe type ultra-sonication

The probe type of ultra-sonication (Branson Digital Sonifier Model 102C at 450 W, 20 Hz in pulsed method, 2 seconds on and 1 second off) is employed to create a stable SWCNTs, rGO and rGO/SWCNTs composite dispersion. The sonication time and amplitude for each dispersion are described in the specific chapter.

2.2.8 Electrical conductivity measurement (4-point-probe)

The electrical conductivity (S/cm) or surface resistance measurement of nanocarbon based materials including rGO, SWCNTs and rGO/SWCNTs composite film is performed by JANDEL RM3four-point probe (Jandel Engineering Ltd, UK). The electrical resistivity could be expressed as [7];

$$\rho = K\,(V/I) * t \quad \text{Eq. (1)}$$

whereas, ρ is the electrical resistivity of the nanocarbon materials based film, K is a geometric factor (K = 4.5324), V is the electric potential across the two inner probes, I is the applied current and *t* is the thickness of the film (cm). The electrical conductivity of the SWCNTs film is calculated by following equation;

$$\sigma = 1/\rho \quad \text{Eq. (2)}$$

The schematic diagram of the four-point probe is presented in the Figure 2.5.

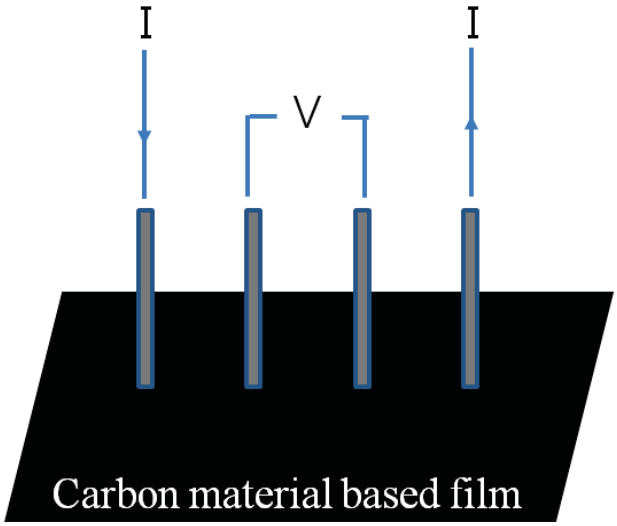

Figure 2.5 Schematic diagram of the four-point probe configuration.

2.2.9 Spray coating

Many technique such as ink-jet printing [8], dip coating [9, 10], vacuum filtration [11, 12] have developed to fabricate nanocarbon base conductive films. Even though these techniques have been used to prepare nanocarbon base films, they present practical challenges for scale up of industrial applications and are time consuming to fabricate thick film with high quality over large areas. Spray coating technique is widely used for industrial applications including, vehicle body painting, industrial coating and graffiti artists. In order to obtain optimal spray coating conditions, main parameters of the spray coating process should be considered including gas flow property, feed rate, working distance, nozzle design, amount of sprayed dispersion and concentration of dispersion.

In this thesis, flexicoat industrial spray coating system with AccuMist atomizing nozzle from Sono-Tek (Figure 2.6) has conducted to fabricate nanocarbon base conductive films. Spray coating technique was able to fabricate conductive single-wall carbon nanotubes (SWCNTs), reduced graphene oxide (rGO) and rGO/SWCNTs composite film with high electrochemical and endurable performances on the stretchable and flexible substrate. All of the employed spraying parameters for preparing stretchable and flexible electrode will be outlined in the each chapter.

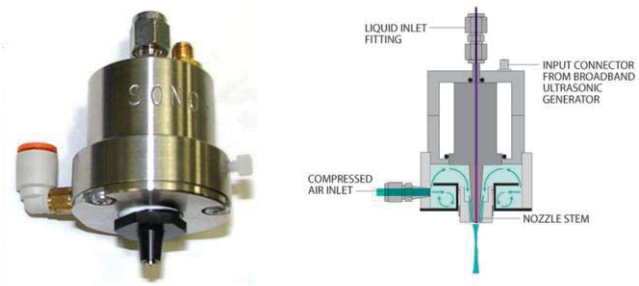

Figure 2.6 AccuMist Ultrasonic Nozzle.

2.3 ELECTROCHEMISTRY

Electrochemistry is a study on the chemical response of an electrode to electrical stimulation. The redox reaction of the material can be obtained from the electrochemical analysis, which is able to provide information of the material including kinetics, concentration, reaction mechanism and other behavior at electrode surface. The electrochemical analysis techniques such as cyclic voltammetry (CV), galvanostatic charge/discharge (GCD) and electrochemical impedance spectroscopy (EIS) are employed in order to characterize the reproducible performance of the electrode or device under various conditions.

2.3.1 Cyclic voltammetry (CV)

Cyclic voltammetry (CV) is an excellent technique to characterize electrochemical system. The CV is concerned with current response between electrodes (two working electrode in the case of full device or one working electrode in the case of three-electrode system) by applying potential (Figure 2.7).

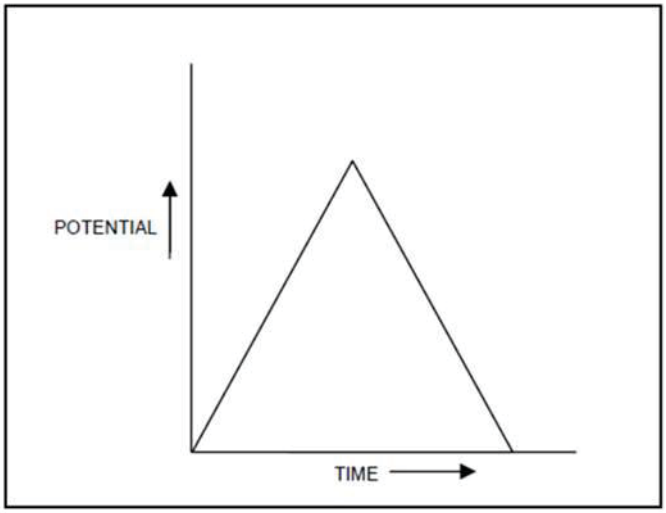

Figure 2.7 Typical triangular potential waveform for cyclic voltammetry.

The CV graph can provide electrochemical information of a material including capacitive properties and electrochemical active surface area for a given electrolyte. In the case of non-faradaic process (no redox reaction between electrode and electrolyte), CV will be illustrated sharp charging and discharging behaviour and rectangular current response (Figure 2.8a).

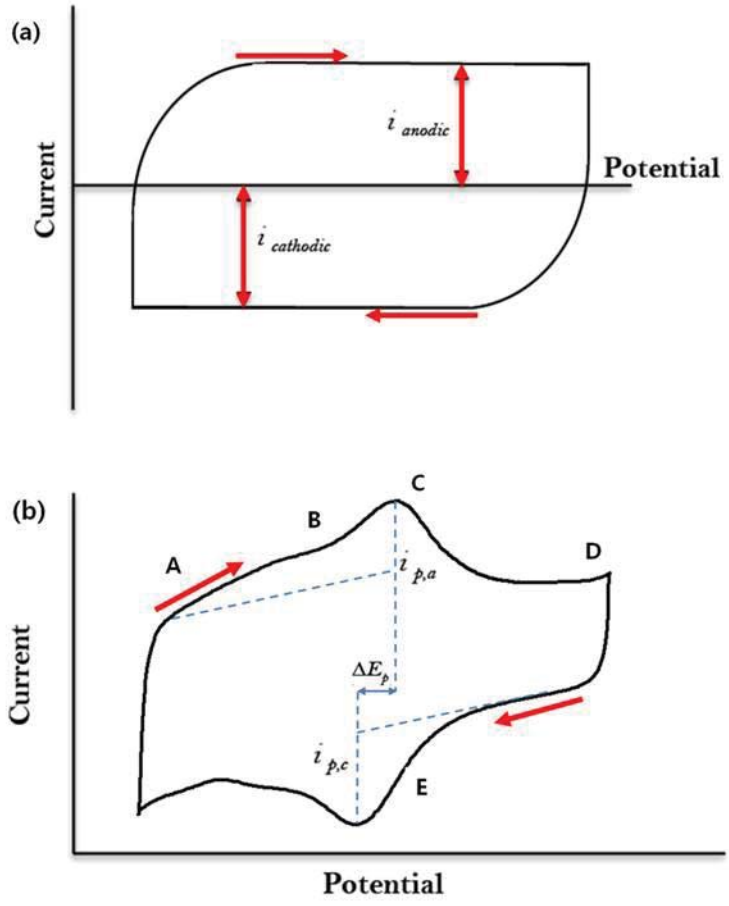

Figure 2.8 (a) Cyclic voltammetry (CV) of a typical non-faradaic response, and (b) CV of graphene/carbon nanotube composite electrode showing a Faradaic response.

The CV normally generates noticeable redox peaks associated with oxidation and reduction when a redox active species is occurred between electrolyte-electrode

interfaces (Figure 2.8b). At the point A, the initial potential is more negative than the formal potential redox species with non-Faradaic currents flow. The potential sweep reaches to the formal redox species, Faradaic current begins flow with oxidation at the electrode surface (point B). At the point C, the system is oxidizing the redox species, this process is limited by the diffusion rate of the redox species in electrolyte to the electrode surface. Point D exhibits the potential at which scan is reversed and oxidized species generated in the previous scan stats to reduction as the scan approaches the formal potential of the redox couple (point E). The oxidation and reduction peaks should be generated identical peak width, height and overall shape for a highly reversible redox system, and also indicated sufficient electron transfer between the electrolyte and electrode.

In this thesis, the CV measurements of the various carbon based electrode were carried out in room temperature with a two or three-electrode system using an electrochemical analyzer (EDAQ Australia) and EChem V2 software (ADI Instruments Pty. Ltd). In the case of the three-electrode system, the carbon based electrode is used as the working electrode with Ag/AgCl (3M NaCl) aqueous solution as the reference electrode and Pt mesh as a counter electrode with approximately 1.8 cm^2 area. For three-electrode system, the specific capacitance values were calculated as following equation [13]:

$$C_{sp} = \int_{E1}^{E2} \mathrm{i}\,(\mathrm{E})dE \;/\; 2(E2 - E1)\, mv \qquad \text{Eq. (3)}$$

where C_{sp} is the specific capacitance of the individual electrode, *E1* and *E2* are the cutoff potentials in CV measurements, *i(E)* is the instantaneous current, *E2 – E1* is the potential window width, *m* is the mass of active material, *v* is the potential scan rate

and $\int_{E1}^{E2} \mathrm{i}\,(\mathrm{E})dE$ is the total voltammetric charge obtained by integration of the positive and negative sweep in the CV measurements. The energy and power density of the electrode is calculated according to the following equation:

$$E = \frac{1}{2} C_{sp} V^2; P = \frac{E}{t} \qquad \text{Eq. (4)}$$

where C_{sp} is the specific capacitance of the electrode, V is the operating voltage and t is the sweep time.

2.3.2 Electrochemical impedance spectroscopy (EIS)

Ohm's law describes resistance (R) in the ratio between voltage (E) and current (I) according to equation 5. However, there is a limitation to define an ideal resistor in terms of circuit elements show more complex behavior in the real world.

$$R = \frac{E}{I} \quad \text{Eq. (5)}$$

Resistance and impedance are similar by measuring ability of circuit to resist the electrical current flow. Electrochemical impedance spectroscopy (EIS) is an electrochemical analysis technique which is the response of electrode to AC signals with different frequencies. The current response to a sinusoidal potential will be a sinusoid at the same frequency in shifted phase (Figure 2.9). Changes in the phase shift at different frequencies give data relate to electrochemical process within the electrochemical device or cell. EIS is able to differentiate between electrode and resistive response and solution capacitive by the phase shift and the magnitude of the current response at different time [14, 15].

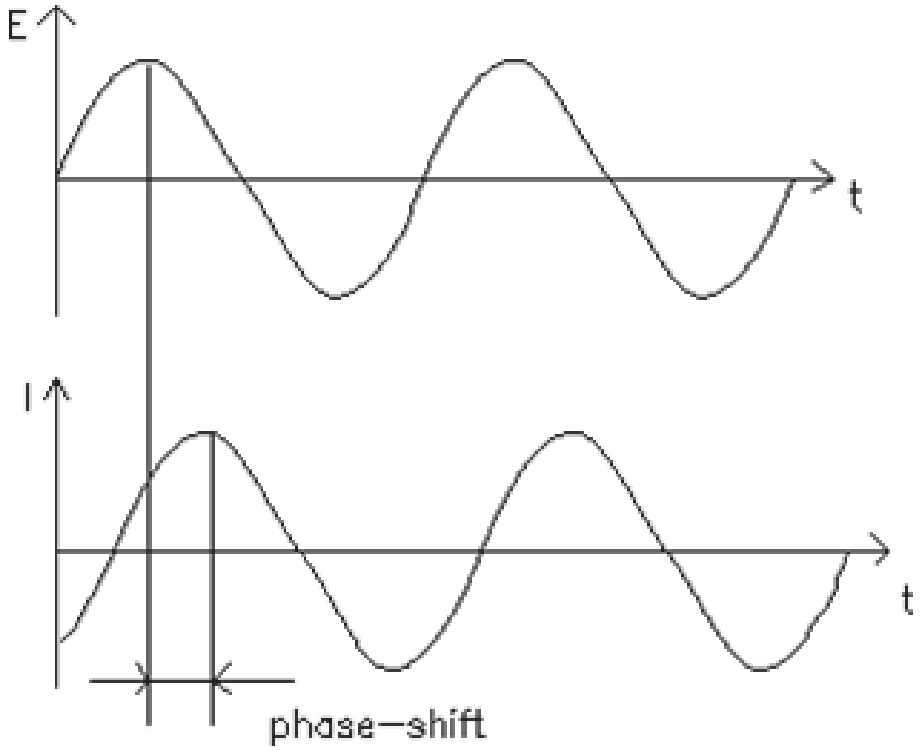

Figure 2.9 Sinusoidal current response in a linear system [16].

However, the data from EIS requires equivalent circuit models to understand of the obtained data. Nyquist plot is a resulting data which plots the real (x-axis) and imaginary (y-axis) part with each point on the impedance plot at one frequency (Figure 2.10). The first point (R_1) on the x-axis is measure of the solution resistance and the next intercept (R_2) indicating the charge transfer resistance (R_{ct}) which is calculated by the difference between two intercepts ($R_{ct} = R_2 - R_1$). The specific value used for EIS will be presented in the each chapter.

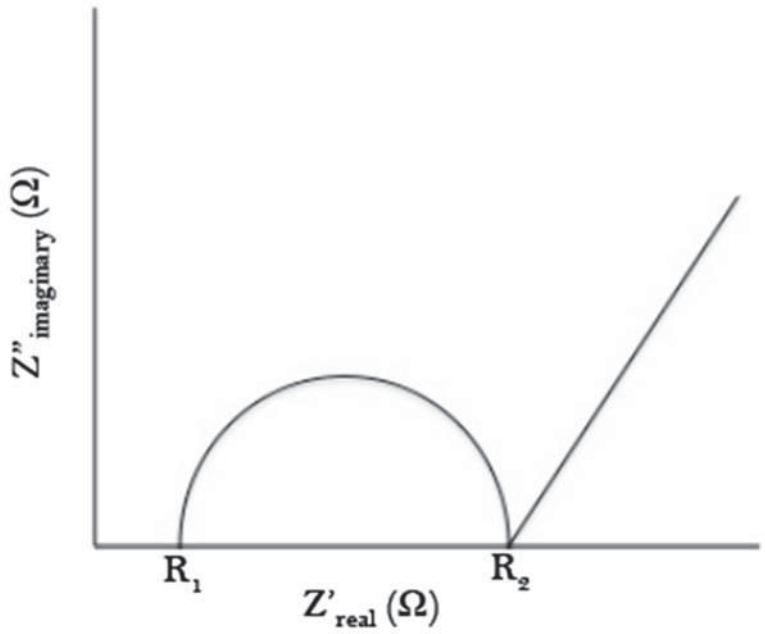

Figure 2.10 Schematic of a typical Nyquist plot.

In this thesis, EIS is used to probe the electrical double layer effects at the electrode/electrolyte interface. All of the EIS measurements are performed at room temperature using a Gamry EIS 3000^{TM} system (Gamry, USA) where the frequency range spanned 100 kHz to 0.01 Hz with an amplitude of 10mV (rms) at open circuit potential. The equivalent circuit values of all samples are obtained by ZView^{TM} V 3.2, Scribner Associates.

In the case of the three-electrode system, the carbon based electrode is used as the working electrode with Ag/AgCl (3M NaCl) aqueous solution as the reference electrode and Pt mesh as a counter electrode with approximately 1.8 cm^2 area. All of the working electrodes are immersed in the aqueous electrolyte for 10 minutes with open circuit monitoring to ensure the stability of the electrode in the electrolyte. In the

case of two-electrode system, the two carbon based electrodes are used as the positive and negative electrode with application of polymer based gel electrolyte.

2.3.3 Galvanostatic charge/discharge

The Galvanostatic charge/discharge tests are performed to evaluate long-term stability of the device using a battery test system (Neware electronic Co.) with V.5.0 software. The potential window is applied between either 0 V and 1.0 V or 0 V and 0.8 V depending on the electrolyte and type of device (details are in each chapter). Specific capacitance (C_{sp}) of the device for two-electrode system is calculated from the Galvanostatic charge-discharge curves on the basis of the equation 5 [17]:

$$C_{sp} = 2(I\Delta t) / (m\Delta V) \quad \text{Eq. (5)}$$

where, I is the discharge current, Δt is the time for a full discharge, m is the total mass of the active material on single electrode and ΔV represents the potential change after a full discharge.

2.4 FABRICATION OF ELECTRODES

See details in chapters.

2.5 FABRICATION OF FULL DEVICES

See details in chapters.

2.6 REFERENCES

[1] M. S. Dresselhaus, G. Dresselhaus, R. Saito, and A. Jorio, "Raman spectroscopy of carbon nanotubes," *Physics Reports,* vol. 409, pp. 47-99, 2005.

[2] R. K. Saini, I. W. Chiang, H. Peng, R. E. Smalley, W. E. Billups, R. H. Hauge, and J. L. Margrave, "Covalent Sidewall Functionalization of Single Wall Carbon Nanotubes," *Journal of the American Chemical Society,* vol. 125, pp. 3617-3621, 2003/03/01 2003.

[3] P. A. Tipler and R. Llewellyn, *Modern physics*: Macmillan, 2003.

[4] P. van der Heide, *X-Ray Photoelectron Spectroscopy : An Introduction to Principles and Practices*. Hoboken, NJ, USA: Wiley, 2011.

[5] B. E. Warren, *X-ray Diffraction*: Courier Dover Publications, 1969.

[6] P. R. Griffiths and J. A. De Haseth, *Fourier Transform Infrared Spectrometry*: Wiley, 2007.

[7] A. P. Schuetze, A. P. Schuetze, W. Lewis, C. Brown, and W. J. Geerts, "A laboratory on the four-point probe technique," *American journal of physics,* vol. 72, pp. 149-153, 2004.

[8] K. Kordás, T. Mustonen, G. Tóth, H. Jantunen, M. Lajunen, C. Soldano, S. Talapatra, S. Kar, R. Vajtai, and P. M. Ajayan, "Inkjet Printing of Electrically Conductive Patterns of Carbon Nanotubes," *Small,* vol. 2, pp. 1021-1025, 2006.

[9] M. H. Kim, J. Y. Choi, H. K. Choi, S. M. Yoon, O. O. Park, D. K. Yi, S. J. Choi, and H. J. Shin, "Carbon Nanotube Network Structuring Using Two-Dimensional Colloidal Crystal Templates," *Advanced Materials,* vol. 20, pp. 457-461, 2008.

[10] M. H. A. Ng, L. T. Hartadi, H. Tan, and C. H. P. Poa, "Efficient coating of transparent and conductive carbon nanotube thin films on plastic substrates," *Nanotechnology,* vol. 19, p. 205703, 2008.

[11] Z. Wu, Z. Chen, X. Du, J. M. Logan, J. Sippel, M. Nikolou, K. Kamaras, J. R. Reynolds, D. B. Tanner, A. F. Hebard, and A. G. Rinzler, "Transparent, Conductive Carbon Nanotube Films," *Science,* vol. 305, pp. 1273-1276, August 27, 2004 2004.

[12] A. A. Green and M. C. Hersam, "Colored Semitransparent Conductive Coatings Consisting of Monodisperse Metallic Single-Walled Carbon Nanotubes," *Nano Letters,* vol. 8, pp. 1417-1422, 2008/05/01 2008.

[13] M. A. Azam, K. Isomura, A. Fujiwara, and T. Shimoda, "Direct growth of vertically aligned single-walled carbon nanotubes on conducting substrate and its electrochemical performance in ionic liquids," *physica status solidi (a),* vol. 209, pp. 2260-2266, 2012.

[14] G. Li and P. G. Pickup, "Measurement of single electrode potentials and impedances in hydrogen and direct methanol PEM fuel cells," *Electrochimica Acta,* vol. 49, pp. 4119-4126, 2004.

[15] A. A. Franco, P. Schott, C. Jallut, and B. Maschke, "A dynamic mechanistic model of an electrochemical interface," *Journal of The Electrochemical Society,* vol. 153, pp. A1053-A1061, 2006.

[16] J. R. Macdonald and E. Barsoukov, "Impedance spectroscopy: theory, experiment, and applications," *History,* vol. 1, p. 8, 2005.

[17] Y. Xu, Z. Lin, X. Huang, Y. Liu, Y. Huang, and X. Duan, "Flexible solid-state supercapacitors based on three-dimensional graphene hydrogel films," *ACS nano,* vol. 7, pp. 4042-4049, 2013.

CHAPTER 3

CAPACITIVE BEHAVIOUR OF LATEX/SINGLE-WALL CARBON NANOTUBES ELECTRODES

3.1 INTRODUCTION

The development of novel energy storage devices is of great significance for applications in wearable electronics [1-3]. Amongst the diverse range of energy storage devices available, electrochemical capacitors (ECs) are promising candidates due to their high power density, long life, durability and safety. Such characteristics are desirable for various applications, including high performance sportswear, wearable displays and embedded health monitoring devices [4, 5]. Developing technologies such as foldable displays [6], functional electronic eyes [7], transistors [8] and photovoltaic devices [9] also require the continued development of stretchable electrodes. These applications demand power systems with high capacitance, but also require the material to be highly flexible and stretchable [10, 11]. Two types of ECs, which store charge by electrochemical means, have been developed. The first is the electrochemical double layer capacitor (EDLC) which, instead of having two plates separated by a thick insulator, is based on the operating principle of an electrical double layer that is formed at the interface between an electrode and electrolyte [1, 4]. The second type is based on Faradaic pseudo-capacitance where charge is transferred at the surface or in the bulk near the surface of the solid electrode materials [3, 5] .

Various materials have been used as substrates for stretchable conductors. These include silicone rubber, polydimethylsiloxane (PDMS), nitrile-butadiene rubber (NBR), natural-latex rubber, polyurethane (PU) and cotton [12-17]. Among the

polymers available, latex rubber is widely available, inexpensive, non-toxic, eco-friendly, highly stretchable and easily processed. Most work to date using latex has focused on sensors and actuators. Kros *et al*. [18] have developed a biosensor based on a polypyrrole/latex composite, while Jung Woo *et al*. [19] have reported a micro-actuator using latex rubber as a membrane. To our knowledge there have been no studies for the capacitive behaviour of SWCNTs coated onto latex rubber as a stretchable substrate.

Single-wall carbon nanotubes (SWCNTs) are highly suitable for preparation of high performance electrochemical supercapacitors due to their high electrical conductivity, thermal and chemical stability and large surface area [20]. In addition, SWCNTs possess high flexibility, low mass density and large aspect ratio (typically >1000), enabling them to maintain conductive pathways by bridging cracked regions under large strain [21-23]. However, a major problem of pristine SWCNTs is aggregation due to van der Waals force, which results in poor dispersability of pristine SWCNTs in most solvents. In order to overcome this issue, acid treatment has been used to improve dispersability and capacitance values of SWCNTs in fabricating supercapacitors [24]. Acid treatment using strong acids, including nitric and sulfuric acid, can introduce oxygen containing functional groups such as carboxylic (-COOH) and hydroxyl (-OH) groups on the surface of SWCNTs. -COOH groups on SWCNTs can enhance surface wettability of SWCNTs to improve ionic conductivity between the electro-electrolyte interface. These functional groups also offer more available sites to enable physisorption of free electrolyte ions. Previous reports have indicated that nitric acid treatment can significantly improve capacitance values of the carbon nanotubes (CNTs) based capacitors [25, 26]. Initial studies of electrochemical

capacitors with SWCNTs electrodes [27, 28], reported significant increases in electrochemical performances [29-33]. Lee *et al*. [34] have reported supercapacitors fabricated from SWCNTs grown by arc discharge and mixed with poly(vinylidene dichloride) as a binder and then dissolved in tetrahydrofuran. They reported a maximum specific capacitance of 180 F g^{-1} and power density of 20 KW kg^{-1} at an energy density of 6.5 Wh kg^{-1} in 7.5N potassium hydroxide (KOH) electrolyte. Pushparaj *et al*. [2] used nanoporous cellulose composite paper embedded with aligned multi-wall carbon nanotubes (MWCNTs) electrodes to improve energy density to 13 Wh kg^{-1} with specific capacitance of 36 F g^{-1} and power density of 1.5 Wh kg^{-1}. Yu *et al*. [11] have reported a stretchable supercapacitor based on buckled SWCNTs macro-films on poly(dimethylsiloxane) (PDMS) that has a maximum specific capacitance of 54 F g^{-1} and power density of 0.5 KW kg^{-1} at 4.2 Wh kg^{-1} energy density. The buckled SWCNTs films could stretch up to 30% strain.

Established methods for the preparation of carbon nanotube films include vacuum filtration [35, 36], dip coating [37, 38], ink-jet printing [39] and electro-spray deposition [40]. Even though the vacuum filtration method has been widely used to fabricate CNTs films (bucky paper), this method presents practical challenges for scale up of industrial applications and is limited to deposition on porous substrates [38]. Dip and spin coating methods allow the preparation of CNTs films on various substrates at the laboratory scale, but are time consuming when thicker films are required and limited by lack of control of film quality over large areas [35].

In this chapter, we report on the preparation of a flexible and stretchable electrode using a simple and inexpensive spray coating technique, which is potentially applicable at an industrial scale. Functionalised (carboxylated) single-wall carbon

nanotubes (SWCNTs) were sprayed onto gold coated latex to create an electrode that displays practically useful electronic properties even after repeated stretching to 100% strain. This is demonstrated through characterization of their electrochemical properties such as changes in specific capacitance under varying mechanical stress and strain. We also describe the surface morphology of SWCNTs films on the latex substrate with respect to the capacitance of the stretchable electrode.

3.2 EXPERIMENTAL SECTION

3.2.1 Materials

Single-wall carbon nanotubes (SWCNTs) were purchased from Carbon Nanotechnologies, Inc (Houston, TX). N, N-Dimethylformamide (AR grade), concentrated nitric acid (70%) and sodium sulfate (AR grade) were obtained from Sigma-Aldrich and used as received. The liquid latex was purchased from AA Rubber and Seals. Pty, Ltd (Belmore, NSW, Australia).

3.2.2 Purification and functionalization of the SWCNTs

Metallic oxides were removed from the pristine SWCNTs by nitric acid treatment. Approximately 200 mg of the SWCNTs were refluxed in 40 mL 5 M nitric acid for 6 hours, then filtered through a polytetrafluoroethylene-coated polypropylene filter (0.2 μm) and rinsed with deionized water. The sample was freeze dried for 2 days [41].

3.2.3 Preparation of the SWCNTs coated stretchable electrode

3.2.3.1 Gold modified latex substrate

A suitable amount of natural liquid latex (with ammonia to prevent bacteria spoilage) was poured into a glass mold (30cm x 5cm x 1mm) and then allowed to dry at room

temperature for 24 hrs. To fabricate the electrode, a section of the latex film (1cm x 5cm x 1mm) was transferred to a glass microscope slide, stretched to introduce a 100% uniaxial pre-strain and then held under tension using double-sided adhesive tape. After stretching, a 150 nm thick layer of gold was coated onto the dried latex film by sputter coating (Edwards Sputter Coater AUTO306, BOC Ltd, United Kingdom), allowing it to be used as a current collector.

3.2.3.2 Preparation of the SWCNTs dispersion

Acid treated SWCNTs (5mg) were mixed with 10mL DMF, then ultrasonicated (Sonics Vibracell ultrasonic processor, 500 watt, 30% amplitude, USA) for 1 hr to create a stable dispersion.

3.2.3.3 Spray coating onto the gold modified latex substrate

Figure 3.1 illustrates the procedure used to prepare the stretchable latex/SWCNTs electrode via spray coating. The latex film (1cm x 5cm x 1mm) is transferred to a glass microscope slide (step 1), stretched to introduce a 100% uniaxial pre-strain and then held under tension using double-sided adhesive tape (step 2). 150 nm of gold is then coated onto the latex film as a current collector (step 3). A hotplate is covered with aluminium foil and the sample/slide assembly was fixed horizontally to the centre of the foil with adhesive tape. Once the hotplate is stabilized at 80°C, the assembly is coated with the SWCNTs dispersion using a small airbrush (Bunnings, Australia) with a nozzle diameter of approximately 1 mm (step 4).

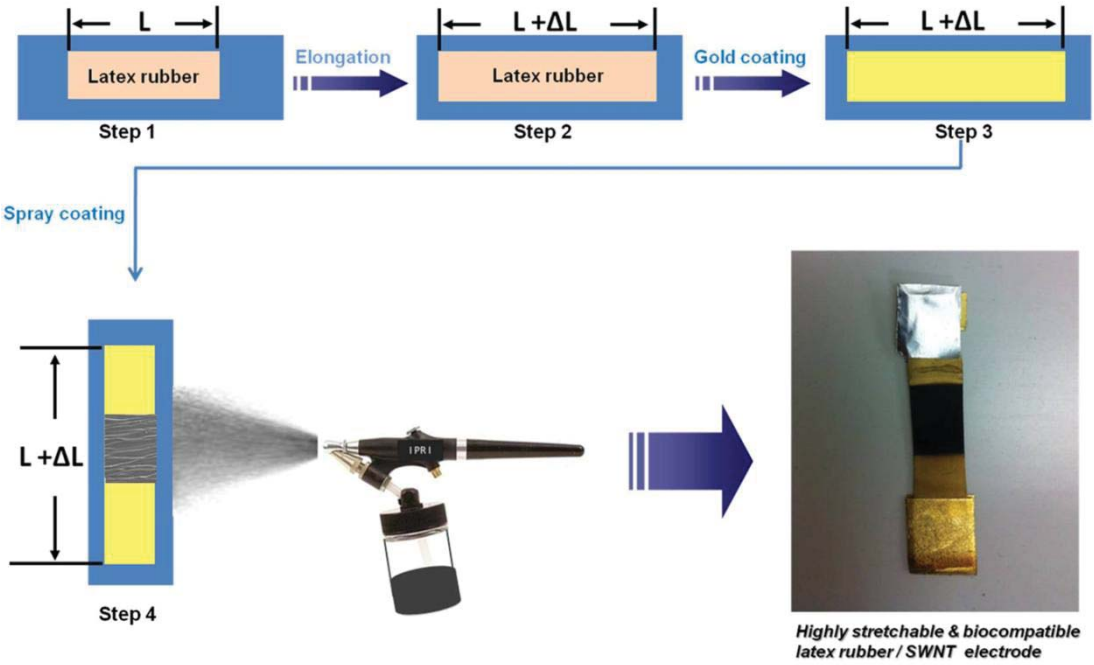

Figure 3.1 Scheme of the stretchable latex/SWCNTs electrode via spray coating technique.

An air pressure of 50 psi was applied and the liquid feed rate is adjusted at the nozzle to approximately 0.15 mL/min. Spraying is performed manually at a distance of 10-15 cm from the latex substrate. Many thin coats are applied, allowing a few seconds for drying between coats, until the entire 10 mL suspension is exhausted. After spray coating, the latex/SWCNTs film is dried in an oven at 120 ^{o}C for 30 min to evaporate residual solvent.

3.3 CHARACTERIZATIONS

3.3.1 Cyclic Voltammetry (CV)

Cyclic Voltammetry (CV) measurements of the latex/SWCNTs electrodes were performed at room temperature with a three electrode system using an electrochemical analyzer (EDAQ Australia) and EChem V2 software (ADI Instruments Pty. Ltd). In all cases, the latex/SWCNTs electrode was used as the working electrode with Ag/AgCl (3M NaCl) aqueous solution as the reference electrode and Pt mesh as a counter electrode. All of the CV measurements were recorded in 1M Na_2SO_4 (aq) under 0 to 100% strain and after 50 and 100 stretches (at 100% strain) over the scan rate range of 5-500 mV s^{-1}. All of the electrodes had stretch and release cycles applied at a speed of 2% s^{-1} for 50 and 100 stretches using a Shimadzu EZ mechanical tester.

3.3.2 Electrochemical impedance spectroscopy

Electrochemical impedance spectroscopy (EIS) was used to probe the electrical double layer effects at the electrode/electrolyte interface. EIS measurements were performed at room temperature using a Gamry EIS 3000^{TM} system (Gamry, USA) where the frequency range spanned 100 kHz to 0.01 Hz with an amplitude of 10mV (rms) at open circuit potential.

3.3.3 Galvanostatic charge/discharge measurement

A pair of latex/SWCNTs film electrodes was set up in a glass beaker for use as the anode and cathode. The constant current charge-discharge measurement was carried

out at 0.25mA/cm^2 in the voltage range between 0.1 and 1 V in 1 M aqueous Na_2SO_4 electrolyte.

3.4 RESULTS AND DISCCUSION

3.4.1 Physical and chemical properties of SWCNTs

Figure 3.2 presents SEM micrographs and FT-IR of pristine and functionalized (acid-treated) single-wall carbon nanotubes (SWCNTs). The pristine SWCNTs are bundled with an average diameter in excess of 100 nm before functionalization (Figure 3.2a), while the functionalized SWCNTs have average bundled diameters of approximately 10 nm (Figure 3.2b). Importantly, the pristine SWCNTs in the DMF (Figure 3.2a see inset photo) were sediment at the bottom of the vial within 1 hr, while the functionalized SWCNTs show good dispersion up to 60 days (Figure 3.2b see inset photo). This indicates that the functional groups on the SWCNTs can significantly improve dispersability and wettability of the SWCNTs in the DMF. It also implies that the π-π interaction and van der Waals force between the nanotubes decreased with functionalization of the SWCNTs [42].

The presence of functional groups on the SWCNTs is confirmed by FT-IR spectroscopy (Figure 3.2c and d). The carbonyl group stretch of the carboxylate anions appears at 1581cm^{-1} for the acid treated SWCNTs (Figure 3.2d). The peaks at 1736cm^{-1} and 3428 cm^{-1}, which are from the O-HCO stretch of the carboxylic acid groups, indicates that the functional group on the SWCNTs is successfully introduced by acid treatment (Figure 3.2d) [24, 43]. In contrast, the same peaks are not observed for the pristine SWCNTs (Figure 3.2c).

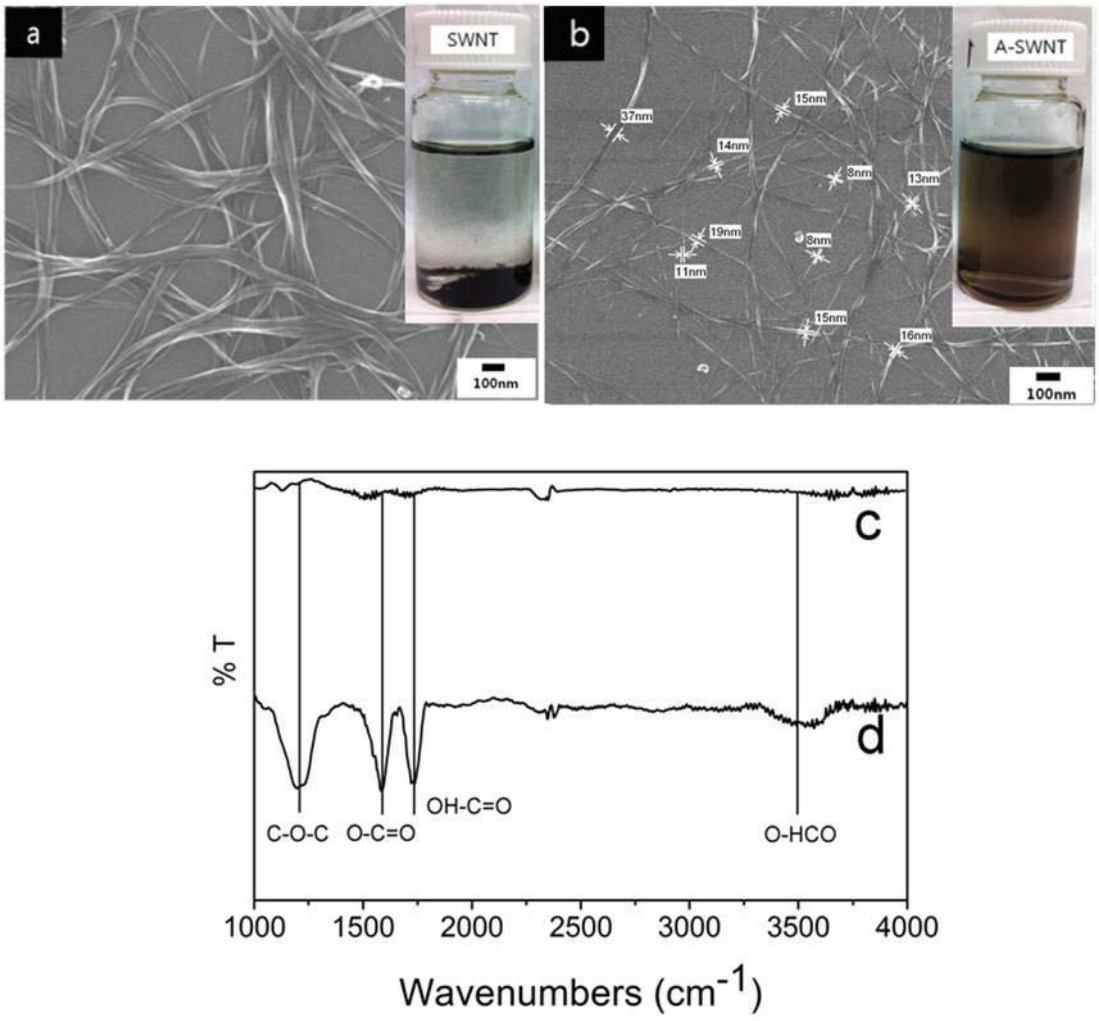

Figure 3.2 SEM images and FT-IR spectrum of the (a, c) pristine SWCNTs and (b, d) functionalized SWCNTs.

Raman spectroscopy in the high frequency range between 1500 and1600 cm^{-1} gives the intensity of the G-band that relates to the arrangement of hexagonal lattices of graphite (Figure 3.3). The other peak at 1200–1400 cm^{-1} or D-band indicates the level of defect or disorder. In the low-frequency range (100–375 cm^{-1}), the measurement of the radial breathing mode (RBM) is a useful way of analysing the SWCNTs diameter distribution. By comparing pristine SWCNTs with acid-treated SWCNTs, the ID/IG ratio of pristine SWCNTs is smaller than that of the acid-treated SWCNTs (Figure 3.3, see table).

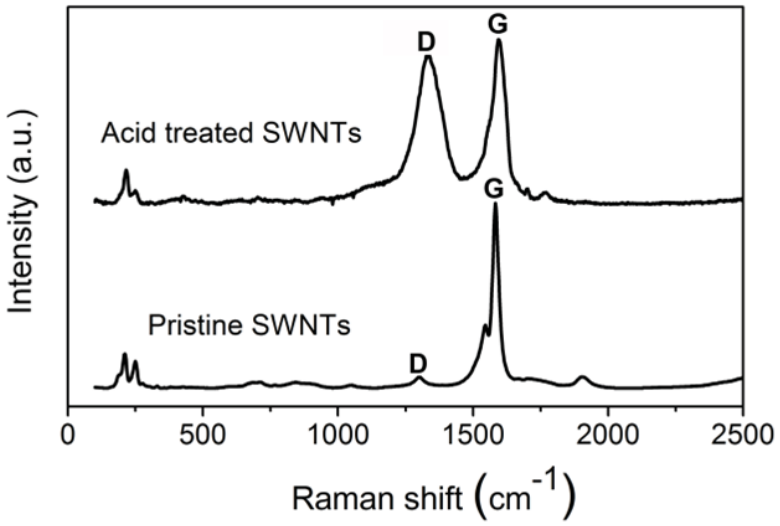

	I_D/I_G	D band	G band	diameter (nm)
Pristine SWNTs	0.05	1300	1583	1.17, 1
Acid treated SWNTs	0.9	1336	1593	1.15, 1

Figure 3.3 Raman spectra of the pristine SWCNTs and functionalized SWCNTs.

This indicates that the pristine SWCNTs have less defects on the carbon structure when compared to the functionalized SWCNTs [44, 45]. The relation $\omega = 248/d$ is used to determine the approximate diameter of SWCNTs, where ω is the RBM frequency in cm^{-1} and d is the diameter of the SWCNTs [46-48]. According to the above equation, the diameter of the pristine SWCNTs is in the range of 1–1.17 nm and the diameter distribution of the functionalized SWCNTs is in the range of 1–1.15 nm. This implies that acid-treatment does not significantly modify the diameter of the SWCNTs. In addition, D and G band peaks for functionalized SWCNTs are slightly shifted right from that of pristine SWCNTs (Figure 3.3, see table), which may be due to the presence of functional groups on the SWCNTs [49].

3.4.2 Electrochemical properties

Cyclic voltammetry (CV) measurements were obtained to investigate the electrochemical properties of the latex/SWCNTs films as a function of stretching and strain (Figure 3.4a, c). The decrease in CV current was observed with respect to increase in number of stretching and level of strain (Figure 3.4a, c). It might be due to decrease electrical conductivity of the latex/SWCNTs electrode after a number of stretching and strain (Figure 3.9a, b). The redox peaks can be attributed to the presence of functional groups (-COOH or -OH) on the carbon nanotubes [50]. The specific capacitance is calculated on the basis of the following equation [51]:

$$C = \int_{E1}^{E2} \mathrm{i}\,(\mathrm{E})dE \;/\; 2(E2 - E1)\, mv \qquad \text{Eq. (1)}$$

where *C* is the specific capacitance of the individual electrode, *E1* and *E2* are the cutoff potentials in cyclic voltammetry, *i(E)* is the instantaneous current, *E2 – E1* is the potential window width, *m* is the mass of active material (the mass difference of the working electrode before and after spray coating), *v* is the potential scan rate and $\int_{E1}^{E2} \mathrm{i}\,(\mathrm{E})dE$ is the total voltammetric charge obtained by integration of the positive and negative sweep in cyclic voltammograms.

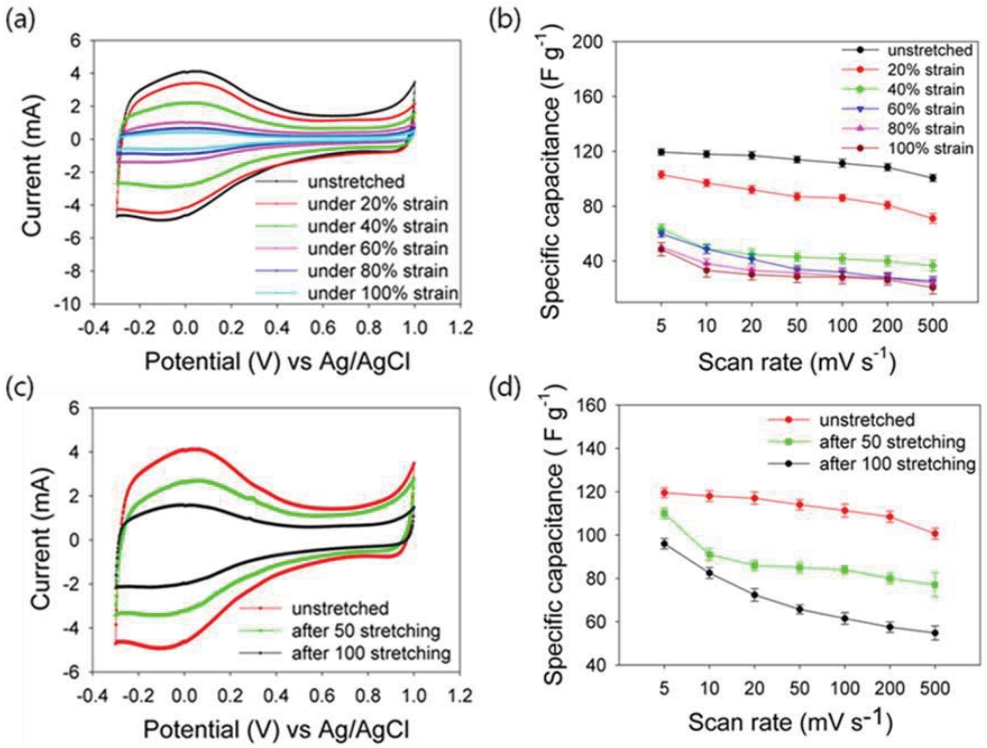

Figure 3.4 Cyclic voltammetry and specific capacitance of latex/SWCNTs electrodes at various strain percentages and stretching in 1M Na_2SO_4; (a) Under various strain percentage (0 ~100% strain with 100 mV s^{-1} scan rate), (b) Specific capacitance under various strain percentage (0 ~100% strain with 5~500 mV s^{-1} scan rate), (c) After various stretching (0, 50 and 100 times stretching at 100% strain with 100 mV s^{-1} scan rate) , (d) Specific capacitance after various stretching (0, 50 and 100 times stretching at 100% strain with 5~500 mV s^{-1} scan rate).

The highest capacitance value obtained for the unstretched SWCNTs electrode is 119 F g^{-1} in 1 M Na_2SO_4 at 5 mV s^{-1}. To assess the reproducibility of the fabrication approach we assessed the specific capacitance of 10 electrodes. The average specific capacitance decreases slightly with an increase in scan rate but retains a value of 100.6 ± 5.0 (mean ± S.D., n = 10 electrodes) F g^{-1} at 500 mV s^{-1}, reflecting an energy density of 33.5 ± 1.6 (mean ± S.D., n = 10 electrodes) Wh kg^{-1} and power density of

50.3 ± 2.4 (mean ± S.D., n = 10 electrodes) KW kg^{-1} (Table 3.1). The energy and power density of the latex electrode is calculated according to the following equation:

$$E = \frac{1}{2} C_{sp} V^2 ; P = \frac{E}{t} \qquad \text{Eq. (2)}$$

where C_{sp} is the specific capacitance of the latex electrode, V is the operating voltage and t is the sweep time. Under fixed strain over the range (20-100%) the capacitance values obtained at 5 mV s^{-1} decreased.

	Specific capacitance ($F\ g^{-1}$)	Energy Density ($Wh\ kg^{-1}$)	Power Density ($KW\ kg^{-1}$)
Unstretched	100.6 (± 5)	33.5 (± 1.6)	50.3 (± 2.4)
Under 20%	71.1 (± 3)	23.7 (± 1)	35.55 (± 1.5)
Under 40%	36.7 (± 4)	12.2 (± 1.3)	18.35 (± 2)
Under 60%	25.4 (± 3)	8.46 (± 1)	12.7 (± 1.5)
Under 80%	24 (± 2)	8 (± 0.6)	12 (± 0.9)
Under 100%	20.7 (± 5)	6.9 (± 1.6)	10.35 (± 2.4)

Table 3.1 Specific capacitance, energy and power density of the latex/SWCNTs electrode under various strains at 500 mV s^{-1} of scan rate.

Specific capacitance versus scan rate is plotted for the electrode under repeated stretching (Figure 3.4d) and strain conditions (Figure 3.4b). The specific capacitance decreased to 110 ± 2.5 (mean ± S.D., n = 10 electrodes) and 96 ± 2.4 (mean ± S.D., n = 10 electrodes) F g^{-1} at 5mV s^{-1} after 50 and 100 stretches (at 100% strain),

respectively (Figure 3.4d). The performance also decreased to 48.7 ± 4.8 (mean ± S.D., n = 10 electrodes) F g^{-1} at 5 mV s^{-1} under 100 % level of strain (Figure 3.4d).

Nyquist plots obtained from impedance measurements show characteristic capacitive behaviour of SWCNTs (Figure 3.5) [52]. In the high frequency domain for stretching (inset Figure 3.5a) and applied strain (inset Figure 3.8b), there are smaller semi-circles that can be attributed to minimization of the contact impedance between the SWCNTs film and current collector as well as electrolyte resistance within the pores of the SWCNTs film [53]. In the middle frequency regime, a small 45^{o} degree inclination is seen for the latex/SWCNTs electrodes. This arises as a result of distribution capacitance/impedance in a porous material [54]. However, the internal resistance of the unstretched latex/SWCNTs electrode is 1.8 Ω, which increases to 7.5 Ω and 10.8 Ω after 50 and 100 stretches, respectively (Figure 3.5a). The internal resistance further increases to 26.9 Ω under 100% strain (Figure 3.5b). This again is mostly likely due to the low electrical conductivity on the SWCNTs film after repetitive stretching to 100% strain.

The cycling stability of the latex/SWCNTs electrodes when subjected to a different number of stretches (Figure 3.6a) and applied strain percentages (Figure 3.6b) shows typical galvanostatic charge/discharge profiles with a constant current density of 0.25mA/cm^2 (1A g^{-1}). The charge/discharge curves of the latex/SWCNTs electrodes indicate good capacitive behavior even after 50 and 100 stretch cycles and under various levels of strain (Figure 3.6a and 3.6b). The symmetrical shape indicates that highly conductive SWCNTs create a pathway for the transfer of ions and electrons, thus decreasing internal resistance. Importantly, it takes 84 seconds for the unstretched latex/SWCNTs electrode to reach one charge/discharge cycles, while after

100 stretch cycles the sample shows a less charge/discharge time of ≈ 67 seconds (Figure 3.6a). A longer cycle time indicates a higher amount of charge stored in the capacitor, since this measurement is carried out under constant current.

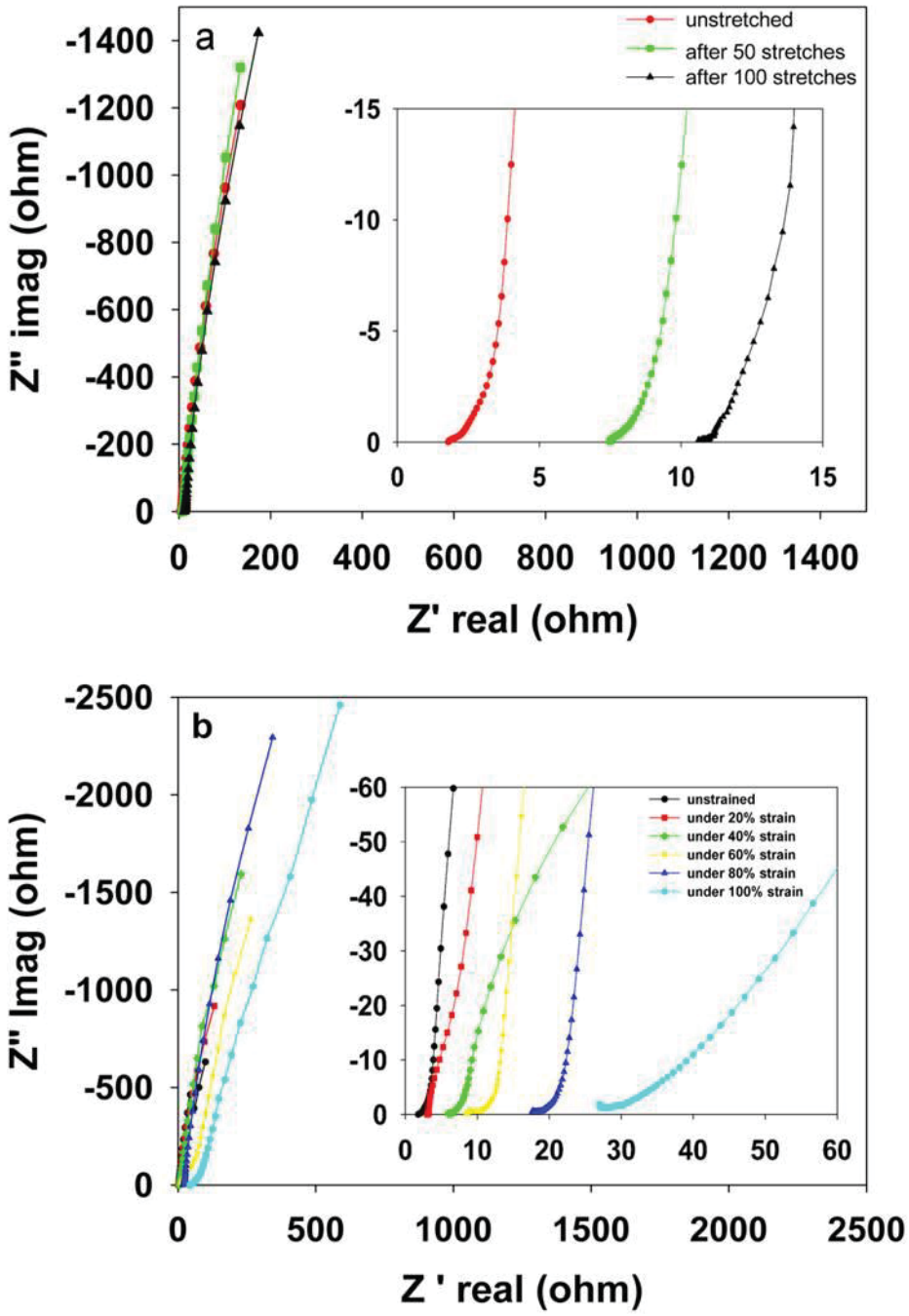

Figure 3.5 Nyquist plots of the latex/SWCNTs electrode applied with (a) various stretching (0, 50 and 100 times stretching) and (b) strain percentage (0 ~100% strain).

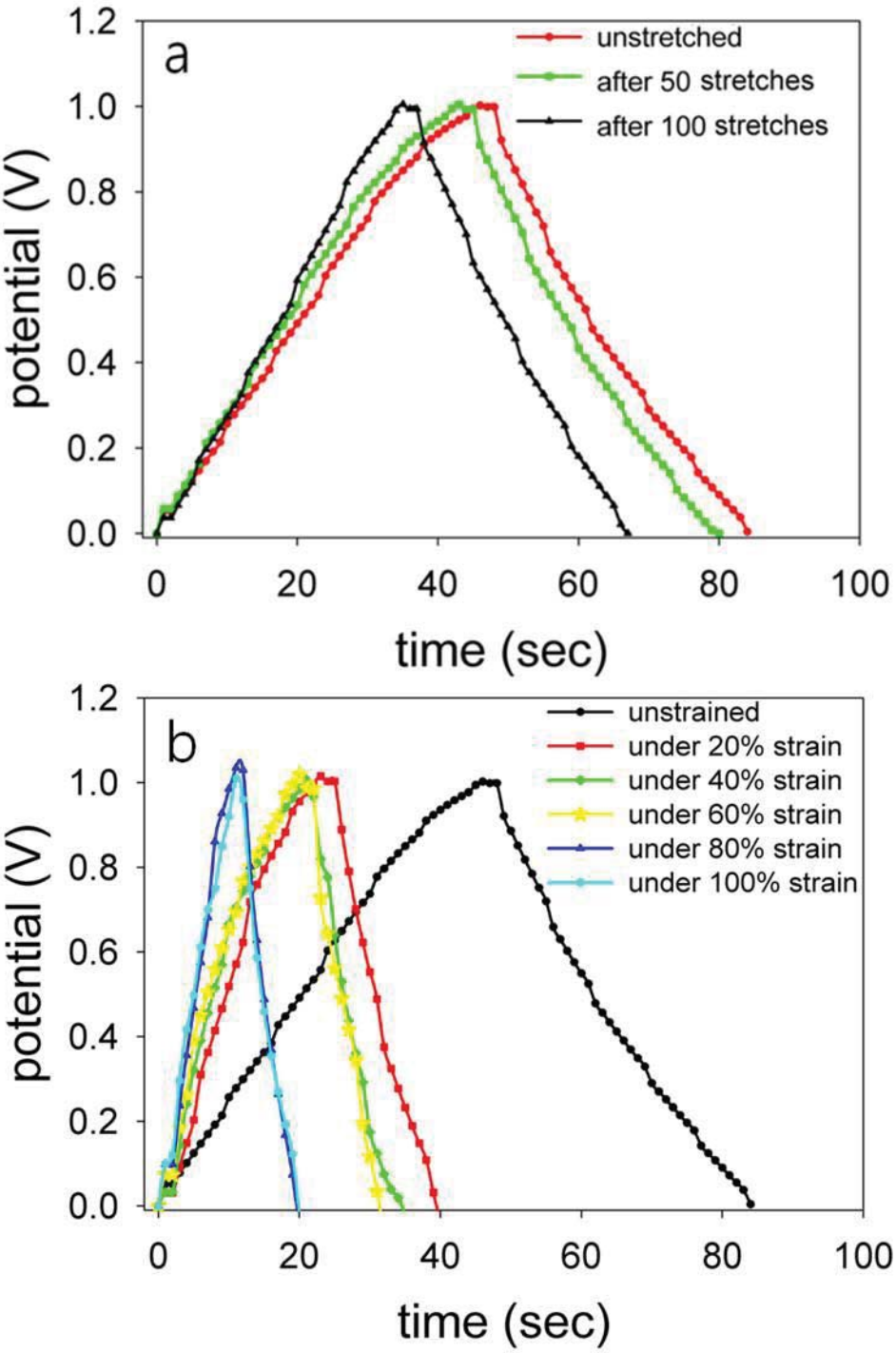

Figure 3.6 Galvanostatic charge/discharge curves of the latex/SWCNTs electrode at constant current (1A g^{-1}) in 1M Na_2SO_4 (a) after various stretching (0, 50 and 100 times stretching), (b) under various strain percentages (0 ~100% strain).

We have also investigated the cycling stability of the unstretched latex/SWCNTs electrode (Figure 3.7a) after applying 50 (Figure 3.7b) and 100 stretch cycles (Figure 3.7c). For these measurements, 1000 CV cycles are performed and the first cycle, 500^{th} cycle and 1000^{th} cycle are shown in Figure 3.7a-c. The CV curves show a slightly decreased current after stretching the electrode 50 times, with a further decrease in current after stretching 100 times. This effect indicates that the internal resistance of the electrode inhibits the charge collection and the lower conductivity of the 1M Na_2SO_4 electrolyte also limits diffusion of Na^+ ions into the nanotube film [55].

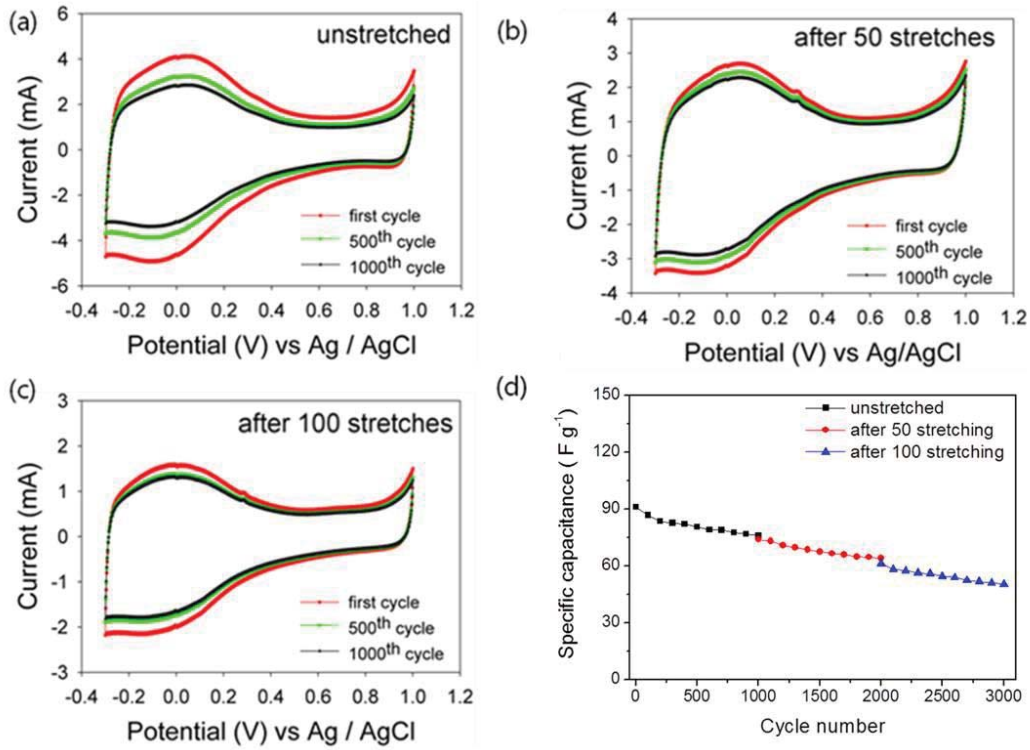

Figure 3.7 Stability and specific capacitance of the latex/SWCNTs at varying cycle number of CV and stretching in 1M Na_2SO_4 at 100mV s^{-1}; (a) unstretched, (b) after 50 stretches, (c) after 100 stretches, (d) specific capacitance as a function of CV cycle number (0~1000^{th} cycles).

However, approximately 55% of the initial capacitance remains after the 100th stretching cycle of the electrode during the 3000th CV cycle at 100 mV s^{-1} scan rate (Figure 3.7d). In addition, there is a consistent decrease in the current and capacitance as a function of the number of stretches and CV cycle. This behaviour can be explained by the initial charge formed by the ion adsorption at the same scan rates. Furthermore, the cracks on the SWCNTs film observed after 50 and 100 stretches could be attributed to irreversible loss of electrons between the surface of the electrode and electrolyte, thus causing degradation of the substrate [55].

3.4.3 Morphological study of the SWCNTs film on the latex

SEM images of the latex/SWCNTs electrodes are shown in Figure 3.8. The surface morphology of the relaxed SWCNTs film shows a lot of islands with a very porous and well-defined periodic buckling structure before prolonged stretching (Figure 3.8a and 3.8b). This characteristic is strongly desirable since it maximizes surface area. However, there are some cracks evident on the SWCNTs film after 100 stretch cycles with applied strain of 100% (Figure 3.8c and 3.8d). The introduction of repeated stresses and strain is likely to result in the formation of these cracks on the SWCNTs films that cause a decrease in electrical conductivity of the SWCNTs film and thus affect the capacitance. We also attribute these cracks to irreversible loss of junctions between SWCNTs [56]. However, approximately 80% and 40% of the initial capacitance remains after 100 stretching cycles and applied strain of 100%, respectively (Figure 3.8b and d).

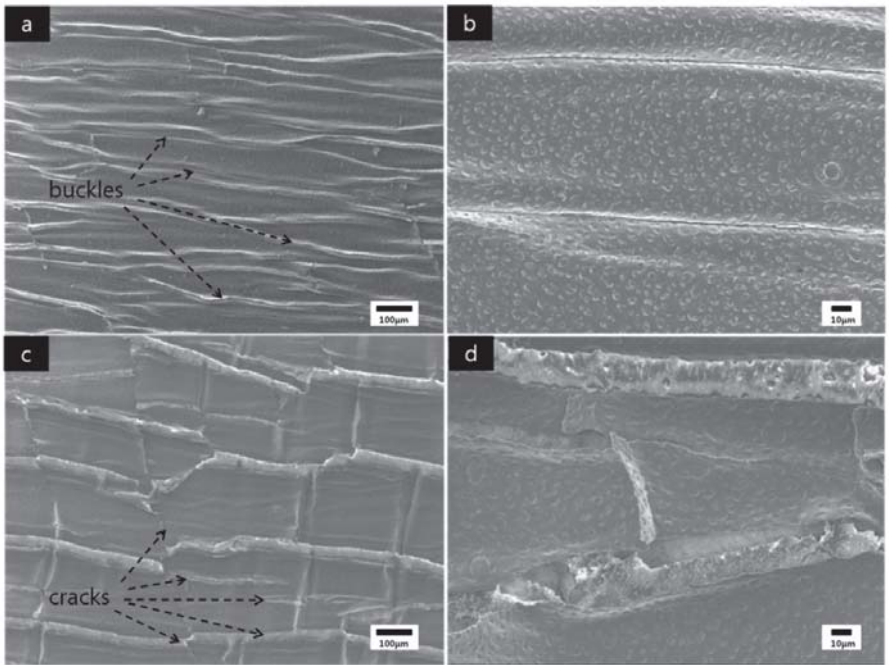

Figure 3.8 SEM images of latex/SWCNTs electrode; (a, b) relaxed from 100% pre-strain, (c, d) under 100% tensile strain with application of 100 stretches.

3.4.4 Electrical conductivity of the latex/SWCNTs electrode as a function of stretching and strain

The electrical conductivities of the latex/SWCNTs electrode decreased with an increasing number of stretches and strain percentage (Figure 3.9). The electrical conductivity of the unstretched SWCNTs film on the latex is 2.5 x 10^3 S cm^{-1}. However, the electrical conductivity of the SWCNTs film decreases to 5.1 S cm^{-1} and 2.35 x 10^2 S cm^{-1} after 100 stretches (Figure 3.9a) and applied strain of 100% (Figure 3.9b), respectively.

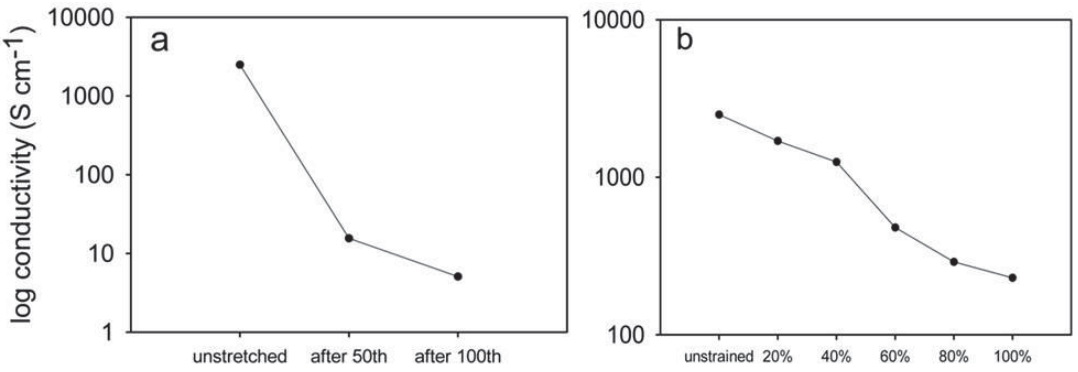

Figure 3.9 Electrical conductivities of the latex/SWCNTs electrode (a) after various stretching (0, 50 and 100 times stretching) and (b) under various strain percentage (0 ~100% strain).

Again, the emergence of cracks (Figure 3.8c and 3.8d) on the SWCNTs film after 100 stretches with applied strain of 100% is the most likely cause of the decrease in conductivity.

3.5 CONCLUSIONS

SWCNTs were characterized using FT-IR and Raman spectroscopy. Three significant peaks on the FT-IR spectroscopy at 1581 cm^{-1}, 1736 cm^{-1} and 3428 cm^{-1} were observed, corresponding to the carbonyl groups stretch of the carboxylate anions and carboxylic acid groups, respectively. In addition, Raman spectroscopy shows that the level of defects on the SWCNTs increased after functionalization.

The latex/SWCNTs electrode was successfully fabricated using a spray coating method. Cyclic voltammetric measurements revealed that the latex/SWCNTs electrode displayed typical capacitive behaviour under various strains even after repetitive stretching to 100%. The highest capacitance value obtained for the unstretched SWCNTs electrode was 119 F g^{-1} in 1 M Na_2SO_4 at 5 mV s^{-1}. However,

the electrochemical performance of the latex/SWCNTs electrode decreased with an increase in the number of stretches and the degree of strain. Approximately 80% of the initial capacitance remained after 100 stretch cycles. The high surface area, high stability and stretchability of the latex/SWCNTs electrode demonstrate that this kind of carbon nanotube film has potential advantages for wearable and biocompatible devices.

3.6 REFERENCES

[1] Y. Sun and J. A. Rogers, "Inorganic Semiconductors for Flexible Electronics," *Advanced Materials,* vol. 19, pp. 1897-1916, 2007.

[2] V. L. Pushparaj, M. M. Shaijumon, A. Kumar, S. Murugesan, L. Ci, R. Vajtai, R. J. Linhardt, O. Nalamasu, and P. M. Ajayan, "Flexible energy storage devices based on nanocomposite paper," *Proceedings of the National Academy of Sciences,* vol. 104, pp. 13574-13577, August 21, 2007 2007.

[3] K. Jain, M. Klosner, M. Zemel, and S. Raghunandan, "Flexible Electronics and Displays: High-Resolution, Roll-to-Roll, Projection Lithography and Photoablation Processing Technologies for High-Throughput Production," *Proceedings of the IEEE,* vol. 93, pp. 1500-1510, 2005.

[4] Y.-k. Zhou, B.-l. He, W.-j. Zhou, and H.-l. Li, "Preparation and Electrochemistry of SWNT/PANI Composite Films for Electrochemical Capacitors," *Journal of The Electrochemical Society,* vol. 151, pp. A1052-A1057, July 1, 2004 2004.

[5] S. W. Lee, J. Kim, S. Chen, P. T. Hammond, and Y. Shao-Horn, "Carbon Nanotube/Manganese Oxide Ultrathin Film Electrodes for Electrochemical Capacitors," *ACS Nano,* vol. 4, pp. 3889-3896, 2010/07/27 2010.

[6] D.-Y. Khang, H. Jiang, Y. Huang, and J. A. Rogers, "A Stretchable Form of Single-Crystal Silicon for High-Performance Electronics on Rubber Substrates," *Science,* vol. 311, pp. 208-212, January 13, 2006 2006.

[7] Y. Sun, W. M. Choi, H. Jiang, Y. Y. Huang, and J. A. Rogers, "Controlled buckling of semiconductor nanoribbons for stretchable electronics," *Nature Nanotechnology,* vol. 1, pp. 201-207, 2006.

[8] D.-H. Kim, J.-H. Ahn, W. M. Choi, H.-S. Kim, T.-H. Kim, J. Song, Y. Y. Huang, Z. Liu, C. Lu, and J. A. Rogers, "Stretchable and Foldable Silicon Integrated Circuits," *Science,* vol. 320, pp. 507-511, April 25, 2008 2008.

[9] H. C. Ko, M. P. Stoykovich, J. Song, V. Malyarchuk, W. M. Choi, C.-J. Yu, J. B. Geddes, III, J. Xiao, S. Wang, Y. Huang, and J. A. Rogers, "A hemispherical electronic eye camera based on compressible silicon optoelectronics," *Nature,* vol. 454, pp. 748-53, 2008 Aug 07 2008.

[10] C. Wang, W. Zheng, Z. Yue, C. O. Too, and G. G. Wallace, "Buckled, Stretchable Polypyrrole Electrodes for Battery Applications," *Advanced Materials,* vol. 23, pp. 3580-3584, 2011.

[11] C. Yu, C. Masarapu, J. Rong, B. Wei, and H. Jiang, "Stretchable Supercapacitors Based on Buckled Single-Walled Carbon-Nanotube Macrofilms," *Advanced Materials,* vol. 21, pp. 4793-4797, 2009.

[12] K. Subramaniam, A. Das, and G. Heinrich, "Development of conducting polychloroprene rubber using imidazolium based ionic liquid modified multi-walled carbon nanotubes," *Composites Science and Technology,* vol. 71, pp. 1441-1449, 2011.

[13] T. A. Kim, H. S. Kim, S. S. Lee, and M. Park, "Single-walled carbon nanotube/silicone rubber composites for compliant electrodes," *Carbon,* vol. 50, pp. 444-449, 2012.

[14] Y. Zhang, C. J. Sheehan, J. Zhai, G. Zou, H. Luo, J. Xiong, Y. T. Zhu, and Q. X. Jia, "Polymer-Embedded Carbon Nanotube Ribbons for Stretchable Conductors," *Advanced Materials,* vol. 22, pp. 3027-3031, 2010.

[15] M. S. Cho, H. J. Seo, J. D. Nam, H. R. Choi, J. C. Koo, K. G. Song, and Y. Lee, "A solid state actuator based on the PEDOT/NBR system," *Sensors and Actuators B: Chemical,* vol. 119, pp. 621-624, 2006.

[16] S. J. Kwon, T. Y. Kim, B. S. Lee, T. H. Lee, J. E. Kim, and K. S. Suh, "Elastomeric conducting polymer nano-composites derived from ionic liquid polymer stabilized-poly(3,4-ethylenedioxythiophene)," *Synthetic Metals,* vol. 160, pp. 1092-1096, 2010.

[17] C. Yuan, L. Hou, D. Li, L. Shen, F. Zhang, and X. Zhang, "Synthesis of flexible and porous cobalt hydroxide/conductive cotton textile sheet and its application in electrochemical capacitors," *Electrochimica Acta,* vol. 56, pp. 6683-6687, 2011.

[18] A. Kros, S. W. F. M. van Hövel, R. J. M. Nolte, and N. A. J. M. Sommerdijk, "A printable glucose sensor based on a poly(pyrrole)-latex hybrid material," *Sensors and Actuators B: Chemical,* vol. 80, pp. 229-233, 2001.

[19] P. Jung Woo, Y. Jung-Hoon, and K. Hanseup, "A large-deflection high-force micro electromagnetic hydraulic Latex membrane actuator for fluid manipulation in micro channels," in *Micro Electro Mechanical Systems (MEMS), 2011 IEEE 24th International Conference on*, 2011, pp. 1209-1212.

[20] S. Ugur, Ö. Yargi, and Ö. Pekcan, "Conductivity percolation of carbon nanotubes (CNT) in polystyrene (PS) latex film," *Canadian Journal of Chemistry,* vol. 88, pp. 267-276, 2010.

[21] Z. Spitalsky, D. Tasis, K. Papagelis, and C. Galiotis, "Carbon nanotube–polymer composites: Chemistry, processing, mechanical and electrical properties," *Progress in Polymer Science,* vol. 35, pp. 357-401, 2010.

[22] L. Hu, W. Yuan, P. Brochu, G. Gruner, and Q. Pei, "Highly stretchable, conductive, and transparent nanotube thin films," *Applied Physics Letters,* vol. 94, pp. -, 2009.

[23] X. Wang, P. D. Bradford, W. Liu, H. Zhao, Y. Inoue, J.-P. Maria, Q. Li, F.-G. Yuan, and Y. Zhu, "Mechanical and electrical property improvement in CNT/Nylon composites through drawing and stretching," *Composites Science and Technology,* vol. 71, pp. 1677-1683, 2011.

[24] J. Shen, A. Liu, Y. Tu, G. Foo, C. Yeo, M. B. Chan-Park, R. Jiang, and Y. Chen, "How carboxylic groups improve the performance of single-walled carbon nanotube electrochemical capacitors?," *Energy & Environmental Science,* vol. 4, pp. 4220-4229, 2011.

[25] Y.-T. Kim, Y. Ito, K. Tadai, T. Mitani, U.-S. Kim, H.-S. Kim, and B.-W. Cho, "Drastic change of electric double layer capacitance by surface functionalization of carbon nanotubes," *Applied Physics Letters,* vol. 87, pp. -, 2005.

[26] M. D. Obradović, G. D. Vuković, S. I. Stevanović, V. V. Panić, P. S. Uskoković, A. Kowal, and S. L. Gojković, "A comparative study of the electrochemical properties of carbon nanotubes and carbon black," *Journal of Electroanalytical Chemistry,* vol. 634, pp. 22-30, 2009.

[27] R. Z. Ma, J. Liang, B. Q. Wei, B. Zhang, C. L. Xu, and D. H. Wu, "Study of electrochemical capacitors utilizing carbon nanotube electrodes," *Journal of Power Sources,* vol. 84, pp. 126-129, 1999.

[28] E. Frackowiak, K. Metenier, V. Bertagna, and F. Beguin, "Supercapacitor electrodes from multiwalled carbon nanotubes," *Applied Physics Letters,* vol. 77, pp. 2421-2423, 2000.

[29] E. Frackowiak, K. Jurewicz, S. Delpeux, and F. Béguin, "Nanotubular materials for supercapacitors," *Journal of Power Sources,* vol. 97–98, pp. 822-825, 2001.

[30] F. Picó, J. M. Rojo, M. L. Sanjuán, A. Ansón, A. M. Benito, M. A. Callejas, W. K. Maser, and M. T. Martínez, "Single-Walled Carbon Nanotubes as Electrodes in Supercapacitors," *Journal of The Electrochemical Society,* vol. 151, pp. A831-A837, June 1, 2004 2004.

[31] H. Pan, C. K. Poh, Y. P. Feng, and J. Lin, "Supercapacitor Electrodes from Tubes-in-Tube Carbon Nanostructures," *Chemistry of Materials,* vol. 19, pp. 6120-6125, 2007/12/01 2007.

[32] C. Liu, F. Li, L.-P. Ma, and H.-M. Cheng, "Advanced Materials for Energy Storage," *Advanced Materials,* vol. 22, pp. E28-E62, 2010.

[33] K. H. An, W. S. Kim, Y. S. Park, Y. C. Choi, S. M. Lee, D. C. Chung, D. J. Bae, S. C. Lim, and Y. H. Lee, "Supercapacitors Using Single-Walled Carbon Nanotube Electrodes," *Advanced Materials,* vol. 13, pp. 497-500, 2001.

[34] K. H. An, W. S. Kim, Y. S. Park, J. M. Moon, D. J. Bae, S. C. Lim, Y. S. Lee, and Y. H. Lee, "Electrochemical Properties of High-Power Supercapacitors Using Single-Walled Carbon Nanotube Electrodes," *Advanced Functional Materials,* vol. 11, pp. 387-392, 2001.

[35] Z. Wu, Z. Chen, X. Du, J. M. Logan, J. Sippel, M. Nikolou, K. Kamaras, J. R. Reynolds, D. B. Tanner, A. F. Hebard, and A. G. Rinzler, "Transparent, Conductive Carbon Nanotube Films," *Science,* vol. 305, pp. 1273-1276, August 27, 2004 2004.

[36] A. A. Green and M. C. Hersam, "Colored Semitransparent Conductive Coatings Consisting of Monodisperse Metallic Single-Walled Carbon Nanotubes," *Nano Letters,* vol. 8, pp. 1417-1422, 2008/05/01 2008.

[37] M. H. Kim, J. Y. Choi, H. K. Choi, S. M. Yoon, O. O. Park, D. K. Yi, S. J. Choi, and H. J. Shin, "Carbon Nanotube Network Structuring Using Two-Dimensional Colloidal Crystal Templates," *Advanced Materials,* vol. 20, pp. 457-461, 2008.

[38] M. H. A. Ng, L. T. Hartadi, H. Tan, and C. H. P. Poa, "Efficient coating of transparent and conductive carbon nanotube thin films on plastic substrates," *Nanotechnology,* vol. 19, p. 205703, 2008.

[39] K. Kordás, T. Mustonen, G. Tóth, H. Jantunen, M. Lajunen, C. Soldano, S. Talapatra, S. Kar, R. Vajtai, and P. M. Ajayan, "Inkjet Printing of Electrically Conductive Patterns of Carbon Nanotubes," *Small,* vol. 2, pp. 1021-1025, 2006.

[40] J. H. Kim, K.-W. Nam, S. B. Ma, and K. B. Kim, "Fabrication and electrochemical properties of carbon nanotube film electrodes," *Carbon,* vol. 44, pp. 1963-1968, 2006.

[41] J.-Y. Kim, C. S. Lee, J. H. Han, J. W. Cho, and J. Bae, "Supercapacitors Using Gel Electrolytes and Thin Multiwalled Carbon Nanotube Films Spray-Deposited on ITO Substrates," *Electrochemical and Solid-State Letters,* vol. 14, pp. A56-A59, April 1, 2011 2011.

[42] H. J. Park, M. Park, J. Y. Chang, and H. Lee, "The effect of pre-treatment methods on morphology and size distribution of multi-walled carbon nanotubes," *Nanotechnology,* vol. 19, p. 335702, 2008.

[43] W. Chidawanyika and T. Nyokong, "Characterization of amine-functionalized single-walled carbon nanotube-low symmetry phthalocyanine conjugates," *Carbon,* vol. 48, pp. 2831-2838, 2010.

[44] M. N. Tchoul, W. T. Ford, G. Lolli, D. E. Resasco, and S. Arepalli, "Effect of Mild Nitric Acid Oxidation on Dispersability, Size, and Structure of Single-Walled Carbon Nanotubes," *Chemistry of Materials,* vol. 19, pp. 5765-5772, 2007/11/01 2007.

[45] H.-Z. Geng, K. K. Kim, K. P. So, Y. S. Lee, Y. Chang, and Y. H. Lee, "Effect of Acid Treatment on Carbon Nanotube-Based Flexible Transparent Conducting Films," *Journal of the American Chemical Society,* vol. 129, pp. 7758-7759, 2007/06/01 2007.

[46] C. Niu, E. K. Sichel, R. Hoch, D. Moy, and H. Tennent, "High power electrochemical capacitors based on carbon nanotube electrodes," *Applied Physics Letters,* vol. 70, pp. 1480-1482, 1997.

[47] R. K. Saini, I. W. Chiang, H. Peng, R. E. Smalley, W. E. Billups, R. H. Hauge, and J. L. Margrave, "Covalent Sidewall Functionalization of Single Wall Carbon Nanotubes," *Journal of the American Chemical Society,* vol. 125, pp. 3617-3621, 2003/03/01 2003.

[48] H. Murphy, P. Papakonstantinou, and T. I. T. Okpalugo, "Raman study of multiwalled carbon nanotubes functionalized with oxygen groups," *Journal of Vacuum Science & Technology B,* vol. 24, pp. 715-720, 2006.

[49] Z.-M. Dang, L. Wang, and L.-P. Zhang, "Surface functionalization of multiwalled carbon nanotube with trifluorophenyl," *Journal of Nanomaterials,* vol. 2006, 2006.

[50] J. N. Barisci, G. G. Wallace, D. Chattopadhyay, F. Papadimitrakopoulos, and R. H. Baughman, "Electrochemical Properties of Single-Wall Carbon Nanotube Electrodes," *Journal of The Electrochemical Society,* vol. 150, pp. E409-E415, September 1, 2003 2003.

[51] M. A. Azam, K. Isomura, A. Fujiwara, and T. Shimoda, "Direct growth of vertically aligned single-walled carbon nanotubes on conducting substrate and its electrochemical performance in ionic liquids," *physica status solidi (a),* vol. 209, pp. 2260-2266, 2012.

[52] J. Segalini, B. Daffos, P. L. Taberna, Y. Gogotsi, and P. Simon, "Qualitative Electrochemical Impedance Spectroscopy study of ion transport into sub-nanometer carbon pores in Electrochemical Double Layer Capacitor electrodes," *Electrochimica Acta,* vol. 55, pp. 7489-7494, 2010.

[53] H. Kurig, A. Jänes, and E. Lust, "Electrochemical Characteristics of Carbide-Derived Carbon | 1 -Ethyl-3-methylimidazolium Tetrafluoroborate Supercapacitor Cells," *Journal of The Electrochemical Society,* vol. 157, pp. A272-A279, March 1, 2010 2010.

[54] P. L. Taberna, P. Simon, and J. F. Fauvarque "Electrochemical Characteristics and Impedance Spectroscopy Studies of Carbon-Carbon Supercapacitors," *Journal of The Electrochemical Society,* vol. 150, pp. A292-A300, March 1, 2003 2003.

[55] S. Nataraj, Q. Song, S. Al-Muhtaseb, S. Dutton, Q. Zhang, and E. Sivaniah, "Thin, flexible supercapacitors made from carbon nanofiber electrodes

decorated at room temperature with manganese oxide nanosheets," *Journal of Nanomaterials,* vol. 2013, 2013.

[56] S. R. S. Prabaharan, R. Vimala, and Z. Zainal, "Nanostructured mesoporous carbon as electrodes for supercapacitors," *Journal of Power Sources,* vol. 161, pp. 730-736, 2006.

CHAPTER 4

REDUCED GRAPHENE OXIDE (RGO)/SINGLE-WALL CARBON NANOTUBES ($SWCNT_S$) ELECTRODES ON POLYURETHANE

4.1 INTRODUCTION

Stretchable electronics have attracted a great deal of attention for potential applications in epidermal electronics [1], organic light emitting diodes (OLEDs) [2] and field effect transistors [3]. Such applications require the electronic materials to show excellent mechanical robustness and electronic functionality under high level of strain and stress [4]. As this industry continues to grow, there will be a need to integrate energy storage devices that are also stretchable, while retaining performance. Supercapacitors are useful energy storage devices that have several advantages compared to batteries. These include rapid charge/discharge response, simple operating mechanisms, long life cycles (>100 000 cycles), high specific power (2 orders of magnitude higher) and high efficiencies (up to 98%) [5]. However, supercapacitors still suffer from low energy density. To overcome this challenge, nanocarbon materials such as carbon nanotubes (CNTs) and graphene have been utilized to increase electroactive surface area, leading to enhanced electrochemical performance of supercapacitors [6-8].

To produce stretchable supercapacitors [9, 10], a variety of highly conductive materials such as metal wires, conducting polymers, carbon nanotubes (CNTs), or graphene films have been applied to polymer substrates [11-13]. Among these conductive materials, CNTs and graphene are promising candidates for supercapacitors due to their high electrical conductivity, high surface area, chemical

stability and outstanding mechanical properties [3, 7]. Yu *et al*. [14] reported on a stretchable supercapacitor based on buckled SWNT-based films applied to polydimethylsiloxane (PDMS). The SWCNTs-based stretchable supercapacitor showed a maximum specific capacitance of 54 F g^{-1} and power density of 0.5 KW kg^{-1} with 4.2 Wh kg^{-1} energy density. A specific capacitance value of 52 F g^{-1} was achieved with the application of 30% strain. Li *et al*. [10] recently developed a fully stretchable supercapacitor using buckled SWCNTs macrofilms as the electrode, polydimethylsiloxane (PDMS) as the substrate, electrospun polyurethane membrane as the separator, and 1M organic electrolyte of tetraethylammonium tetrafluoroborate in propylene carbonate. The buckled SWCNTs macrofilms could stretch up to 30% strain with 50 F g^{-1} of specific capacitance at a scan rate of 100 mV s^{-1}. Nevertheless, capacitance values for stretchable supercapacitors based on the SWCNTs are not capable of reaching their theoretical performance [15, 16]. Thus, more work is required to develop the electrodes such that their capacitance values are continually being improved as a function of stress and strain.

Reduced graphene oxide (rGO) has been identified as a suitable nanocarbon material for supercapacitors mainly due to their high surface area. A single graphene layer has a theoretical surface area of 2630 m^2 g^{-1} [7]. However, there are limitations in using rGO as an electrode material. Firstly, rGO has an electrical conductivity of 100~200 S m^{-1}, which is lower than the conductivity of SWCNTs (10,000 S m^{-1}) [7, 8]. Secondly, rGO is very likely to form irreversible agglomerates due to Van der Waals interactions during the drying process, leading to “re-stacking” of layers with a concomitant reduced electroactive surface area and lower specific capacitance [7]. Related to this, rGO-based electrodes operate more effectively with a ‘spacer’

material, although addition of the latter may decrease the capacitance. Thus, it is preferable to use a 'spacer' material with high conductivity and high surface area.

SWCNTs have been used as a "binder" between graphene layers to reduce the internal resistance of the resultant electrode structure [17]. The SWCNTs can also act to prevent re-stacking of the graphene layers [7]. These attributes of SWCNTs as constituents in graphene electrodes are believed to provide synergistic benefits in increasing the accessibility of electrolyte and electroactive surface area. Yu and co-workers [8] reported on poly(ethyleneimine) (PEI) modified graphene combined with CNTs. The PEI modified graphene/CNTs composite was prepared via a layer-by-layer technique and exhibited a capacitance of 120 F g^{-1} in 1 M sulfuric acid (H_2SO_4) aqueous electrolyte. Fan *et al.* [18] used drop-casting to produce graphene/CNT composite electrodes, which showed a specific capacitance of 385 F g^{-1} in 6 M potassium hydroxide (KOH) electrolyte. Whilst further work on graphene/CNTs composite electrodes and other carbon nanomaterial 'spacer' materials to improve capacitance values is expected to progress developments in this area, there is to our knowledge no report as yet on their performance under high strain conditions. Such performance characteristics are critical to determine their usefulness as stretchable electrodes.

In this chapter, rGO/SWCNTs stretchable, composite electrodes have been formed by spray coating onto gold-coated polyurethane (PU). The rGO/SWCNTs composite electrodes were characterized to quantify their electrochemical properties, including specific capacitance, impedance and charging/discharge properties as a function of strain. We also describe the surface morphology with respect to the capacitance of the stretchable electrodes.

4.2 EXPERIMENTAL SECTION

4.2.1 Materials

Graphite powder was obtained from Bay Carbon. Milli-Q water with a resistivity of 18.2 mΩ cm^{-1} was used in all preparations. Potassium permanganate, phosphorous penta-oxide, hydrazine hydrate and triethylamine were sourced from Sigma-Aldrich. Ammonia solution in water (28%) was sourced from Labtech and used as received. Single-walled carbon nanotubes (SWCNTs) were purchased from Carbon Nanotechnologies, Inc (Houston, TX). N, N-Dimethylformamide (DMF) and concentrated nitric acid (70%) were obtained from Sigma Aldrich. The polyurethane (PU) was purchased from Advan Source Biomaterials Corp. and used as the stretchable substrate. 1M Sulfuric acid (H_2SO_4) (Sigma Aldrich) was used as electrolyte to measure all of the electrochemical properties of the stretchable electrode.

4.2.2 Preparation of rGO and its dispersion in N, N-dimethylformamide (DMF)

Graphene oxide was synthesized from natural graphite powder using a modified Hummers' method in two steps of oxidation using $K_2S_2O_8$, P_2O_5 and H_2SO_4 followed by H_2SO_4, $KMnO_4$ and H_2O_2 to achieve better oxidation of graphite [19]**.** Graphene oxide (62.5 g) is diluted with deionised water (2 L) and sonicated for 80 min. Then, hydrazine (400 µL) and ammonia (4 mL) are added and the solution is heated at 90 ℃ for 1 hr. A further aliquot of hydrazine (3 mL) is added to the solution and the mixture is heated and kept at 90 ^{O}C for two hours under constant stirring. After cooling to the room temperature, the solution is acidified with H_2SO_4 (aq. 30%), then the agglomerated graphene powder is filtered and washed until the waste water is at a

neutral pH. The agglomerated graphene powder (dried chemically converted graphene) is filtered and dried in a vacuum oven at 50 ^{O}C for 2 days.

To form a stable suspension, rGO (300 mg) is added to DMF (150 ml, moisture content ≤ 350 ppm by Karl-Fischer). Triethylamine (50 µl) is added and the solution is extensively sonicated with continuous cooling under a dry nitrogen purge. DMF (300 ml) and triethylamine (500 µl) are then added and the suspension is further sonicated under nitrogen. The dispersion is centrifuged to separate any agglomerated graphene sheets and the resulting supernatant (0.5 mg ml^{-1}) [20].

4.2.3 Preparation of a stretchable polyurethane mat as a stretchable electrode substrate

4.2.3.1 Electrospining of the polyurethane mat

In order to prepare polyurethane (PU) nanofibers as a substrate, medical grade polyurethane was dissolved in DMF with a 15wt% concentration. The polyurethane solution was loaded into an electrospinning system consisting of a plastic syringe equipped with a 21 gauge needle that was connected to a high voltage supply. During electrospinning, the syringe pumping rate was adjusted to 0.2 mL/h and a voltage of 23 kV was maintained between the tip of the needle and the drum collector, which were separated by a distance of 10 cm. After electrospinning, the electrospun polyurethane mat was lifted from the collector and used as a stretchable substrate.

4.2.3.2 Gold coating onto the polyurethane mat

An Edwards Auto 306 Sputter Coater was used to deposit a 150nm thick layer of gold onto the 100% pre-strain polyurethane substrate. The gold coating functioned as a

current collector and was critical for reducing the contact resistance between the PU substrate and rGO, SWCNTs and rGO/SWCNTs composite layers (described below). The gold coating also provided a good electrical contact for the working electrode.

4.2.3.3 Fabrication of rGO/SWCNTs electrodes on indium tin oxide (ITO) coated glass

In order to optimize the electrochemical performance of the rGO/SWCNTs electrode, we initially assessed dispersions with different % ratios between the rGO and SWCNTs. Firstly, the SWCNTs and rGO were separately dispersed in DMF at a concentration of 0.5 mg mL^{-1} using a probe type ultrasonicator (Sonics Vibracell ultrasonic processor, 500 watt, 30% amplitude, USA) for 1hr to produce the dispersions. The rGO and SWCNTs dispersions were then mixed by using an ultrasonicator for 30 min at 30% amplitude (2 s on/2 s off pulse) to produce the rGO/SWCNTs dispersions with %weight ratios of 100/0, 90/10, 80/20, 50/50, 20/80, 10/90 and 0/100. Each of the different rGO/SWCNTs dispersions were spray coated on indium tin oxide (ITO) coated glass using a small airbrush (Bunnings, Australia) with approximately 0.15mL/min of feeding rate and 1 mm of nozzle diameter. For this coating procedure, the ITO glass was initially cut to a length of 50 mm and width of 10 mm, then fixed onto a hotplate covered with aluminium foil and heated to 70 °C prior to spray coating with the 5 mL rGO/SWCNTs dispersions with different % weight ratios. After the spray coating, each rGO/SWCNTs composite electrode was dried at 100 °C in an oven for 30 min to remove residual solvent.

4.2.3.4 Preparation of the stretchable rGO, SWCNTs and rGO/SWCNTs electrodes on gold-coated polyurethane via spray coating

To prepare dispersions for spray coating, acid treated SWCNTs [13] (9 mL) were mixed with the rGO solution (1 mL) to form a 10% rGO/ 90% SWCNTs dispersion, as described above. The rGO/SWCNTs solution was ultrasonicated (Sonics Vibracell ultrasonic processor, 500 watt, 30% amplitude, USA) for 30min. Pure 100% SWNT and 100% rGO dispersions were also prepared. The polyurethane (PU) film (10 mm x 50 mm x 0.2 mm) was transferred to a glass microscope slide and fixed to 100% pre-strain by using double-sided adhesive tape and then gold was deposited onto the pre-strain polyurethane. The sample/slide assembly was fixed to a hotplate covered with aluminium foil, heated to 70°C and then spray coated with either rGO, SWCNTs or rGO/SWCNTs dispersions. Spray coating was performed using a small and inexpensive craft airbrush (Bunnings, Australia) with a nozzle diameter of approximately 1mm. An air pressure of 50 psi was employed and the liquid feed rate adjusted to approximately 0.15mL/min. Spraying was performed manually at a distance of 15-20 cm from the polyurethane substrate. Many thin coats were applied, allowing a few seconds for drying between coats, until the entire 10 mL suspension was exhausted. After spray coating, the rGO, SWCNTs and rGO/SWCNTs composite electrodes were dried at 100 ℃ in an oven for 30 min to evaporate residual solvent.

4.3 RESULTS AND DISCUSSION

4.3.1 Physical and chemical properties of graphene oxide (GO) and reduced graphene oxide (rGO)

4.3.1.1 X-ray diffraction (XRD) of the GO and rGO

The X-ray diffraction (XRD) pattern of the GO was compared with rGO presented in the Figure 4.1. The peak position for GO was observed 2 θ = 11.02° (d-spacing ~ 8.05 Å). A typical broad peak near 24.08° (d-spacing ~ 3.7 Å) was observed for the rGO. The peak of rGO showed a dramatic shift to higher 2 θ angles (24.08°, d-spacing ~ 3.7 Å) compared with the parent GO, suggesting that rGO was disordered with two-dimensional sheets and there was a decrease in the average interlayer spacing of the rGO layers [21].

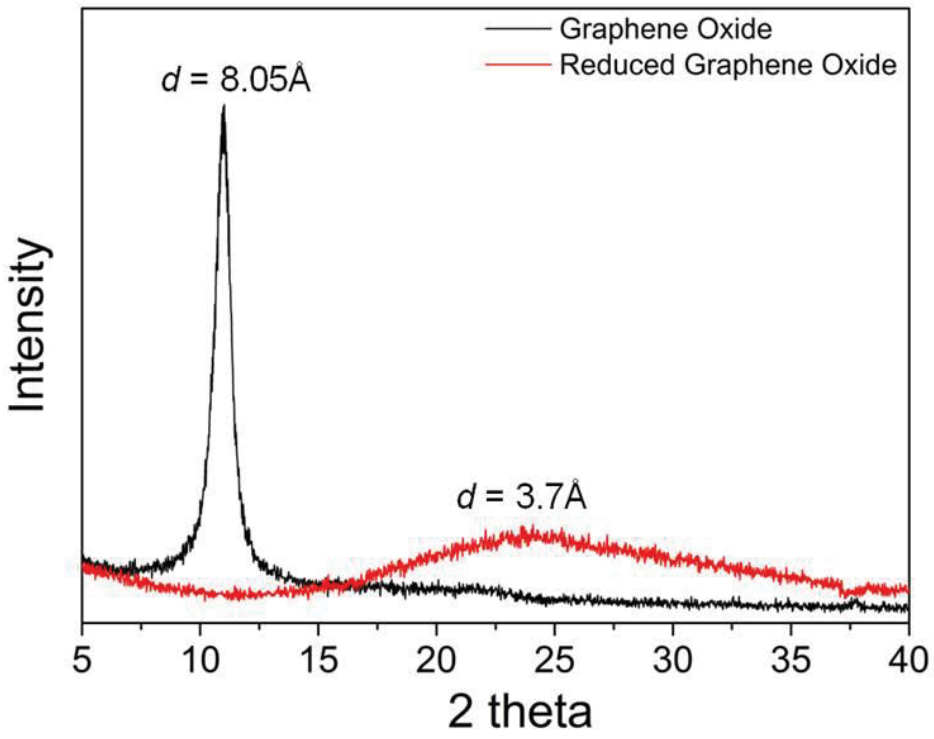

Figure 4.1 X-ray diffraction (XRD) patterns of GO and rGO.

4.3.1.2 Raman spectroscopy of the GO and rGO

Raman spectroscopy is a powerful tool for characterizing crystal structure, disorder and defects in nanocarbon-based materials such as carbon nanotubes (CNTs) and graphene [22]. The Raman spectra of the GO and rGO were depicted in Figure 4.2. The G-band of rGO occurred at 1578 cm^{-1}, which corresponds to the recovery of the hexagonal network of carbon atoms with defects [21]. The increase of I_D/I_G ratio was observed after reduction of GO, indicating that the process of reduction could affect the structure of GO with a high quantity of structural defects and decrease in the average size of the sp^2 domains on the reduction of exfoliated GO [23, 24].

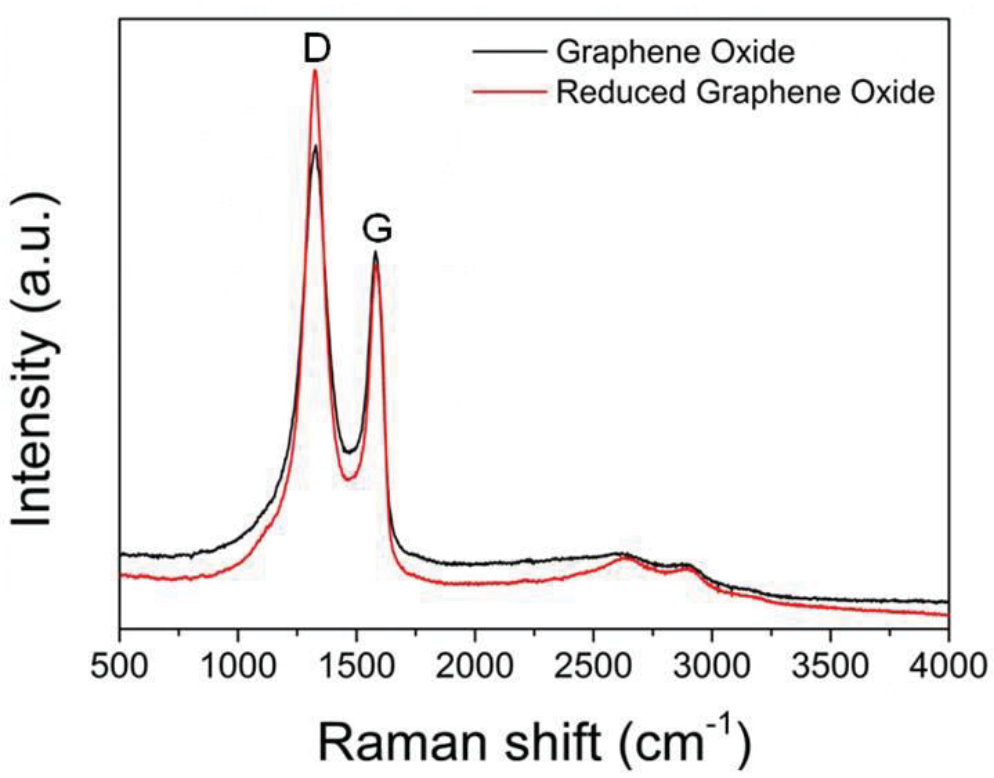

Figure 4.2 Raman spectroscopy of the GO and rGO.

4.3.1.3 X-ray photoelectron spectroscopy (XPS) of the GO and rGO

X-ray photoelectron spectroscopy (XPS) was carried out to examine the element binding configuration in the graphene oxide (GO) and reduced graphene oxide (rGO). Figure 4.3a and c demonstrate XPS survey spectra of rGO and GO, respectively. The C_{1s} and O_{1s} peaks were observed at 287 and 535 eV, respectively. The atomic ratios (O_{1s}/C_{1s}) and peak intensities of the rGO in the Figure 4.3a and b were significantly decreased in comparison with GO. which indicated considerable de-oxygenation by the reduction process [25]. The physical values including XRD, Raman and XPS of GO and rGO were presented in Figure 4.3e.

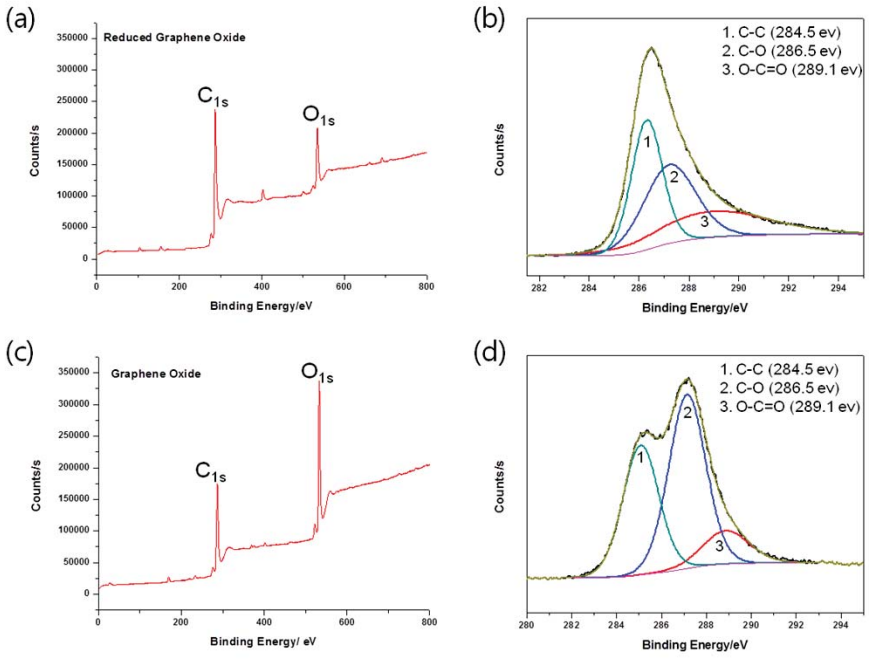

(e)

	XRD	Raman			XPS
	d-spacing (nm)	D band (cm^{-1})	G band (cm^{-1})	I_D/I_G (%)	O_{1s}/C_{1s} (atomic ratio)
GO	8.05	1328	1580	1.27	1.5
rGO	3.7	1326	1578	1.51	0.8

Figure 4.3 The X-ray photoelectron spectroscopy (XPS) of: (a), (b) rGO and (c), (d) GO, (e) physical properties of the GO and rGO.

4.3.2 Optimization of the rGO and SWCNTs ratio

Using the spray coating procedures described above, adherent, robust, reproducible coatings of nanostructured carbons could be obtained on the polyurethane (PU) substrates. To determine the optimal % weight ratios of rGO and SWNT the mixed dispersions were firstly spray coated onto ITO glass using spray coating. CV measurements of the rGO/SWCNTs electrodes with different % ratios of rGO and SWCNTs are presented in Figure 4.4a. The rGO (10%)/SWCNTs (90%) composite electrode showed the largest current in the CV measurements (Fig. 4.4a), which correlated to a specific capacitance of 95 F g^{-1} (Table 4.1). This value was higher than those of the pure SWCNTs (100%) and other electrodes with different % ratios of the rGO/SWCNTs, suggesting that the addition of rGO into SWCNTs at % ratio of 10/90 improves the electroactive surface area and/or conductivity of the electrode. The SWCNTs may assist by preventing re-stacking of the rGO [6, 7]. The capacitance value of the rGO/SWCNTs composite electrode decreased with an increase in the % ratio of rGO, indicating an increase in the internal resistance and/or decrease of the electroactive surface area [7]. The capacitance values correlated with Nyquist plots from impedance measurements that indicated the rGO (10%)/SWCNTs (90%) had the lowest internal resistance (19 Ω), increasing with an increase in the % ratio of rGO (Table 4.1).

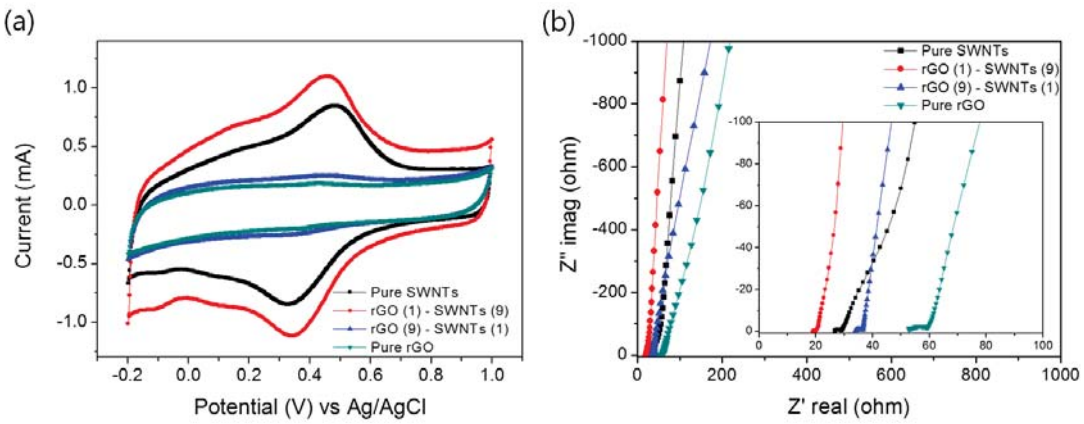

Figure 4.4 Cyclic voltammetry (CV) and Nyquist plot of the rGO/SWCNTs composite on ITO coated glass with different composition between rGO and SWCNTs ; (a) CV of rGO/SWCNTs composite at 100 mV s^{-1} in 1M H_2SO_4, (b) Nyquist plot of the rGO/SWCNTs composite.

Ratio b/w rGO and SWCNTs	Specific capacitance (F g^{-1})	Internal resistance (ohm)
rGO/SWCNTs (10:0)	32 (±2.1, mean±S.D., n=5 electrodes)	53
rGO/SWCNTs (9:1)	35 (±1.8, mean±S.D., n=5 electrodes)	36
rGO/SWCNTs (8:2)	41 (±2.3, mean±S.D., n=5 electrodes)	35
rGO/SWCNTs (5:5)	63 (±2.5, mean±S.D., n=5 electrodes)	32
rGO/SWCNTs (2:8)	79 (±1.9, mean±S.D., n=5 electrodes)	24
rGO/SWCNTs (1:9)	95 (±2.2, mean±S.D., n=5 electrodes)	19
rGO/SWCNTs (0:10)	84 (±2.4, mean±S.D., n=5 electrodes)	27

Table 4.1 Specific capacitance and internal resistance values of the different % ratio rGO/SWCNTs composites on ITO coated glass.

Having established an optimal ratio % of rGO (10%)/SWCNTs (90%), we proceeded to investigate this composite and those of pure rGO (100%) and SWCNTs (100%) when applied to gold-coated polyurethane (PU) substrates. Figure 4.5 describes the process for fabricating these stretchable rGO, SWCNTs and rGO/SWCNTs electrodes via spray coating. To summarize the process, the PU film (10mm x 50mm x 0.2mm) was firstly transferred to a glass microscope slide, stretched to introduce a 100% uniaxial pre-strain and then held under tension using double-sided adhesive tape (Step 1). 150 nm of gold was then coated onto the PU film as a current collector (Step 2).

The gold modified PU film was spray coated with the rGO, SWCNTs and/or rGO/SWCNTs dispersions using a small airbrush (Bunnings, Australia) (Step 3). After spray coating, the composite electrode was dried thoroughly and removed from the glass (Step 4).

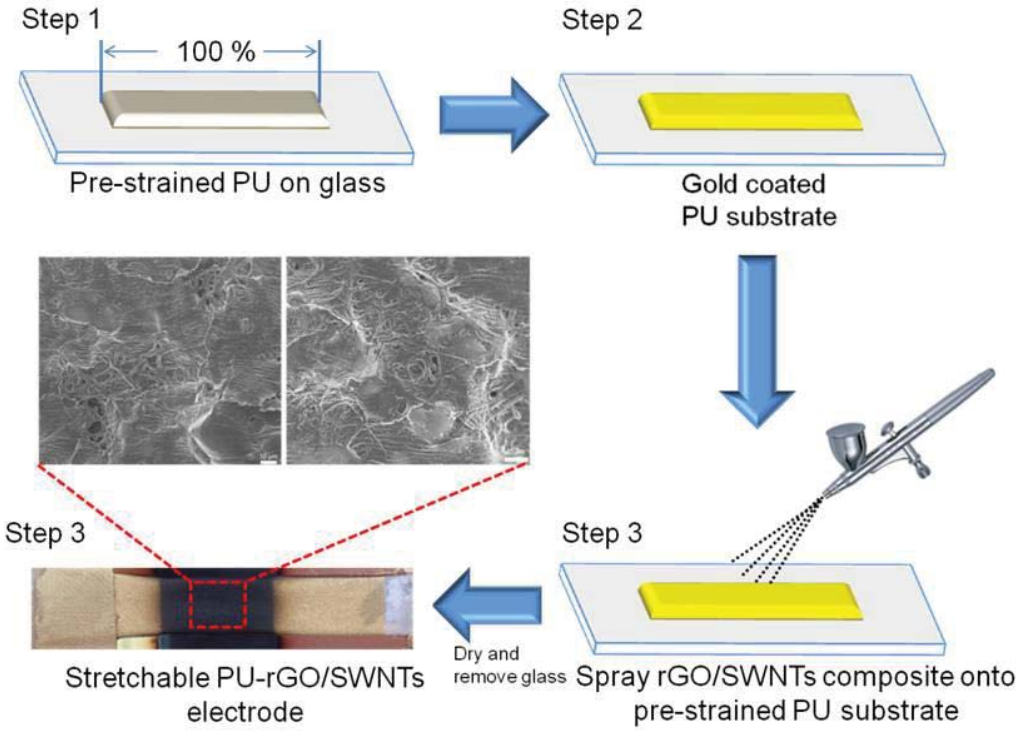

Figure 4.5 Preparation of the stretchable rGO, SWCNTs and rGO/SWCNTs electrode on gold-coated polyurethane via spray coating.

4.3.3 Electrochemical properties

CV measurements were carried out in aqueous 1M H_2SO_4 electrolyte to investigate the electrochemical properties of the 100% rGO, 100% SWCNTs and rGO (10%)/SWCNTs (90%) electrodes as a function of strain (Fig. 4.6) and number of stretching cycles (Fig. 4.7). The redox peaks observed on the CV curves of the SWCNTs and rGO/SWCNTs composite electrodes were attributed to the presence of functional groups (-COOH or -OH) on the carbon nanotubes [13, 26]. In comparison to the rGO/SWCNTs composite electrode, the SWCNTs electrode gave a lower

current and notable distortion of the CV as the level of strain increased to 100% (Fig. 4.6a-e). From these CV measurements, the calculated specific capacitance value of the rGO (10%)/SWCNTs (90%) composite electrode was 148 F g^{-1} under 20 % strain, and this decreased to 115 F g^{-1} under 100 % strain (Fig. 3f). Comparative values for pure rGO and SWCNTs under 100% strain were 31 F g^{-1} and 79 F g^{-1}, respectively.

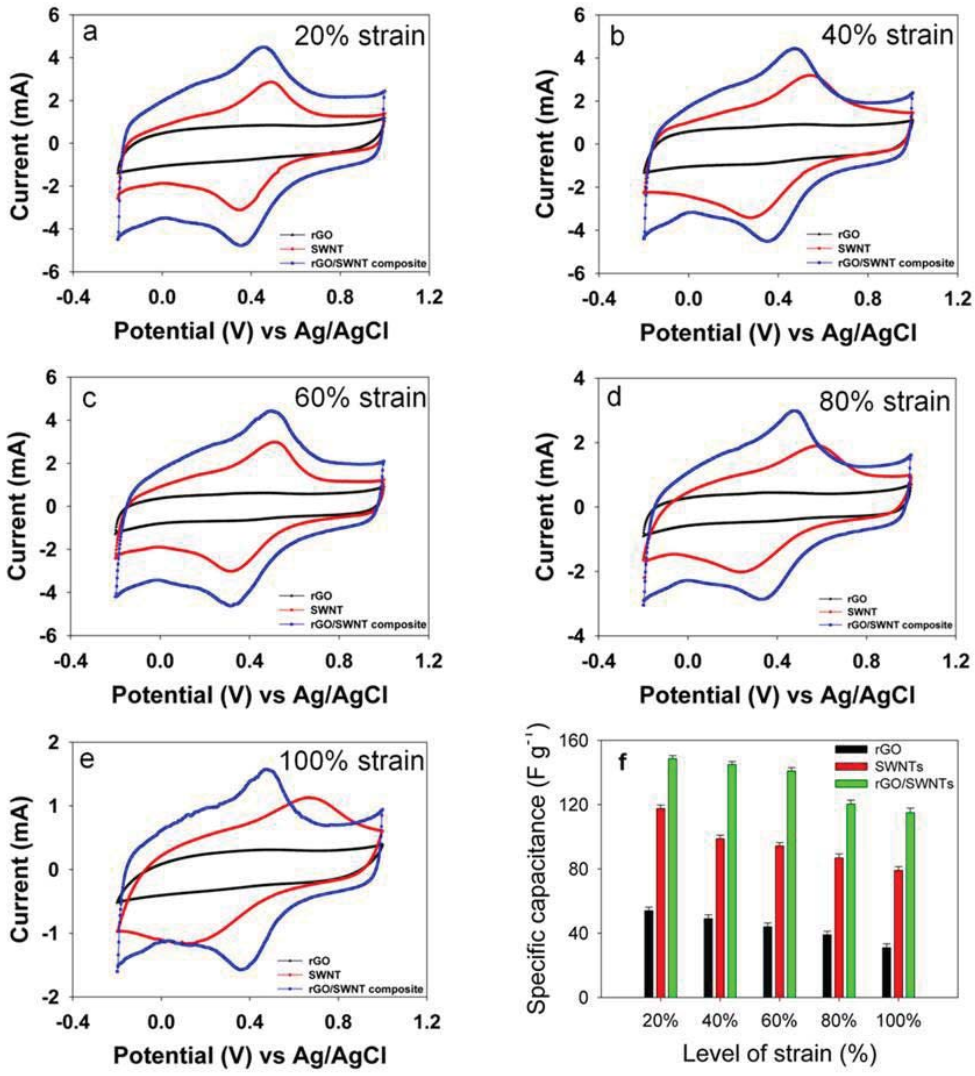

Figure 4.6 Cyclic voltammetry (CV) and specific capacitance of the rGO, SWCNTs and rGO/SWCNTs composite electrode under 20 ~ 100% strain at 100 mV s^{-1} in 1M H_2SO_4; (a) under 20% strain, (b) under 40% strain, (c) under 60% strain, (d) under 80% strain, (e) under 100% strain, (f) comparison of specific capacitance for the rGO, SWCNTs and rGO/SWCNTs composite electrodes.

In Figure 4.7a-c, the rGO/SWCNTs composite electrode also gave the largest current on the CV curves after 50 and 100 stretching cycles. The unstretched rGO (10%)/SWCNTs (90%) composite electrode gave 153 F g^{-1} of specific capacitance at 100 mV s^{-1}, which was higher than the unstretched pure rGO and SWCNTs electrodes that gave values of 60 and 121 F g^{-1}, respectively (Fig. 4.7d). Interestingly, the unstretched rGO (10%)/SWCNTs (90%) composite electrode on PU substrates showed a higher specific capacitance value in comparison rGO (10%)/SWCNTs (90%) composite electrode on ITO coated glass. This was most likely due to the PU substrate's porous fiber structure that has increased the surface area, thus resulting in increased capacitance. The specific capacitance value of the unstretched rGO/SWCNTs composite electrode decreased to 105 F g^{-1} after 100 stretching cycles, which remained higher than values for the pure rGO (40 F g^{-1}) and SWCNTs (77 F g^{-1}) electrode under the same conditions (Fig. 4.7d).

Electrochemical impedance spectroscopy (EIS) was carried out to obtain insight into the electrochemical interfacial properties of the rGO, SWCNTs and rGO/SWCNTs electrodes as a function of strain (Figure 4.8) and stretching (Figure 4.9). In the complex plain, the Z'' imag part indicated the imaginary capacitive property that was dependent on the frequency and real component, while the Z' Re part related to the ohmic properties of the electrode. The Nyquist plot of the supercapacitor can be divided into three regimes based on the measurement frequency (nb: All of the measurements have been carried out in the frequency between 0.01 Hz and 100 KHz).

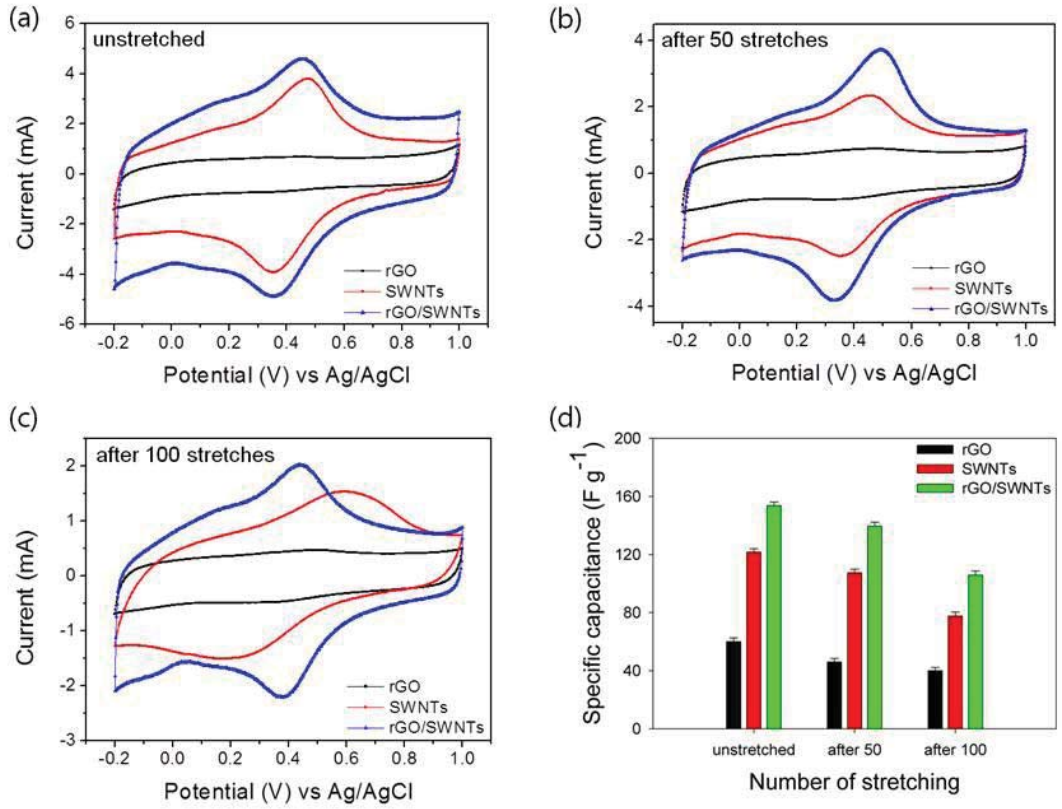

Figure 4.7 Cyclic voltammetry (CV) and specific capacitance of the rGO, SWCNTs and rGO/SWCNTs composite electrodes after 0, 50 and 100 stretching at 100 mV s^{-1} in 1M H_2SO_4; (a) unstretched electrodes, (b) after 50 stretchings, (c) after 100 stretchings, (d) comparison of specific capacitance for the rGO, SWCNTs and rGO/SWCNTs composite electrodes.

At low frequencies, the Z" imag (imaginary part) increased linearly to indicate pristine capacitive behavior of the electrode [27]. The middle frequency regime, termed the Warburg region [28, 29], is related to diffusion of the electrolyte within the electrode and infers on the extent of electrode porosity. Under fixed 20 ~ 100 % strain (Fig. 4.8a-e) and after 50 (Fig. 4.9b) and 100 (Fig. 4.9c) stretching cycles, the length of the Warburg region increased for all electrode types. The rGO (10%)/SWCNTs (90%) electrode showed the smallest Warburg region under all strain and stretching conditions, indicating that the rGO (10%)/SWCNTs (90%) composite electrode had

enhanced accessibility of ions within the composite electrode structure [7, 8]. Whilst a difference in this regime between pure SWCNTs and rGO (10%)/SWCNTs (90%) electrodes was difficult to distinguish, the length of the Warburg region for the pure rGO was significantly longer when unstretched (Fig. 4.9a). In the high frequency domain, the presence of a semicircular region defined the ability for ions to diffuse between the electrolyte/electrode interface. This semicircular region for all electrode types was observed to be negligible when under fixed 20 ~ 100 % strain (Fig. 4.8a-e), and unstretched (Fig. 4.9a), and after 50 (Fig. 4.9b) to 100 (Fig. 4.9c) stretching cycles. However, the internal resistance, corresponding to Z real value on the x-axis, of the rGO (10%)/SWCNTs (90%) electrode was lower in comparison with rGO and SWCNTs electrodes after strain and stretching cycles (see insets, Z' real-axis, in Figures 4.8 and 4.9). More specifically, the internal resistance of the unstretched rGO (10%)/SWCNTs (90%) electrode was calculated to be 3.3 Ω, which increased to 18 Ω and 14 Ω under 100% strain (Fig. 4.8e) and after 100 stretching cycles (Fig. 4.9c), respectively.

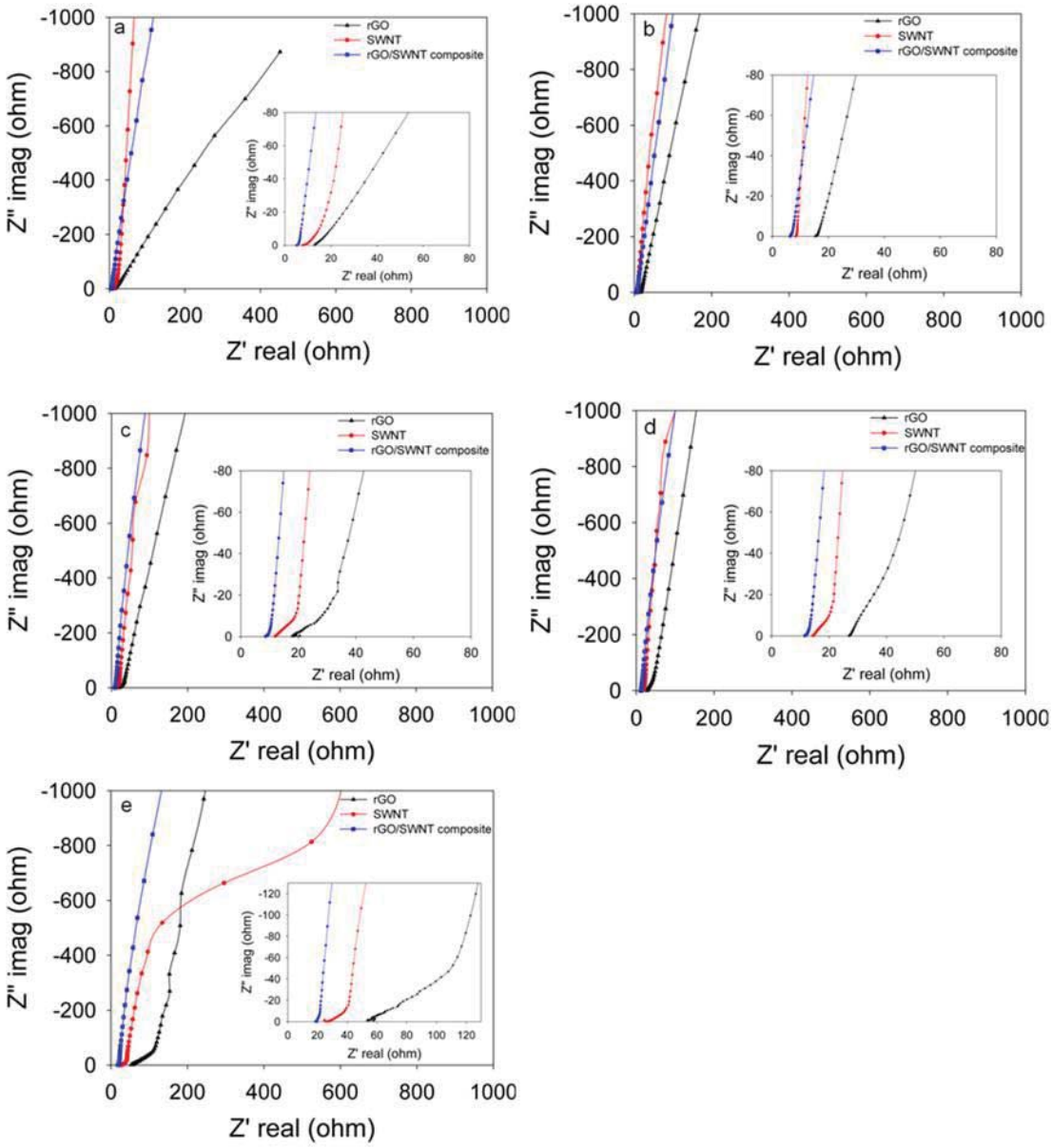

Figure 4.8 Nyquist plots of the rGO, SWCNTs and rGO/SWCNTs composite electrodes; (a) under 20% strain, (b) under 40% strain, (c) under 60% strain, (d) under 80% strain and (e) under 100% strain.

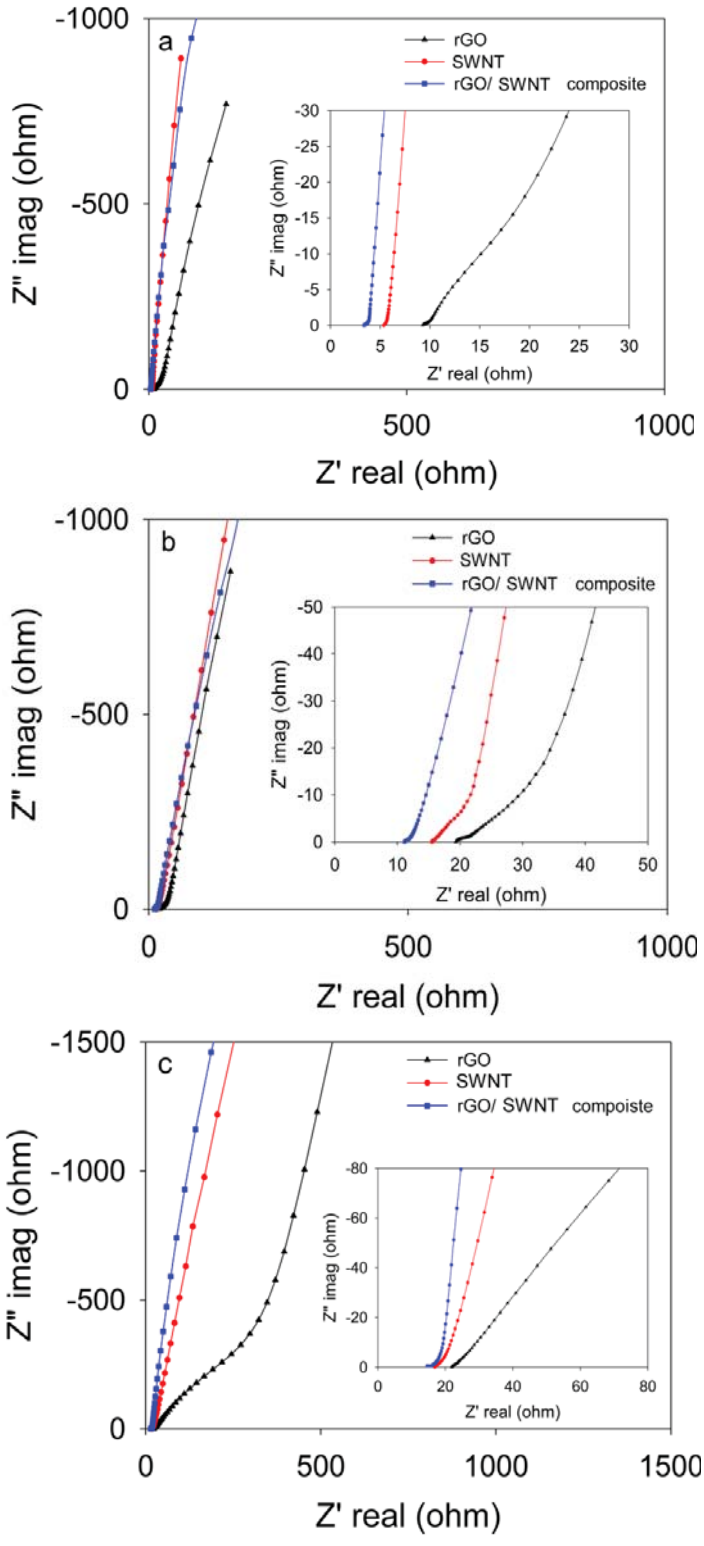

Figure 4.9 Nyquist plots of the rGO, SWCNTs and rGO/SWCNTs composite electrodes; (a) unstretched electrodes, (b) after 50 stretchings, (c) after 100 stretchings.

Galvanostatic charge/discharge curves of the rGO, SWCNTs and rGO (10%)/SWCNTs (90%) electrodes as a function of strain (Fig. 4.10) and stretching (Fig. 4.11) were demonstrated with a constant current density of 1 A g^{-1} up to one cycle. The charge/discharge curves of the rGO, SWCNTs and rGO (10%)/SWCNTs (90%) electrodes showed a symmetrical shape during the charge/discharge process, indicating good capacitive behavior of all electrode types. A longer discharge cycle time indicated that a higher amount of charge could be stored in the electrode with measurement under constant current [13], suggesting that the highly conductive rGO (10%)/SWCNTs (90%) electrode created a pathway for the transfer of ions and electrons, thus reducing internal resistance [30, 31]. In comparison to pure rGO and SWCNTs electrodes, the rGO (10%)/SWCNTs (90%) electrode gave the longest discharge time under 20 ~ 100% strain (Fig. 4.10a-e) and after 50 (Fig. 4.11b), 100 (Fig. 4.11c) stretching cycles. The discharge time of the rGO/SWCNTs electrode decreased with increased level of strain (Fig. 4.10) and stretching cycles (Fig. 4.11).

Hereafter, we focused on the electrochemical properties of the optimal rGO (10%)/SWCNTs (90%) electrode as a function of strain and stretching, particularly at different scan rates (Fig. 4.12) and number of CV cycles (Fig. 4.13). Firstly, Figure 4.12a and b show previous CV measurements of the rGO (10%)/SWCNTs (90%) electrode superimposed to directly compare the effect of the levels of strain (Fig. 4.12a) and different stretching conditions (Fig. 4.12b) This enabled clear observation of the decrease in CV current and capacitance as a function of strain and stretching, with no significant distortion of the CV. As mentioned, specific capacitance versus scan rate was also plotted for the rGO/SWCNTs composite electrode as a function of strain (Figure 4.12c) and stretching (Fig. 4.12d). The highest capacitance value obtained for the unstretched rGO/SWCNTs electrode was 265 F g^{-1} in 1 M H_2SO_4 at 5

mV s^{-1} (Fig. 4.12d). This capacitance value of the unstretched rGO/SWCNTs electrode decreased to 147 ± 4.8 (mean ± S.D., n = 10 electrodes) F g^{-1} at 5 mV s^{-1} under the maximum strain level of 100% (Fig. 4.12c). At the same scan rate of 5 mV s^{-1}, the specific capacitance of the unstretched rGO/SWCNTs composite electrode decreased to 219 and 162 F g^{-1} after 50 and 100 stretches, respectively (Fig. 4.12d).

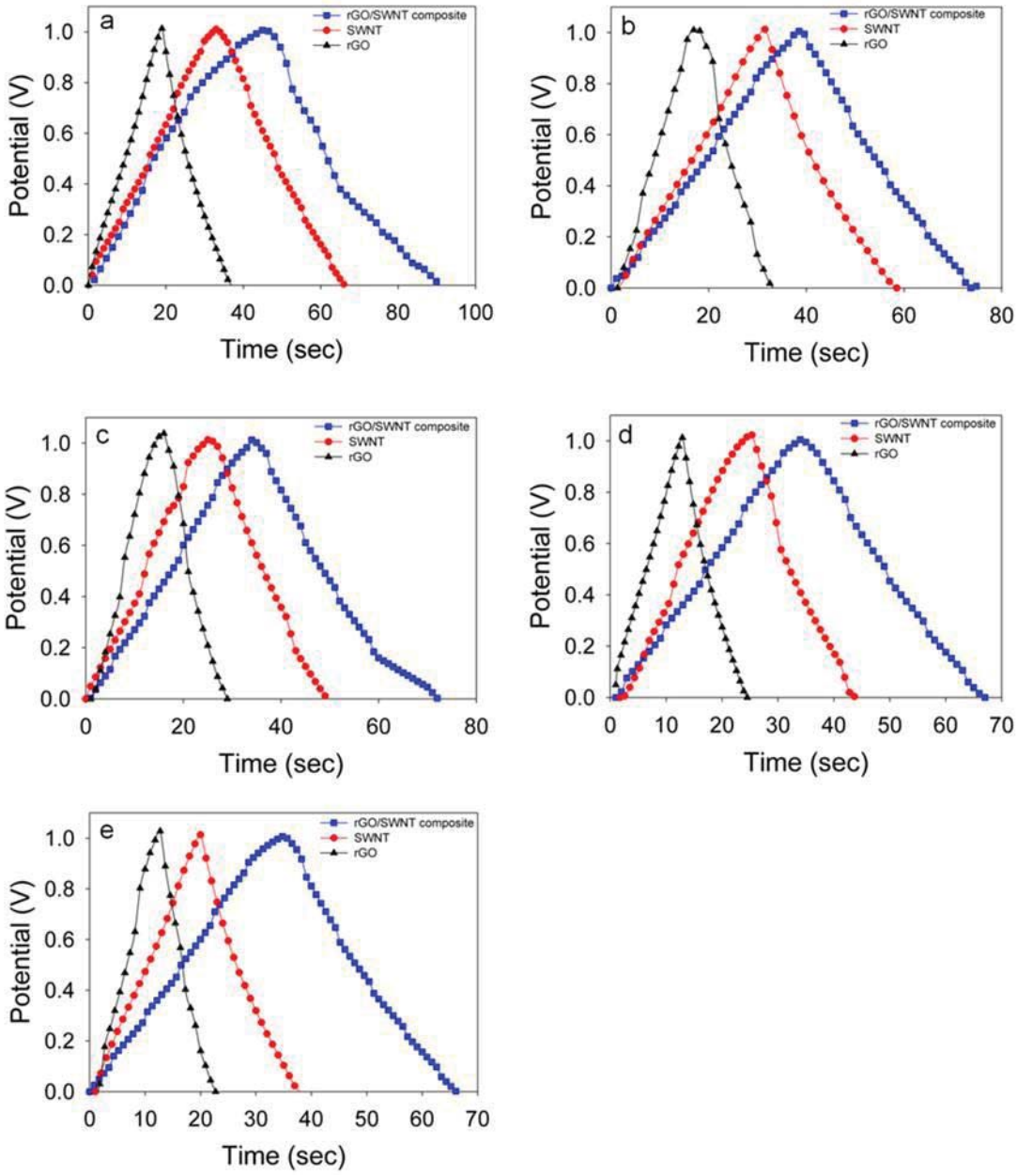

Figure 4.10 Galvanostatic charge/discharge curves of the rGO, SWCNTs and rGO/SWCNTs composite electrodes at a constant current of 1 A g^{-1} in 1M H_2SO_4; (a) under 20% strain, (b) under 40% strain, (c) under 60% strain, (d) under 80% strain and (e) under 100% strain.

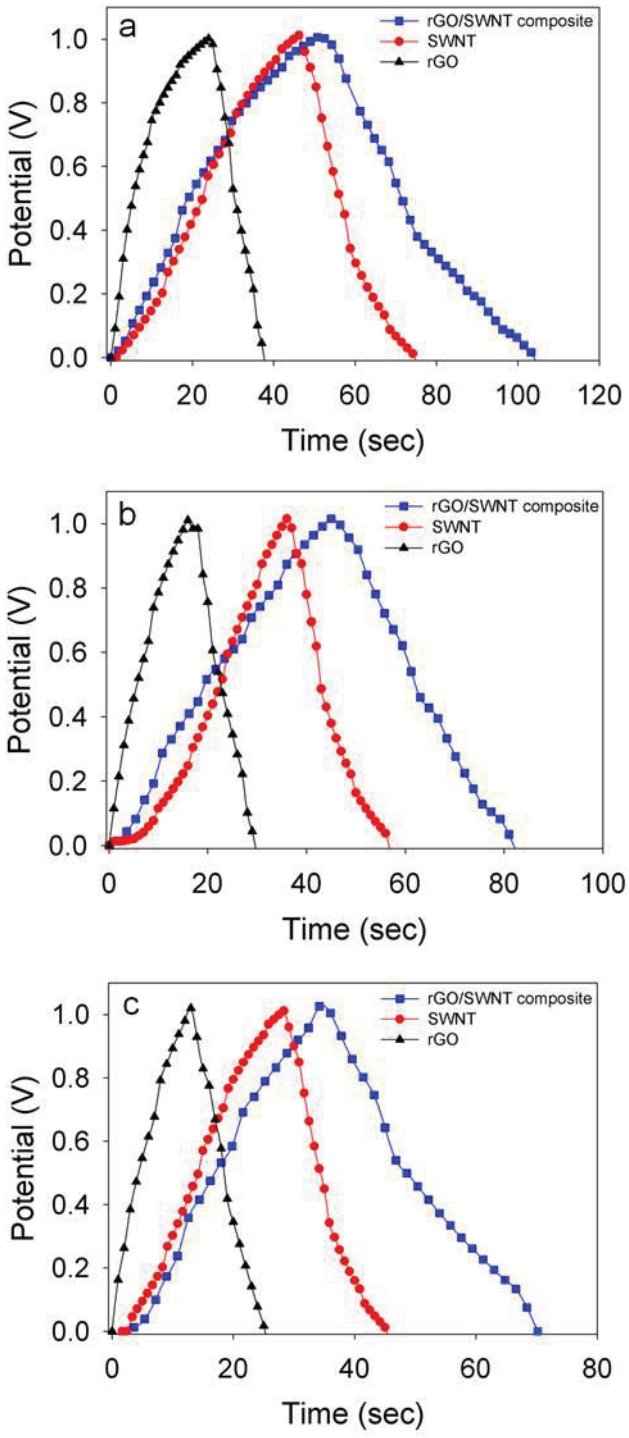

Figure 4.11 Galvanostatic charge/discharge curves of the rGO, SWCNTs and rGO/SWCNTs composite electrodes at a constant current (1 A g^{-1}) in 1M H_2SO_4; (a) unstretched electrodes, (b) after 50 stretchings, (c) after 100 stretchings.

Hereafter, we focused on the electrochemical properties of the optimal rGO (10%)/SWCNTs (90%) electrode as a function of strain and stretching, particularly at different scan rates (Fig. 4.12) and number of CV cycles (Fig. 4.13). Firstly, Figure 4.12a and b show previous CV measurements of the rGO (10%)/SWCNTs (90%) electrode superimposed to directly compare the effect of the levels of strain (Fig. 4.12a) and different stretching conditions (Fig. 4.12b) This enabled clear observation of the decrease in CV current and capacitance as a function of strain and stretching, with no significant distortion of the CV. As mentioned, specific capacitance versus scan rate was also plotted for the rGO/SWCNTs composite electrode as a function of strain (Figure 4.12c) and stretching (Fig. 4.12d). The highest capacitance value obtained for the unstretched rGO/SWCNTs electrode was 265 F g^{-1} in 1 M H_2SO_4 at 5 mV s^{-1} (Fig. 4.12d). This capacitance value of the unstretched rGO/SWCNTs electrode decreased to 147 ± 4.8 (mean ± S.D., n = 10 electrodes) F g^{-1} at 5 mV s^{-1} under the maximum strain level of 100% (Fig. 4.12c). At the same scan rate of 5 mV s^{-1}, the specific capacitance of the unstretched rGO/SWCNTs composite electrode decreased to 219 and 162 F g^{-1} after 50 and 100 stretches, respectively (Fig. 4.12d).

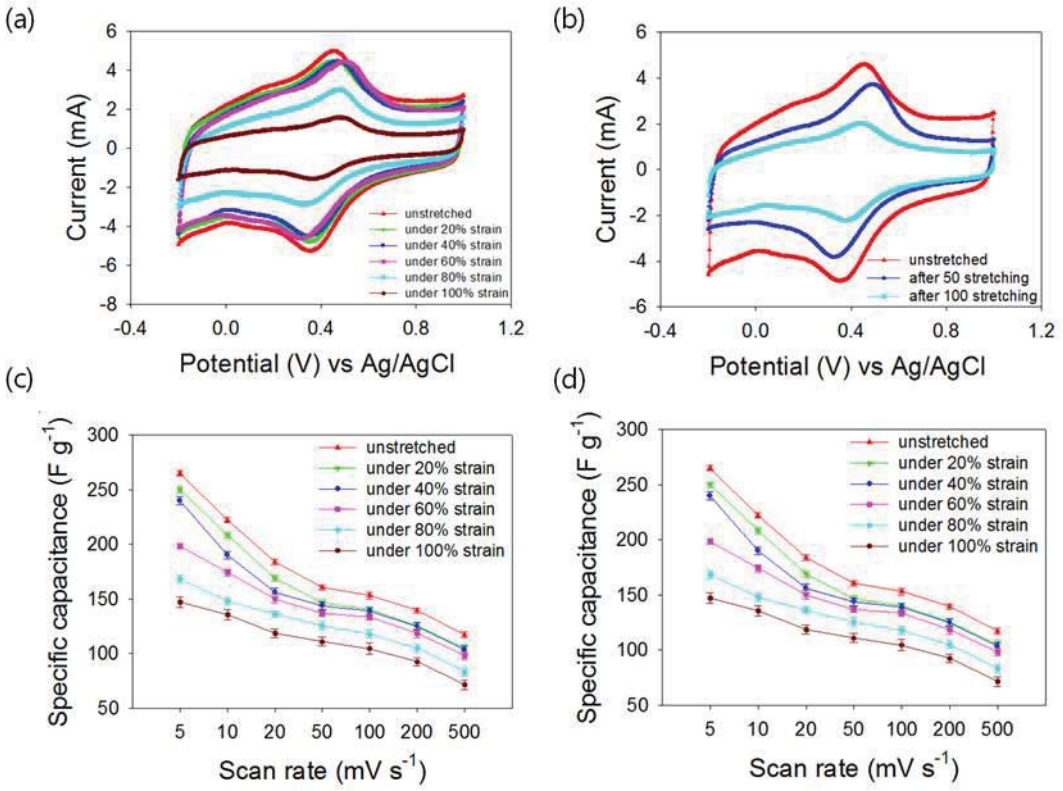

Figure 4.12 Cyclic voltammetry (CV) and specific capacitance of the rGO/SWCNTs composite electrodes as a function of stretching and strain in 1M Na_2SO_4 at 5 ~ 500 mV s^{-1} scan rates; (a) after various stretching (0, 50 and 100 times stretching at 100 mV s^{-1} scan rate), (b) under various strain percentage (0 ~100% strain at 100 mV s^{-1} scan rate), (c) specific capacitance after various stretching (0, 50 and 100 times stretching at 5 ~ 500 mV s^{-1} scan rates), (d) specific capacitance under various strain percentage (0 ~100% strain at 5~500 mV s^{-1} scan rates).

We also investigated the electrochemical stability of the rGO (10%)/SWCNTs (90%) electrode whereby the electrodes were subjected to 1000 CV cycles in the unstretched condition (Fig. 4.13a), then another 1000 CV cycles after applying 50 stretches (Fig. 4.13b) and finally another 1000 CV cycles after 100 stretching cycles (Fig. 4.13c), with all stretching done at 100% strain. Therefore, an electrode had been subjected to a total of 100 stretches and 3000 CV cycles at the conclusion of the measurement. For comparison, CV's at the 1st, 500th and 1000th (unstretched, Figure 10a), 1000th, 1500th

and 2000th cycle (50 stretches, Figure 10b) and 2000th, 2500th and 3000th cycle (100 stretches, Figure 4.13c) are shown in Figure 4.13. Under each stretching condition, there was only a small decrease in CV current with an increase in the number of CV cycles. Furthermore, the rate of change in capacitance as a function of CV cycle number did not significantly change as the electrode underwent more stretching cycles, which was similar to our previous study of SWCNTs spray coated on latex substrates [13].

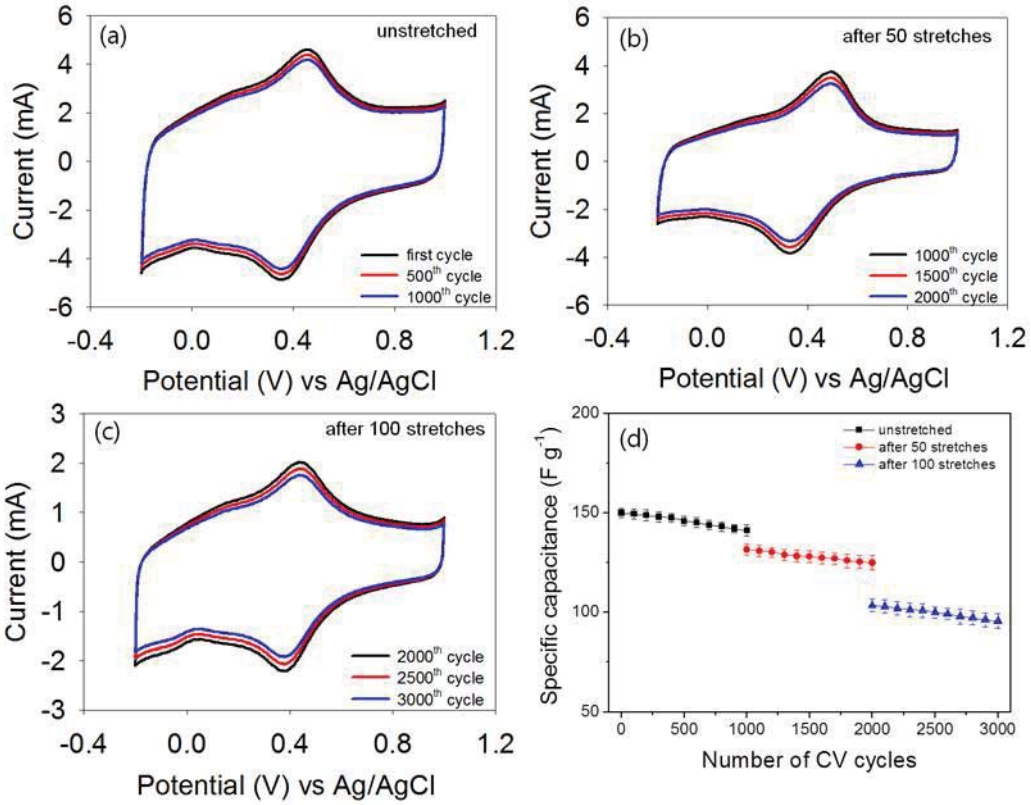

Figure 4.13 Stability and specific capacitance of the rGO/SWCNTs composite electrode as a function of CV cycles and stretching in 1M Na_2SO_4 at 100 mV s^{-1}; (a) unstretched, (b) after 50 stretchings, (c) after 100 stretchings, (d) specific capacitance as a function of CV cycles (0~1000th cycles).

4.3.4 Morphological study of the rGO/SWCNTs composite film on the PU

To better understand the structural-dependent electrochemical properties of the rGO/SWCNTs composite electrode versus the pure rGO electrode, a cross-sectional SEM image of the two different types of electrodes are shown in Figure 4.14. The pristine rGO appeared to show re-stacking of the rGO layers and a less-expanded structure (Fig. 4.14a). In contrast, the rGO (10%) /SWCNTs (90%) composite showed an expanded structure with SWCNTs between, and running perpendicular to, the rGO layers (Fig. 4.14b). This latter morphology suggested that the SWCNTs may have acted as a 'spacer' and binder between the rGO to prevent its re-stacking, further enhancing the accessibility of ions into the rGO layers. The presence of the SWCNTs, as a conducting additive between the rGO layers, may also have reduced the internal resistance between the electrode and electrolyte, leading to enhanced diffusion of electrolyte and conductive pathways across the electrode/electrolyte interface [7].

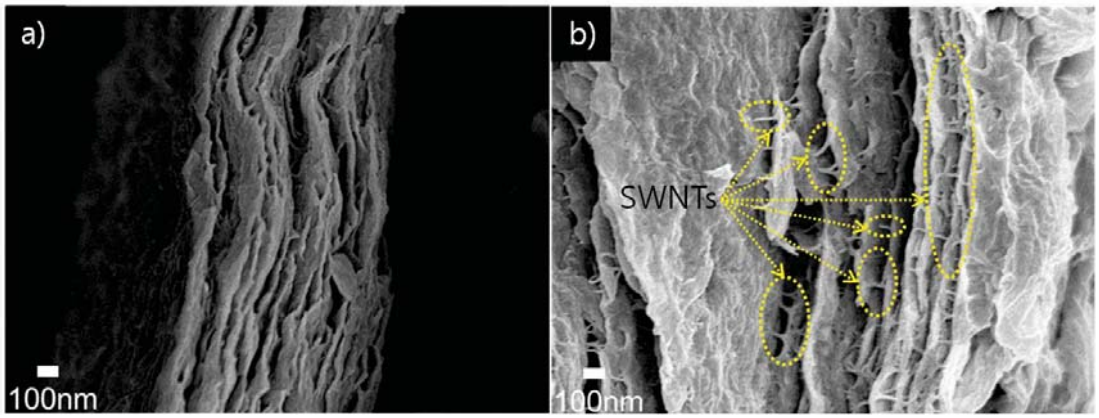

Figure 4.14 SEM images of the pristine rGO and rGO (10%) / SWCNTs (90%) composite; (a) rGO, (b) rGO/SWCNTs composite.

The effect of strain and stretching on the rGO/SWCNTs electrodes are evident in SEM images taken from two different regions (Figure 4.15). Firstly, the surface morphology of the unstretched rGO/SWCNTs electrode has a porous fiber structure (Fig. 4.15a and 4.15c). However, cracks were evident on the rGO/SWCNTs composite film after 100 stretches done at 100% strain (Fig. 4.15b and d). The introduction of repeated strain thus resulted in the formation of cracks on the rGO/SWCNTs composite films that are likely to have caused a decrease in electrical conductivity and observed capacitance shown in Figures 4.6 and 4.7. The cracks may also have caused an irreversible loss of junctions between the rGO/SWCNTs electrode and electrolyte. [32].

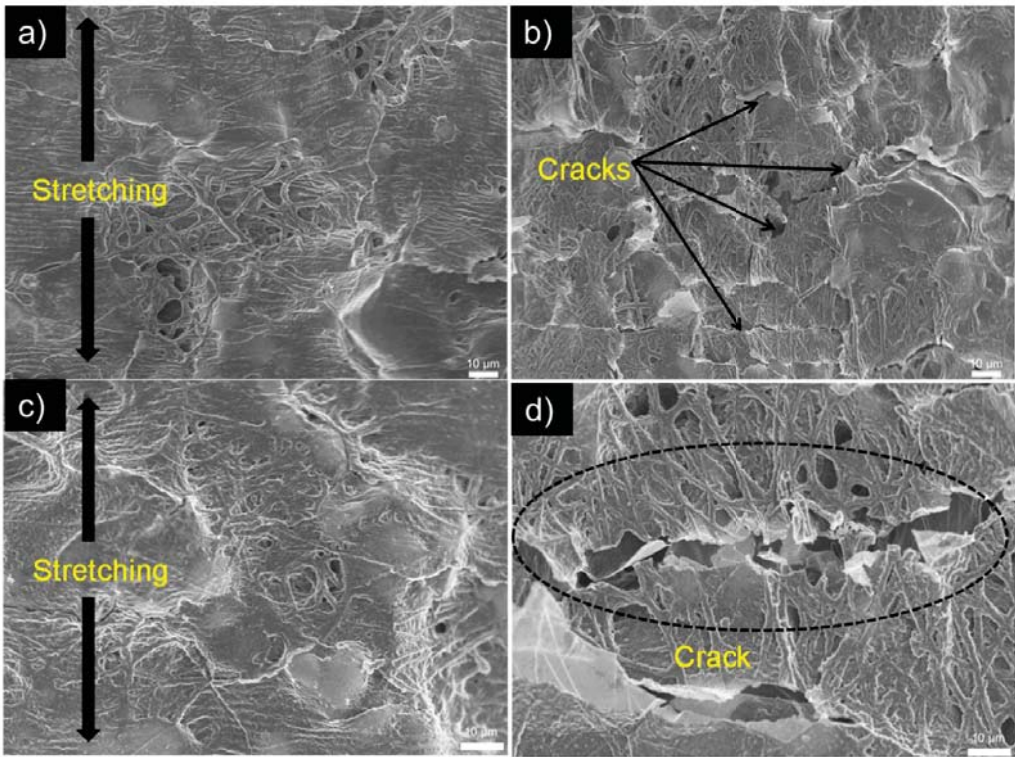

Figure 4.15 SEM images of the rGO/SWCNTs film on the polyurethane (PU); (a), (c) unstretched rGO/SWCNTs film on the PU and (b), (d) rGO/SWCNTs film on the PU after 100 stretchings with application of 100% strain.

4.4 CONCLUSIONS

We have successfully fabricated highly stretchable rGO (10%)/SWCNTs (90%) electrodes via a spray coating technique. The electrochemical properties of the rGO (10%)/SWCNTs (90%) electrodes were characterized by cyclic voltammetry (CV), impedance and charge/discharge measurements. The rGO (10%)/SWCNTs (90%) electrodes showed good capacitive behavior under various strains even after repetitive stretching to 100%. The highest capacitance value obtained for the rGO (10%)/SWCNTs (90%) electrode was 265 F g^{-1} in 1 M H_2SO_4 at 5 mV s^{-1}. Approximately 65% of the initial capacitance for the unstretched rGO (10%)/SWCNTs (90%) electrode was retained after 100 stretching cycles under 100% strain and was then maintained at this level up to the application of the 3000^{th} CV cycle. SEM images suggested the observed decline in capacitance as a function of stretching and strain was due to the appearance of cracks on the rGO (10%)/SWCNTs (90%) electrodes. The high surface area, high stability and stretchability of the rGO (10%)/SWCNTs (90%) composites , in addition to the scalable method of deposition on the electrode, demonstrate that this kind of highly stretchable electrode has potential advantages for scaling up which offers new possibilities for wearable and biocompatible devices.

4.5 REFERENCES

[1] D.-H. Kim, N. Lu, R. Ma, Y.-S. Kim, R.-H. Kim, S. Wang, J. Wu, S. M. Won, H. Tao, A. Islam, K. J. Yu, T.-i. Kim, R. Chowdhury, M. Ying, L. Xu, M. Li, H.-J. Chung, H. Keum, M. McCormick, P. Liu, Y.-W. Zhang, F. G. Omenetto, Y. Huang, T. Coleman, and J. A. Rogers, "Epidermal Electronics," *Science,* vol. 333, pp. 838-843, August 12, 2011 2011.

[2] T. Sekitani, H. Nakajima, H. Maeda, T. Fukushima, T. Aida, K. Hata, and T. Someya, "Stretchable active-matrix organic light-emitting diode display using printable elastic conductors," *Nature materials,* vol. 8, pp. 494-499, 2009.

[3] J. Viventi, D.-H. Kim, L. Vigeland, E. S. Frechette, J. A. Blanco, Y.-S. Kim, A. E. Avrin, V. R. Tiruvadi, S.-W. Hwang, and A. C. Vanleer, "Flexible, foldable, actively multiplexed, high-density electrode array for mapping brain activity in vivo," *Nature neuroscience,* vol. 14, pp. 1599-1605, 2011.

[4] J. A. Rogers, T. Someya, and Y. Huang, "Materials and mechanics for stretchable electronics," *Science,* vol. 327, pp. 1603-1607, 2010.

[5] P. J. Hall and E. J. Bain, "Energy-storage technologies and electricity generation," *Energy Policy,* vol. 36, pp. 4352-4355, 2008.

[6] D. Antiohos, M. S. Romano, J. M. Razal, S. Beirne, P. Aitchison, A. I. Minett, G. G. Wallace, and J. Chen, "Performance enhancement of single-walled nanotube–microwave exfoliated graphene oxide composite electrodes using a stacked electrode configuration," *Journal of Materials Chemistry A,* 2014.

[7] Q. Cheng, J. Tang, J. Ma, H. Zhang, N. Shinya, and L.-C. Qin, "Graphene and carbon nanotube composite electrodes for supercapacitors with ultra-high energy density," *Physical Chemistry Chemical Physics,* vol. 13, pp. 17615-17624, 2011.

[8] D. Yu and L. Dai, "Self-assembled graphene/carbon nanotube hybrid films for supercapacitors," *The Journal of Physical Chemistry Letters,* vol. 1, pp. 467-470, 2009.

[9] D.-H. Kim, J.-H. Ahn, W. M. Choi, H.-S. Kim, T.-H. Kim, J. Song, Y. Y. Huang, Z. Liu, C. Lu, and J. A. Rogers, "Stretchable and Foldable Silicon Integrated Circuits," *Science,* vol. 320, pp. 507-511, April 25, 2008 2008.

[10] X. Li, T. Gu, and B. Wei, "Dynamic and Galvanic Stability of Stretchable Supercapacitors," *Nano Letters,* vol. 12, pp. 6366-6371, 2012/12/12 2012.

[11] L. L. Zhang, R. Zhou, and X. S. Zhao, "Graphene-based materials as supercapacitor electrodes," *Journal of Materials Chemistry,* vol. 20, pp. 5983-5992, 2010.

[12] T. Sekitani, Y. Noguchi, K. Hata, T. Fukushima, T. Aida, and T. Someya, "A Rubberlike Stretchable Active Matrix Using Elastic Conductors," *Science,* vol. 321, pp. 1468-1472, September 12, 2008 2008.

[13] H. T. Jeong, B. C. Kim, R. Gorkin, M. J. Higgins, and G. G. Wallace, "Capacitive behavior of a stretchable single-wall carbon nanotube on latex electrode," *Electrochimica Acta,* 2014.

[14] C. Yu, C. Masarapu, J. Rong, B. Wei, and H. Jiang, "Stretchable Supercapacitors Based on Buckled Single-Walled Carbon-Nanotube Macrofilms," *Advanced Materials,* vol. 21, pp. 4793-4797, 2009.

[15] J. Oh, M. E. Kozlov, B. G. Kim, H.-K. Kim, R. H. Baughman, and Y. H. Hwang, "Preparation and electrochemical characterization of porous SWNT–PPy nanocomposite sheets for supercapacitor applications," *Synthetic Metals,* vol. 158, pp. 638-641, 2008.

[16] M. Pasta, F. La Mantia, L. Hu, H. D. Deshazer, and Y. Cui, "Aqueous supercapacitors on conductive cotton," *Nano research,* vol. 3, pp. 452-458, 2010.

[17] S. Ugur, Ö. Yargi, and Ö. Pekcan, "Conductivity percolation of carbon nanotubes (CNT) in polystyrene (PS) latex film," *Canadian Journal of Chemistry,* vol. 88, pp. 267-276, 2010.

[18] Z. Fan, J. Yan, L. Zhi, Q. Zhang, T. Wei, J. Feng, M. Zhang, W. Qian, and F. Wei, "A Three-Dimensional Carbon Nanotube/Graphene Sandwich and Its Application as Electrode in Supercapacitors," *Advanced Materials,* vol. 22, pp. 3723-3728, 2010.

[19] S. Park, J. An, R. D. Piner, I. Jung, D. Yang, A. Velamakanni, S. T. Nguyen, and R. S. Ruoff, "Aqueous Suspension and Characterization of Chemically Modified Graphene Sheets," *Chemistry of Materials,* vol. 20, pp. 6592-6594, 2008/11/11 2008.

[20] M. K. Shin, B. Lee, S. H. Kim, J. A. Lee, G. M. Spinks, S. Gambhir, G. G. Wallace, M. E. Kozlov, R. H. Baughman, and S. J. Kim, "Synergistic toughening of composite fibres by self-alignment of reduced graphene oxide and carbon nanotubes," *Nature communications,* vol. 3, p. 650, 2012.

[21] I. K. Moon, J. Lee, R. S. Ruoff, and H. Lee, "Reduced graphene oxide by chemical graphitization," *Nature communications,* vol. 1, p. 73, 2010.

[22] G. Sobon, J. Sotor, J. Jagiello, R. Kozinski, M. Zdrojek, M. Holdynski, P. Paletko, J. Boguslawski, L. Lipinska, and K. M. Abramski, "Graphene oxide vs. reduced graphene oxide as saturable absorbers for Er-doped passively mode-locked fiber laser," *Optics express,* vol. 20, pp. 19463-19473, 2012.

[23] S. Stankovich, D. A. Dikin, R. D. Piner, K. A. Kohlhaas, A. Kleinhammes, Y. Jia, Y. Wu, S. T. Nguyen, and R. S. Ruoff, "Synthesis of graphene-based nanosheets via chemical reduction of exfoliated graphite oxide," *Carbon,* vol. 45, pp. 1558-1565, 2007.

[24] F. Tuinstra and J. L. Koenig, "Raman spectrum of graphite," *The Journal of Chemical Physics,* vol. 53, pp. 1126-1130, 1970.

[25] Z. Xu and C. Gao, "In situ polymerization approach to graphene-reinforced nylon-6 composites," *Macromolecules,* vol. 43, pp. 6716-6723, 2010.

[26] J. N. Barisci, G. G. Wallace, and R. H. Baughman, "Electrochemical Characterization of Single-Walled Carbon Nanotube Electrodes," *Journal of the electrochemical society,* vol. 147, pp. 4580-4583, 2000.

[27] H. Kurig, A. Jänes, and E. Lust, "Electrochemical Characteristics of Carbide-Derived Carbon | 1 -Ethyl-3-methylimidazolium Tetrafluoroborate Supercapacitor Cells," *Journal of The Electrochemical Society,* vol. 157, pp. A272-A279, March 1, 2010 2010.

[28] T. Y. Kim, H. W. Lee, M. Stoller, D. R. Dreyer, C. W. Bielawski, R. S. Ruoff, and K. S. Suh, "High-Performance Supercapacitors Based on Poly(ionic liquid)-Modified Graphene Electrodes," *ACS Nano,* vol. 5, pp. 436-442, 2011/01/25 2010.

[29] C. Portet, P. Taberna, P. Simon, and C. Laberty-Robert, "Modification of Al current collector surface by sol–gel deposit for carbon–carbon supercapacitor applications," *Electrochimica Acta,* vol. 49, pp. 905-912, 2004.

[30] K. H. An, K. K. Jeon, J. K. Heo, S. C. Lim, D. J. Bae, and Y. H. Lee, "High-Capacitance Supercapacitor Using a Nanocomposite Electrode of Single-Walled Carbon Nanotube and Polypyrrole," *Journal of The Electrochemical Society,* vol. 149, pp. A1058-A1062, August 1, 2002 2002.

[31] Y. Show and K. Imaizumi, "Decrease in equivalent series resistance of electric double-layer capacitor by addition of carbon nanotube into the activated carbon electrode," *Diamond and related materials,* vol. 15, pp. 2086-2089, 2006.

[32] S. Prabaharan, R. Vimala, and Z. Zainal, "Nanostructured mesoporous carbon as electrodes for supercapacitors," *Journal of Power Sources,* vol. 161, pp. 730-736, 2006.

CHAPTER 5

STRETCHABLE LATEX AND POLYURETHANE (PU) SUPERCAPACITOR COMPOSED OF REDUCED GRAPHENE OXIDE (RGO)/SINGLE-WALL CARBON NANOTUBES ($SWCNT_S$) COMPOSITE ELECTRODE

5.1 INTRODUCTION

Stretchable electronics such as wearable, biomedical devices and wireless sensors have gained considerable attention from scientific and technological communities owing to their promising applications including, epidermal electronics [1], pressure and strain sensor [2-4], transistor [5-7], organic light emitting diode (OLED) devices [8, 9], electronic eyes [10], radio frequency (RF) devices [11], and interconnects [12].

To accommodate the needs of the emerging stretchable electronics, stretchable power source devices such as supercapacitors are a key component.[13]. Supercapacitors as energy-storage devices have been intensively studied due to their high specific power density, durability, safety and long cycle life in comparison with conventional batteries [14-16]. In addition, there has been interest in using carbon-based materials for supercapacitor electrodes due to several advantages, including high electrical conductivity, chemical stability, large surface area and light weight [17-20]. Stretchable carbon-based electrodes for energy-storage devices that have been previously reported include buckled single wall carbon nanotubes (SWCNTs) macrofilms [21] and graphene [22]. Li *et al* [23] developed a new type of stretchable supercapacitor based on SWCNTs that had been chemical vapour deposited onto pre-strained poly(dimethylsiloxane) (PDMS). The buckled SWCNTs supercapacitor

obtained upon release of the strain applied to the PDMS substrate exhibited 50 F g^{-1} at 31.5 % applied strain. Chen *et al.* [24] have similarly introduced a stretchable supercapacitor based on wrinkled graphene on a PDMS substrate and a PVA/H_3PO_4 electrolyte. This stretchable supercapacitor gave a specific capacitance value of 7.6 F g^{-1} and maintained its performance following hundreds of stretching cycles of up to 40 % strain. Yue *et al.* [25] have reported stretchable electrode for supercapacitor application based on polypyrrole (Ppy) coated nylon lycra. It presented specific capacitance of 125.1 F g^{-1} at 60% strain and maintained 55% of its initial capacitance value after 500 charge/discharge cycles. Yu *et al*. [21] have developed stretchable supercapacitor by using buckled SWCNTs film on the PDMS. The buckled SWCNTs supercapacitor exhibited a specific capacitance of 52 F g^{-1} at 30 % strain and retained this value after 1000 charge/discharge cycles without application of stress and strain. This buckled SWCNTs supercapacitor cannot meet the demand for highly stretchable supercapacitor (> 100% elongation) with high stability after number of stretching cycles. According to the reported studies, a fully stretchable (i.e. 100 % strain) nanocarbon-based supercapacitor with high specific capacitance value and stability is yet to be developed for practical applications.

In this chapter, we extend our previous study of a stretchable, electrochemical latex and polyurethane (PU) electrode to a highly durable and fully stretchable supercapacitor and characterized the electrochemical properties as a function of strain (0 to 100%) and stretching/release cycles (up to 100^{th}). To prepare the fully stretchable devices, the rGO/SWCNTs composite electrodes on gold-coated latex and PU substrates were prepared using a Flexicoat industrial spray coating system from

Sono-Tek (USA) and two electrodes assembled with polymer-based electrolyte in a sandwich conformation.

5.2 EXPERIMENTAL SECTION

5.2.1 Materials

Graphite powder was obtained from Bay Carbon. Milli-Q water with a resistivity of 18.2 mΩ cm^{-1} was used in all preparations. Potassium permanganate, phosphorous pentaoxide, hydrazine hydrate, triethylamine were sourced from Sigma-Aldrich and used as received. Ammonia solution in water (28%) from labtech and used as received. Single-wall carbon nanotubes (SWCNTs) were purchased from Carbon Nanotechnologies, Inc (Houston, TX) and used as an active material. N, N-Dimethylformamide (DMF) and concentrate nitric acid (70%) were obtained from Sigma Aldrich and used as received. The liquid latex was purchased from AA rubber and Seals. Pty, Ltd (Belmore, NSW, Australia) and polyurethane (PU) was obtained from Advan Source Biomaterials Corp. Polyvinyl alcohol (PVA, Mw = 124,000-186,000 g mol^{-1}) was obtained from Sigma-Aldrich. Orthophosphoric acid (85%) was purchased from Ajax Finechemicals.

5.2.2 Preparation of stretchable polymer electrolyte

Stretchable polymer electrolyte was prepared by a solvent casting method. PVA (1 g) was dissolved in Milli-Q water (10 mL) at 90 ℃ under vigorous stirring until the solution became clear, then H_3PO_4 (1.5 g) was added into the hot solution and stirred at room temperature overnight. The viscous PVA/H_3PO_4 solution was used to as a stretchable electrolyte to fabricate latex and PU full devices.

5.2.3 Preparation of latex and PU stretchable substrates

A suitable amount of natural liquid latex (with ammonia to prevent bacteria spoilage) was poured into a glass mold (30cm x 5cm x 1mm) and then allowed to dry at room temperature for 24 hrs. To fabricate the electrode, a section of the latex film (1cm x 5cm x 1mm) was transferred to a glass microscope slide, stretched to introduce a 100% uniaxial pre-strain and then held under tension using double-sided adhesive tape.

In order to prepare the polyurethane (PU) mat to use as a substrate, PU is dissolved in DMF with a 15wt% concentration. The PU solution was loaded into a plastic syringe equipped with a 21 gauge needle. The needle was connected to a high voltage supply, and the syringe pumping rate for adjusted to 0.2 mL/h. A distance of 10 cm and voltage of 23 kV are maintained between the tip of the needle and the drum collector. After electrospinning, the as-spun polyurethane mat was pill off from the collector and transferred to a glass microscope slide, stretched to introduce a 100% uniaxial pre-strain and then held under tension using double-sided adhesive tape. After stretching, a 150 nm thick layer of gold was coated onto the dried latex and PU film by sputter coating (Edwards Sputter Coater AUTO306, BOC Ltd, United Kingdom), allowing it to be used as a current collector.

5.2.4 Fabrication of stretchable rGO/SWCNTs composite electrode

Buckled, stretchable rGO/SWCNTs composite electrodes on gold-coated latex and PU substrate were prepared using a Flexicoat industrial spray coating system from Sono-Tek (USA). A 150 nm thickness of gold was first sputter coated on pre-strained (at 100% strain) latex and PU substrate using an Edwards Auto 306 Sputter Coater to use as a current collector. The gold-modified latex and PU was then coated with

rGO/SWCNTs composite dispersion. After spray coating, the rGO/SWCNTs composite electrodes were dried in an oven at 100 ℃ for 30 min to evaporate residual solvent.

5.2.5 Preparation of stretchable latex and/or PU full device

The stretchable latex and/or PU supercapacitor was fabricated by assembling the stretchable rGO/SWCNTs composite electrodes and stretchable polymer electrolyte in a sandwich conformation (Figure. 5.1a). Copper tapes were attached at the edge of the gold coated substrate for electrical contacts (Fig. 5.1a). The rGO/SWNT macrofilms electrodes were prepared by spray coating onto the pre-strained (at 100% strain) latex and/or PU to form a buckled structure as the stretchable electrodes. The PVA/H_3PO_4 solution was heated to 80 ℃ then the buckled rGO/SWCNTs composite electrodes on the latex and PU were soaked in the solution for 10 min to diffuse electrolyte into the rGO/SWCNTs composite film. The electrodes were then placed into a fume hood for 4 h to remove most of the water solvent. Two such stretchable rGO/SWCNTs composite electrodes with PVA/H_3PO_4 electrolyte were pressed together face-to-face to form a sandwich structure. The whole device was dried at room temperature overnight. Characterization of the electrochemical properties were carried out on a two-electrode configuration under fixed 0 to 100% of strain and 50 or 100 stretching/releasing cycles at 100% strain using a Shimadzu EZ mechanical tester (Fig. 5.1b). This approach enables the electrochemical behaviour of a full stretchable latex and/or PU device to be tested under more rigours conditions, and provides a means to test the practicality of their performance.

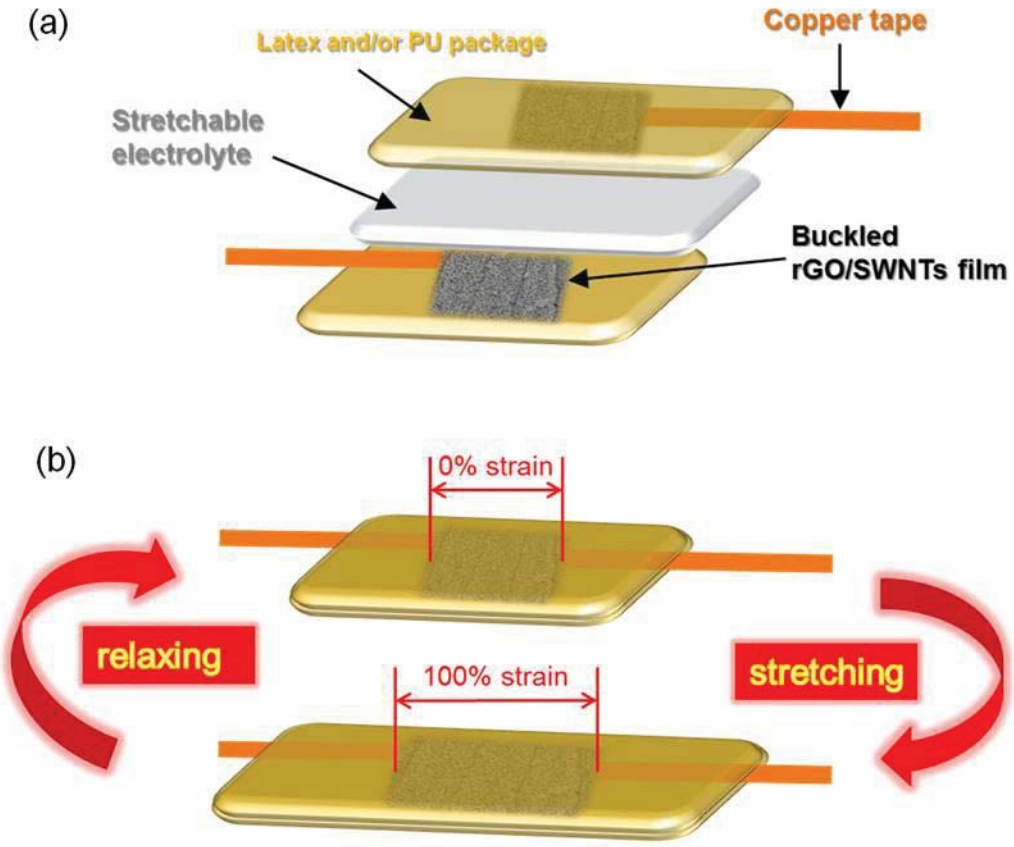

Figure 5.1 (a) Schematic of the main components for the stretchable latex and/or PU supercapacitor. (b) Schematic of the stretchable latex and/or PU supercapacitor under reversible stretching and relaxing from 0% to 100% strain.

5.3 CHARACTERIZATIONS

5.3.1 Cyclic Voltammetry (CV)

Cyclic Voltammetry (CV) measurements of the latex and/or PU supercapacitor were performed at room temperature with a two electrode system using an electrochemical analyzer (EDAQ Australia) and EChem V2 software (ADI Instruments Pty. Ltd).

All of the CV measurements were recorded under 0 to 100% strain and after 50 and 100 stretching (at 100% strain) over the scan rate range of 5~500 mV s^{-1}. All of the

electrodes had stretch and release cycles applied at a speed of 2 % s^{-1} for 50 and 100 stretching cycles using a Shimadzu EZ mechanical tester.

5.3.2 Electrochemical impedance spectroscopy (EIS)

Electrochemical impedance spectroscopy (EIS) was used to probe the electrical double layer effects at the electrode/electrolyte interface. EIS measurements were performed at room temperature using a Gamry EIS 3000^{TM} system (Gamry, USA) where the frequency range spanned 100 kHz to 0.01 Hz with an amplitude of 10mV (rms) at open circuit potential. All of the EIS measurements carried out under 0 to 100% strain and after 50 and 100 stretching (at 100% strain).

5.3.3 Galvanostatic charge/discharge measurement

Galvanostatic charge/discharge tests of the stretchable latex and PU supercapacitor were performed using a battery test system (Neware electronic Co.) between 0 V and 0.8 V with constant current density as 1 A g^{-1}. All of the charge-discharge tests performed under 0 to 100% strain and after 50 and 100 stretching (at 100% strain).

5.4 RESULTS AND DISCUSSION

The device was assembled as above and a robust structure substrate for handling was obtained.

5.4.1 Stretchable latex supercapacitor

By using the latex substrate and the fabrication assembly protocols described above, robust devices that could be easily handled were obtained.

5.4.1.1 Morphological study on the rGO/SWCNTs composite film and polymer electrolyte

The surface morphology of the relaxed rGO/SWCNTs composite film on the latex substrate exhibited a lot of islands with a porous and well-defined periodic buckling structure along the elongation direction with wavelength of ≈ 20 μm (Figure 5.2a and 5.2b). These structural characteristics are strongly desirable for increasing the electroactive surface area. In addition, the highly stretchable electrolyte layer between the two latex electrodes acts as separator and electrolyte but also provides flexibility. The thickness of the electrolyte layer was approximately 90 μm (Figure 5.2c) and the whole device had approximately 2 mm thickness (Figure 5.2c inset). The schematic configuration of the stretchable latex supercapacitor is also illustrated in Figure 5.2d.

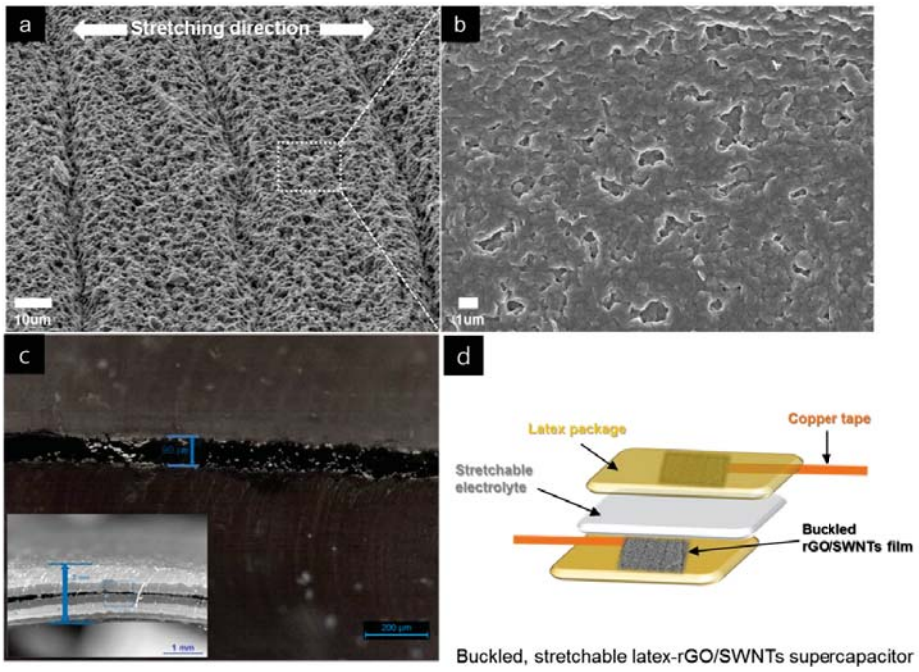

Figure 5.2 SEM images of buckled rGO/SWCNTs composite electrodes; (a) at low magnification (b) at high magnification, (c) Optical image of the cross-section of the stretchable latex supercapacitor, (d) Schematic configuration of the stretchable latex supercapacitor.

5.4.1.2 Electrochemical properties

Cyclic voltammetry (CV) was used to determine electrochemical behaviour of the stretchable latex supercapacitor as a function of number of stretches (Figure 5.3a) and under constant strain (Figure 5.3b) over a scan rate range 5-100 mV s^{-1}. The stretchable latex supercapacitor shows rectangular CV responses even after 50 stretching cycles (Figure 5.3a), which indicates that the charge/discharge processes is highly reversible. However, after 100 stretches of the latex supercapacitor, the rectangular CV shape became distorted. This is attributed to a decrease in electrical conductivity of the latex supercapacitor electrodes [26]. CV responses as a function of strain (0 to 100 %) are illustrated in Figure 5.3b. The CV curves show a slightly decreased current with an increase in level of strain, which implies that the introduction of repeated stresses and strain is likely to result in the formation of cracks on the rGO/SWCNTs films that attribute to irreversible loss of junctions between rGO/SWCNTs composite film [26].

Electrochemical impedance spectroscopy (EIS) was used to obtain an insight into the electrochemical interface properties of the stretchable latex supercapacitor. The Nyquist plots of the stretchable latex supercapacitor as a function of stretching and strain are shown in Figure 5.3c and 5.3d. The stretchable supercapacitor gave a line close to 90º at low frequency even after repetitive stretching and applied with 0 to 100% of strain, indicating a good capacitive behavior (Figure 5.3c and 5.3d) [27, 28]. At high frequency, the intercept point on the real axis represents the resistance of the electrolyte and the internal resistance of the electrodes, which can be called bulk resistance, and the diameter of compressed semicircle is attributed to charge transfer

resistance [28]. Both the bulk resistance and charge transfer resistance increase with the application of the stretching and strain, which corresponded to the CV results.

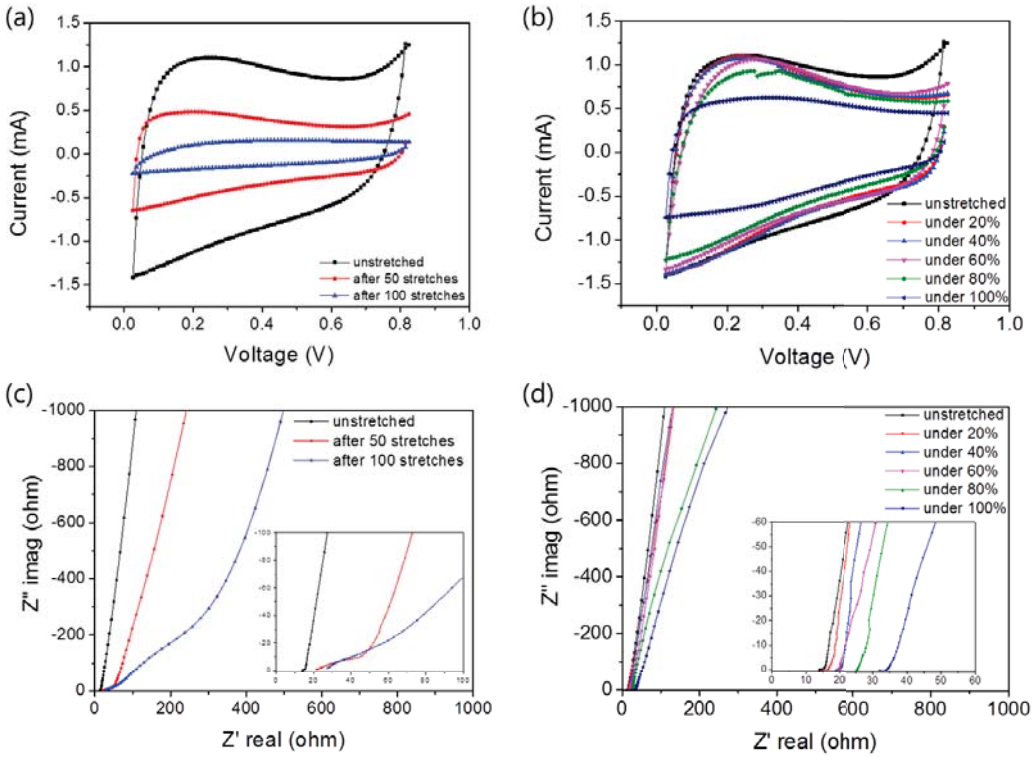

Figure 5.3 CV curves of the stretchable latex supercapacitor as a function of stretching (a) and strain (b) at a scan rate of 100 mV s^{-1}. (c) Nyquist plots of the stretchable latex supercapacitor as a function of stretching (c) and strain (d) with frequency ranging from 100 kHz to 0.01 Hz.

Galvanostatic charge/discharge curves of the latex supercapacitor as a function of the stretching and strain with a current density of 1 A g^{-1} are presented in Figure 5.4a and 5.4b. The charge/discharge curves of the latex supercapacitor show good capacitive behavior even after 50 and 100 stretching cycles and under various levels of strain (0 ~100 % strain) (Figure 5.4a and 5.4b). However, an iR drop is observed on the discharge curves after 50 stretching cycles of the latex supercapacitor (Figure 5.4a), that is ascribed to low conductivity of the latex supercapacitor induced by the cracks

on the buckled rGO/SWCNTs composite film after prolonged stretching. The cycling stability of the latex supercapacitor when subjected to a 50 and 100 stretching with 1000th charge/discharge cycles are showed by galvanostatic charge/discharge profiles with constant current density (1 A g^{-1}) (Figure 5.4c). The average specific capacitance of the unstretched latex supercapacitor was 61.3 ± 1.1 (mean ± S.D., n = 10 devices) F g^{-1}, 70% of the capacitance was retained (41.7 F g^{-1}) after 100 stretching cycles (Figure 5.4c) and also, 66 % retention of the capacitance at 100% elongation (Figure 5.4d). The latex supercapacitor still retained 67% of its initial capacitance (61.3 F g^{-1}) after 100 stretching and 3000th CV cycles, suggesting the high stretchability of the latex supercapacitor.

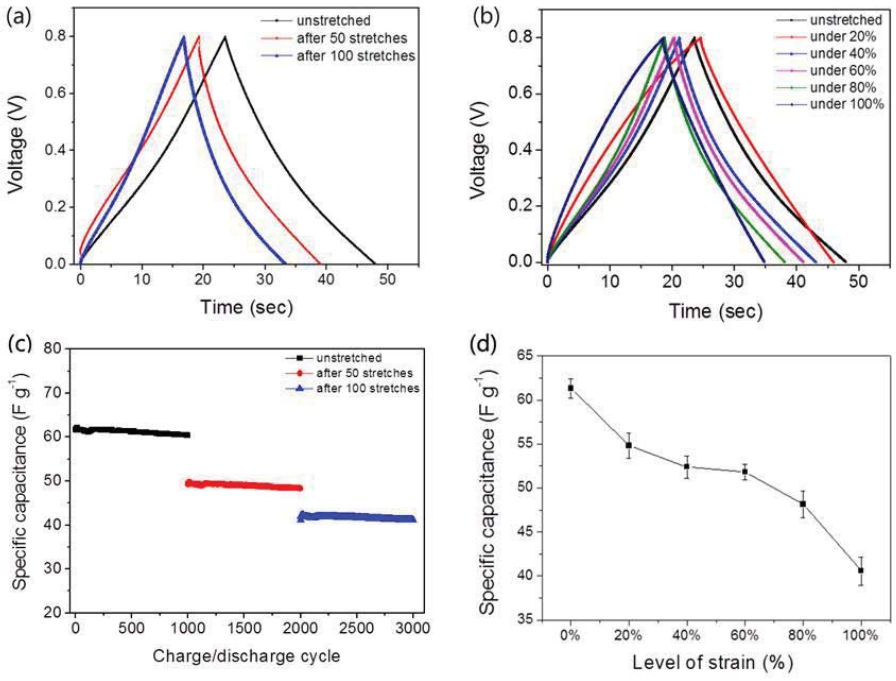

Figure 5.4 Galvanostatic charge/discharge curves of the latex supercapacitor as a function of stretching (a) and strain (b) at a current density of 1 A g^{-1}. (c) Specific capacitance of the stretchable latex supercapacitor after 50 and 100 stretching as a function of charge-discharge cycles. (d) Specific capacitance of the stretchable latex supercapacitor under 0 to 100% of strain.

5.4.2 Stretchable polyurethane (PU) supercapacitor

By using the PU substrate and the fabrication assembly protocols described above, robust devices that could be easily handled were obtained.

5.4.2.1 Morphological study on the rGO/SWCNTs composite film and polymer electrolyte

SEM images of the rGO/SWCNTs composite film on the PU are presented in Figure 5.5. The surface morphology of the relaxed rGO/SWCNTs composite film on the PU substrate showed porous fiber structure before prolonged stretching (Figure 5.5b). This characteristic is suitable to maximize surface area. Similarly, the stretchable PVA-H_3PO_4 electrolyte layer formed between two rGO/SWCNTs composite electrodes acts as separator and electrolyte, and enables flexibility and stretchability [29]. The thickness of the electrolyte layer is an approximately 200 μm (Figure 5.5c) and whole PU device had an approximately 500 μm thickness as well. The schematic conformation of the stretchable PU supercapacitor is also illustrated for easy understanding (Figure 5.5d).

5.4.2.2 Electrochemical properties

Cyclic voltammetry (CV) was used to investigate the electrochemical properties of the stretchable PU supercapacitor as a function of strain. The CV responses under 0% ~ 100% strain at a scan rate of 100 mV s^{-1} are presented in Figure 5.6a. A slight decrease in CV current is observed with an increase in level of strain that may be due to low electrical conductivity of the rGO/SWCNTs electrodes induced by strain. Electrochemical impedance spectroscopy (EIS) is carried out to confirm the electrochemical interfacial properties. Nyquist plots of the stretchable PU

supercapacitor under 0% ~ 100% strains are given to Figure 5.6b. The plots showed a line close to 90º at low frequency, indicating good capacitive behaviour of the stretchable PU supercapacitor [30]. However, in the high frequency domain, both the bulk resistance and charge transfer resistance increases with an increase in level of strain. This agrees with the results from CV [31, 32]. The charge-discharge curves of the stretchable PU supercapacitor under 0% ~ 100% strain with a current density of 1 A g^{-1} are illustrated in Figure 5.6c. The charge/discharge curves of the PU supercapacitor indicate good capacitive behaviour and symmetrical shape, implying that the highly conductive rGO/SWCNTs composite create a pathway for the transfer of ions and electrons, thus decreasing internal resistance. However, a notable IR drop is observed under 100% strain (Figure 5.6c), which is ascribed to the resistance increase induced by cracks formed on the buckled rGO/SWCNTs composite film under high level of strain [33]. The specific capacitance of the PU supercapacitor under 0% strain is 42.9 ±1.2 (mean ± S.D., n = 10 devices) F g^{-1}, and 90% of its capacitance is maintained (37 F g^{-1}) at 100% strain.

Electrochemical properties of the PU stretchable supercapacitor are also investigated after 50 and 100 stretching cycles (Figure 5.7a). A significant decrease in CV current is observed after 100 stretching cycles (at 100% strain), most likely due to the decreased electrical conductivity of the rGO/SWCNTs electrodes induced by the stretching cycles (at 100% strain). The stretchable PU supercapacitor shows a specific capacitance of 39.3 F g^{-1} and 31.1 F g^{-1} after 50 and 100 stretching cycles, respectively (Figure 5.7d).

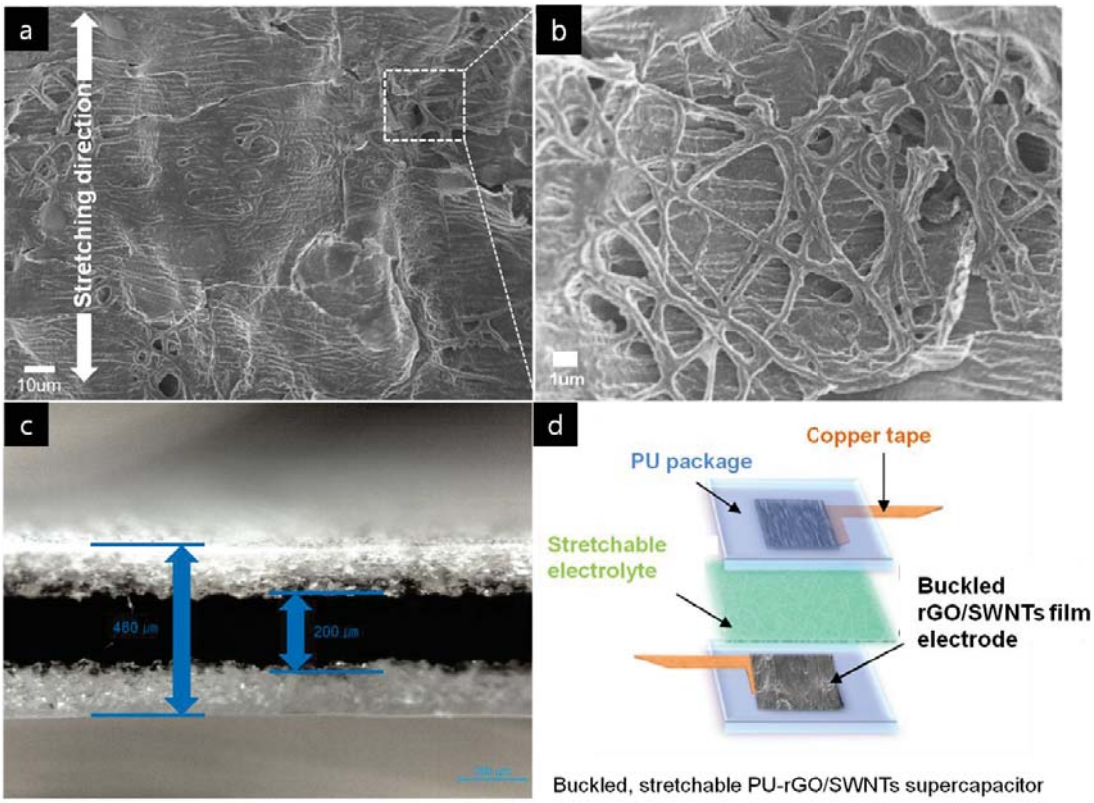

Figure 5.5 SEM images of buckled rGO/SWCNTs composite film on the PU substrate; (a) at low magnification (b) at high magnification, (c) Optical image of the cross-section of the stretchable PU supercapacitor, (d) Schematic configuration of the stretchable PU supercapacitor.

72% of the initial capacitance (42.9 F g^{-1}) is maintained after 100 stretching and 3000th charge/discharge cycles, indicating a high stretchability of the PU supercapacitor. The Nyquist plots of the PU supercapacitor after 50 and 100 stretching cycles are demonstrated in Figure 5.7b. The internal resistance of the PU supercapacitor increases with increasing number of stretching cycles, which is mostly likely due to the low electrical conductivity on the rGO/SWCNTs film after repetitive stretching to 100% strain. The semicircle region of the PU supercapacitor after 50 and 100 stretching is larger than unstretched sample, indicating that the charge transfer

resistance increases (Figure 5.7b). The charge-discharge curves after 50 and 100 stretching cycles with a current density of 1 A g^{-1} are given in Figure 5.7c.

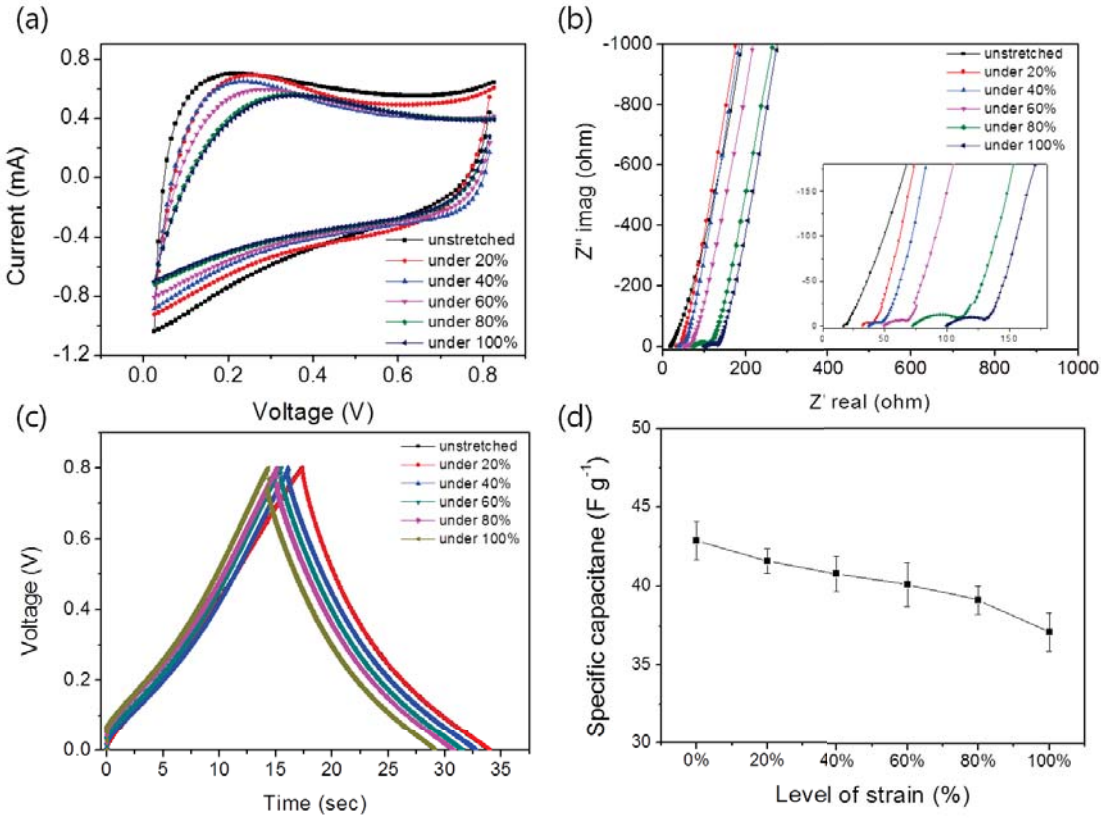

Figure 5.6 Electrochemical properties of the stretchable polyurethane (PU) supercapacitor as a function of strain; (a) Cyclic voltammetry (CV), (b) Electrochemical impedance spectroscopy (EIS), (c) Charge/discharge test and (d) Specific capacitance of the stretchable PU supercapacitor as a function of strain.

A notable iR drop is also observed after 100 stretching cycles (Figure 5.7c). Again this may be due to the high resistance induced by cracks on the rGO/SWCNTs film after continuous stretching. These cracks also contribute to irreversible loss of junctions between rGO/SWCNTs composite [34].

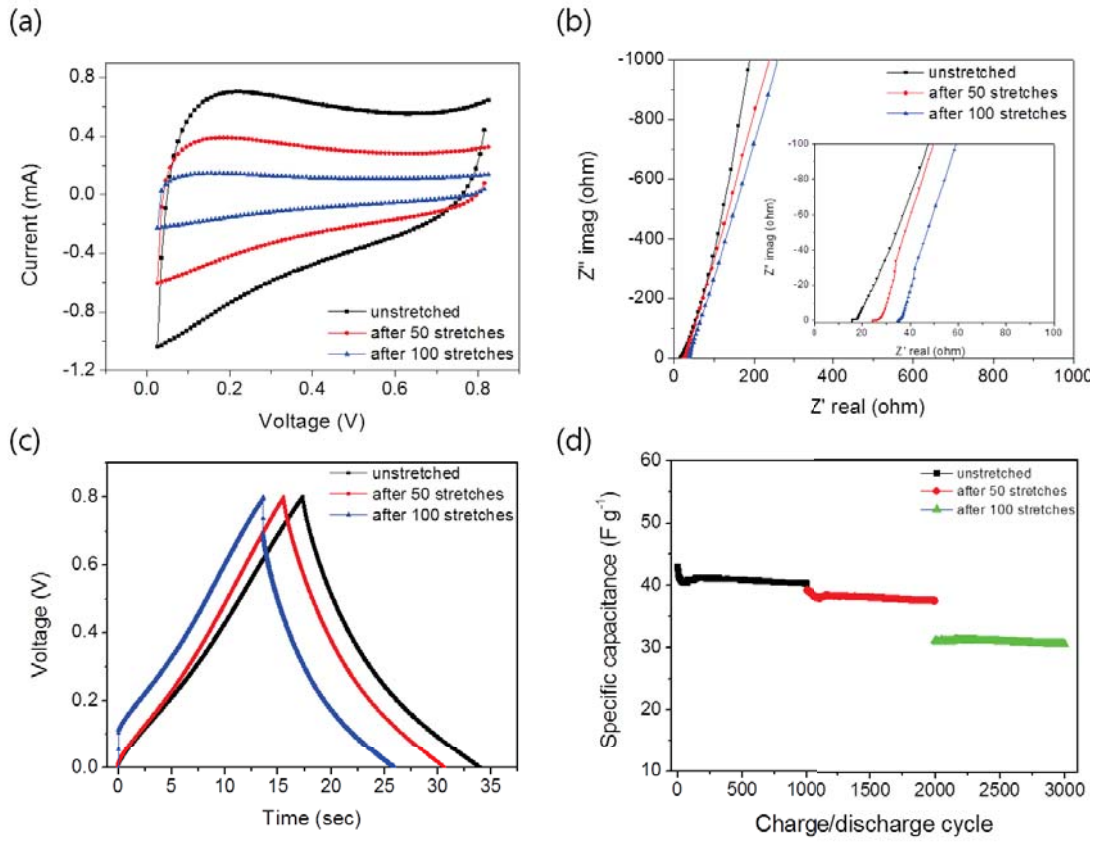

Figure 5.7 Electrochemical properties of the stretchable polyurethane (PU) supercapacitor as a function of stretching; (a) Cyclic voltammetry (CV), (b) Electrochemical impedance spectroscopy (EIS), (c) Charge/discharge test and (d) stability tests of the stretchable PU supercapacitor as a function of stretching and charge/discharge cycle.

5.5 CONCLUSIONS

In this chapter, the highly stretchable latex and PU supercapacitors have been fabricated with a polymer based stretchable electrolyte (PVA-H_3PO_4). The use of the stretchable polymer electrolyte as a separator imparts additional flexibility into the device. The stretchable latex supercapacitor (unstretched) showed 61.3 F g^{-1} of specific capacitance value that decreases to 41.7 F g^{-1} after 100 stretching cycles at

100% strain (70 % capacitance retention). The PU supercapacitor (unstretched) showed 42.9 F g^{-1} of specific capacitance value and decreased to 31.1 F g^{-1} after being 100 stretched (72 % capacitance retention). The stretchable latex and PU supercapacitor retained 74 % and 89 % of initial capacitance at 100% strain, respectively. It should be noted that the electrochemical window of the polymer based stretchable electrolyte and device is limited to less than 1 V. The latter could be greatly improved by using an organic salt or ionic liquids based polymer electrolyte. The high stability and stretchability of the latex and PU supercapacitor demonstrates that nanocarbon-based stretchable energy storage devices as supercapacitors have potential application for wearable and biocompatible devices.

5.6 REFERENCES

[1] D.-H. Kim, N. Lu, R. Ma, Y.-S. Kim, R.-H. Kim, S. Wang, J. Wu, S. M. Won, H. Tao, A. Islam, K. J. Yu, T.-i. Kim, R. Chowdhury, M. Ying, L. Xu, M. Li, H.-J. Chung, H. Keum, M. McCormick, P. Liu, Y.-W. Zhang, F. G. Omenetto, Y. Huang, T. Coleman, and J. A. Rogers, "Epidermal Electronics," *Science,* vol. 333, pp. 838-843, August 12, 2011 2011.

[2] S. C. B. Mannsfeld, B. C. k. Tee, R. M. Stoltenberg, C. V. H. h. Chen, S. Barman, B. V. O. Muir, A. N. Sokolov, C. Reese, and Z. Bao, "Highly sensitive flexible pressure sensors with microstructured rubber dielectric layers," *Nature Materials,* vol. 9, pp. 859-64, Oct 2010 2010.

[3] T. Yamada, Y. Hayamizu, Y. Yamamoto, Y. Yomogida, A. Izadi-najafabadi, D. N. Futaba, and K. Hata, "A stretchable carbon nanotube strain sensor for human-motion detection," *Nature Nanotechnology,* vol. 6, pp. 296-301, May 2011 2011.

[4] D. J. Lipomi, M. Vosgueritchian, B. C. k. Tee, S. L. Hellstrom, J. A. Lee, C. H. Fox, and Z. Bao, "Skin-like pressure and strain sensors based on transparent elastic films of carbon nanotubes," *Nature Nanotechnology,* vol. 6, pp. 788-92, Dec 2011 2011.

[5] J.-Y. Kim, C. S. Lee, J. H. Han, J. W. Cho, and J. Bae, "Supercapacitors Using Gel Electrolytes and Thin Multiwalled Carbon Nanotube Films Spray-Deposited on ITO Substrates," *Electrochemical and Solid-State Letters,* vol. 14, pp. A56-A59, April 1, 2011 2011.

[6] K. Park, D.-K. Lee, B.-S. Kim, H. Jeon, N.-E. Lee, D. Whang, H.-J. Lee, Y. J. Kim, and J.-H. Ahn, "Stretchable, Transparent Zinc Oxide Thin Film Transistors," *Advanced Functional Materials,* vol. 20, pp. 3577-3582, 2010.

[7] G. Shin, C. H. Yoon, M. Y. Bae, Y. C. Kim, S. K. Hong, J. A. Rogers, and J. S. Ha, "Stretchable Field-Effect-Transistor Array of Suspended SnO2 Nanowires," *Small,* vol. 7, pp. 1181-1185, 2011.

[8] T. Sekitani, H. Nakajima, H. Maeda, T. Fukushima, T. Aida, K. Hata, and T. Someya, "Stretchable active-matrix organic light-emitting diode display using printable elastic conductors," *Nature materials,* vol. 8, pp. 494-499, 2009.

[9] Z. Yu, X. Niu, Z. Liu, and Q. Pei, "Intrinsically Stretchable Polymer Light-Emitting Devices Using Carbon Nanotube-Polymer Composite Electrodes," *Advanced Materials,* vol. 23, pp. 3989-3994, 2011.

[10] H. C. Ko, M. P. Stoykovich, J. Song, V. Malyarchuk, W. M. Choi, C.-J. Yu, J. B. Geddes Iii, J. Xiao, S. Wang, and Y. Huang, "A hemispherical electronic eye camera based on compressible silicon optoelectronics," *Nature,* vol. 454, pp. 748-753, 2008.

[11] S. Cheng and Z. Wu, "Microfluidic stretchable RF electronics," *Lab on a Chip,* vol. 10, pp. 3227-3234, 2010.

[12] R.-H. Kim, M.-H. Bae, D. G. Kim, H. Cheng, B. H. Kim, D.-H. Kim, M. Li, J. Wu, F. Du, H.-S. Kim, S. Kim, D. Estrada, S. W. Hong, Y. Huang, E. Pop, and J. A. Rogers, "Stretchable, Transparent Graphene Interconnects for Arrays of Microscale Inorganic Light Emitting Diodes on Rubber Substrates," *Nano Letters,* vol. 11, pp. 3881-3886, 2011/09/14 2011.

[13] J. A. Rogers, T. Someya, and Y. Huang, "Materials and Mechanics for Stretchable Electronics," *Science,* vol. 327, pp. 1603-1607, March 26, 2010 2010.

[14] M. Winter and R. J. Brodd, "What Are Batteries, Fuel Cells, and Supercapacitors?," *Chemical Reviews,* vol. 104, pp. 4245-4270, 2004/10/01 2004.

[15] Y. Sun and J. A. Rogers, "Inorganic Semiconductors for Flexible Electronics," *Advanced Materials,* vol. 19, pp. 1897-1916, 2007.

[16] Y.-k. Zhou, B.-l. He, W.-j. Zhou, and H.-l. Li, "Preparation and Electrochemistry of SWNT/PANI Composite Films for Electrochemical Capacitors," *Journal of The Electrochemical Society,* vol. 151, pp. A1052-A1057, July 1, 2004 2004.

[17] S. Ugur, Ö. Yargi, and Ö. Pekcan, "Conductivity percolation of carbon nanotubes (CNT) in polystyrene (PS) latex film," *Canadian Journal of Chemistry,* vol. 88, pp. 267-276, 2010.

[18] Z. Spitalsky, D. Tasis, K. Papagelis, and C. Galiotis, "Carbon nanotube–polymer composites: Chemistry, processing, mechanical and electrical properties," *Progress in Polymer Science,* vol. 35, pp. 357-401, 2010.

[19] L. Hu, W. Yuan, P. Brochu, G. Gruner, and Q. Pei, "Highly stretchable, conductive, and transparent nanotube thin films," *Applied Physics Letters,* vol. 94, pp. -, 2009.

[20] X. Wang, P. D. Bradford, W. Liu, H. Zhao, Y. Inoue, J.-P. Maria, Q. Li, F.-G. Yuan, and Y. Zhu, "Mechanical and electrical property improvement in CNT/Nylon composites through drawing and stretching," *Composites Science and Technology,* vol. 71, pp. 1677-1683, 2011.

[21] C. Yu, C. Masarapu, J. Rong, B. Wei, and H. Jiang, "Stretchable Supercapacitors Based on Buckled Single-Walled Carbon-Nanotube Macrofilms," *Advanced Materials,* vol. 21, pp. 4793-4797, 2009.

[22] K. S. Kim, Y. Zhao, H. Jang, S. Y. Lee, J. M. Kim, K. S. Kim, J.-H. Ahn, P. Kim, J.-Y. Choi, and B. H. Hong, "Large-scale pattern growth of graphene

films for stretchable transparent electrodes," *Nature,* vol. 457, pp. 706-10, 2009 Feb 05 2009.

[23] X. Li, T. Gu, and B. Wei, "Dynamic and Galvanic Stability of Stretchable Supercapacitors," *Nano Letters,* vol. 12, pp. 6366-6371, 2012/12/12 2012.

[24] T. Chen, Y. Xue, A. K. Roy, and L. Dai, "Transparent and Stretchable High-Performance Supercapacitors Based on Wrinkled Graphene Electrodes," *ACS Nano,* vol. 8, pp. 1039-1046, 2014/01/28 2013.

[25] B. Yue, C. Wang, X. Ding, and G. G. Wallace, "Polypyrrole coated nylon lycra fabric as stretchable electrode for supercapacitor applications," *Electrochimica Acta,* vol. 68, pp. 18-24, 2012.

[26] H. T. Jeong, B. C. Kim, R. Gorkin, M. J. Higgins, and G. G. Wallace, "Capacitive behavior of a stretchable single-wall carbon nanotube on latex electrode," *Electrochimica Acta,* 2014.

[27] J. Gamby, P. L. Taberna, P. Simon, J. F. Fauvarque, and M. Chesneau, "Studies and characterisations of various activated carbons used for carbon/carbon supercapacitors," *Journal of Power Sources,* vol. 101, pp. 109-116, 2001.

[28] A. Di Fabio, A. Giorgi, M. Mastragostino, and F. Soavi "Carbon-Poly(3-methylthiophene) Hybrid Supercapacitors," *Journal of The Electrochemical Society,* vol. 148, pp. A845-A850, August 1, 2001 2001.

[29] C. Zhao, C. Wang, Z. Yue, K. Shu, and G. G. Wallace, "Intrinsically Stretchable Supercapacitors Composed of Polypyrrole Electrodes and Highly Stretchable Gel Electrolyte," *ACS Applied Materials & Interfaces,* vol. 5, pp. 9008-9014, 2013/09/25 2013.

[30] J. Segalini, B. Daffos, P. L. Taberna, Y. Gogotsi, and P. Simon, "Qualitative Electrochemical Impedance Spectroscopy study of ion transport into sub-nanometer carbon pores in Electrochemical Double Layer Capacitor electrodes," *Electrochimica Acta,* vol. 55, pp. 7489-7494, 2010.

[31] P. L. Taberna, P. Simon, and J. F. Fauvarque "Electrochemical Characteristics and Impedance Spectroscopy Studies of Carbon-Carbon Supercapacitors," *Journal of The Electrochemical Society,* vol. 150, pp. A292-A300, March 1, 2003 2003.

[32] H. Kurig, A. Jänes, and E. Lust, "Electrochemical Characteristics of Carbide-Derived Carbon | 1 -Ethyl-3-methylimidazolium Tetrafluoroborate Supercapacitor Cells," *Journal of The Electrochemical Society,* vol. 157, pp. A272-A279, March 1, 2010 2010.

[33] S. Nataraj, Q. Song, S. Al-Muhtaseb, S. Dutton, Q. Zhang, and E. Sivaniah, "Thin, flexible supercapacitors made from carbon nanofiber electrodes

decorated at room temperature with manganese oxide nanosheets," *Journal of Nanomaterials,* vol. 2013, 2013.

[34] S. Prabaharan, R. Vimala, and Z. Zainal, "Nanostructured mesoporous carbon as electrodes for supercapacitors," *Journal of Power Sources,* vol. 161, pp. 730-736, 2006.

CHAPTER 6

FLEXIBLE POLYCAPROLACTONE (PCL) SUPERCAPACITORS

6.1 INTRODUCTION

Recent studies on flexible devices have demonstrated a great deal of attention in a wide range of applications, such as *in vitro* diagnostics, robotics and advanced therapies [1-8]. These studies have employed electroactive materials on flexible substrates to achieve various functions, including high bendability or well-designed human-device interfaces [9-12]. Flexible energy storage devices like supercapacitors are essential components for fully implantable and flexible devices. In addition, to be generating electrical and mechanical function simultaneously, a variety of components involving graphene, hybrid composites or carbon nanotube assemblies need to integrated on flexible substrates [13-17] . Furthermore, flexible polymers should also be considered as a substrate to achieve flexible, implantable or wearable devices. Polycaprolactone (PCL) is a biodegradable, aliphatic polyester based polymer that has good resistance to solvents, water and oil. It also has unique chemical and mechanical properties resulting in its considerable commercial development for biomedical applications [18-21]. The addition of nanocarbon-based conducting materials like carbon nanotubes (CNTs) and graphene enables further possible applications, such as flexible supercapacitors.

Nanocarbon materials such as carbon nanotubes (CNTs) and graphene have been widely used as electrode materials in flexible supercapacitors due to their remarkable properties including excellent mechanical, electrical properties, large surface area,

chemical stability and electrochemical properties [22-26]. Previous studies have demonstrated that nanocarbon based materials have potential for flexible supercapacitors. For this purpose, CNTs could be spray coated onto flexible substrates and used as an electrode [27-30]. Kaempgen *et al*. [27] have developed flexible, thin film supercapacitors based on the single-wall carbon nanotubes (SWCNTs) spray-coated on poly (ethylene therephthalate) (PET) films. In order to fabricate fully printable devices, a polymer based solid state electrolyte was introduced as both a separator and electrolyte. The full device showed a specific capacitance of 36 F g^{-1}. Kang and co-workers [31] have reported low-cost and light weight flexible office paper and CNTs based supercapacitors with good chemical stability, high flexibility and large specific surface area. These exhibited 46.9 F g^{-1} of specific capacitance at 0.1 V s^{-1} of scan rate. And also it has excellent cycle stability with 0.5 % decrease of capacitance after 5000 charge/discharge cycles at a current density of 10 A g^{-1}.

Graphene also has been exploited as an electrode material, in particular for flexible supercapacitors [32-35]. The specific capacitance values from these graphene-based flexible supercapacitors ranged from 80 to 118 F g^{-1}, which are much lower than theoretical values (550 F g^{-1}) [36]. This is due to restacking of the graphene layers which decrease the electroactive area, resulting in lower capacitance values. In order to overcome this limitation, the CNTs can assist in separating graphene sheets and improving electroactive area [37]. CNTs are able to maintain graphene's high surface area and provide conductive pathways for efficient electron and ion transport [38-41]. For instance, Gao *et al*. [42] have developed a free-standing CNTs/graphene composite paper which was prepared by filtration method. It obtained a specific capacitance of 99.7 to 212.9 and 302 F g^{-1} when the mass ratio of the CNTs increased

from 0 to 20 % and 40 %, respectively. Although there has been a great deal of investigation on CNTs, graphene and CNTs/graphene composite bases supercapacitors, there use in flexible supercapacitors has been explored to a much lesser extent.

In this chapter, we have investigated flexible supercapacitors with high durability and flexibility based on CNTs/graphene composites. To fabricate the fully flexible devices, the CNTs/graphene composite electrodes on gold-coated polycaprolactone (PCL) substrate were prepared using a Flexicoat industrial automatic spray coating system from Sono-Tek (USA) and by assembling two electrodes with polymer based electrolyte (PVA-H_3PO_4) in a sandwich configuration. This electrolyte was used as it is readily available and has appropriate mechanical properties. Although it is not cytocompatible [43, 44].

In order to assess the practical and realistic electrochemical performance of the flexible supercapacitors, all of the electrochemical properties were characterized on a two-electrode system under various bending angles and bend/release cycles.

6.2 EXPERIMENTAL SECTION

6.2.1 Materials

Ammonia solution in water (28%) was from labtech and used as received. Single-wall carbon nanotubes (SWCNTs) were obtained from Carbon Nanotechnologies, Inc (Houston, TX) and used as an electrode material. Graphite powder was purchased from Bay Carbon. Milli-Q water with a resistivity of 18.2 mΩ cm^{-1} was used in all preparations. Potassium permanganate, hydrazine hydrate, phosphorous pentaoxide,

triethylamine, concentrate nitric acid (70%) and N, N-Dimethylformamide (DMF) were sourced from Sigma-Aldrich and used as received. Polyvinyl alcohol (PVA, Mw = 124,000-186,000 g mol^{-1}) and polycaprolactone (PCL) (Mw = 80,000) were obtained from Sigma-Aldrich. Orthophosphoric acid (H_3PO_4) (85%) was purchased from Ajax Finechemicals.

6.2.2 Preparation of stretchable polymer electrolyte

Stretchable polymer electrolyte is fabricated by solvent casting method. Polyvinyl alcohol (PVA) (1g) was dissolved in Milli-Q water (10 mL) at 90 ℃ under vigorous stirring until the solution became clear, then orthophosphoric acid (H_3PO_4) (1.5 g) is added into the PVA solution and stirred at room temperature overnight. The viscous PVA/H_3PO_4 solution was used as a stretchable electrolyte and separator to fabricate polycaprolactone (PCL) full devices.

6.2.3 Fabrication of flexible rGO/SWCNTs composite electrode

In order to prepare flexible polycaprolactone (PCL) substrates, the pellet type of PCL was hot pressed at 90 ℃ to obtain approximately 0.5 mm thick films. The film was then cut to strips with a length of 5 cm and a width of 1 cm. After cutting the film, a 150 nm thick layer of gold was coated onto the PCL film by sputter coating (Edwards Sputter Coater AUTO306, BOC Ltd, United Kingdom), enabling it to be used as a current collector. The PCL film (1 cm x 5 cm x 0.5 mm) was transferred to a glass microscope slide, and then held using adhesive tape. The PCL film/slide assembly was fixed horizontally to the centre of the hotplate in the spray coating instrument. Once the hotplate is stabilized at 40°C, rGO/SWCNTs dispersions were spray coated

onto the PCL using a Sono-Tek Flexicoat industrial spray coating system (USA) with a 60 kHz Accumist nozzle and the dispersion feed rate of approximately 0.15 mL/min. Spraying is performed automatically at a distance of 15 cm from the PCL substrate. Many thin coats are applied, allowing a few seconds for drying between coats, until the entire 10 mL suspension is exhausted. After spray coating, the rGO/SWCNTs composite electrodes were dried in a vacuum oven at room temperature overnight to evaporate residual solvent.

6.2.4 Preparation of flexible Polycaprolactone (PCL) full device

The flexible PCL supercapacitor was fabricated by assembling the flexible rGO/SWCNTs composite electrodes and polymer (PVA-H_3PO_4) electrolyte in a sandwich conformation (Figure 6.1a and b). Copper tapes were attached at the edge of gold coated substrate for electrical contacts (Figure 6.1a). The PVA/H_3PO_4 solution was heated to 50 ℃ then the fabricated rGO/SWCNTs composite electrodes were soaked in the solution for 10 min to diffuse electrolyte into the rGO/SWCNTs composite film, then the electrodes were placed into a fume hood for 4 hrs to remove most of the water. Two such flexible rGO/SWCNTs composite electrodes with PVA/H_3PO_4 electrolyte were pressed together face-to-face to form a sandwich configuration. The whole device was dried at room temperature overnight prior to further measurements. The surface morphology of the rGO/SWCNTs composite film on the PCL substrate showed very rough and porous structure which is desirable for maximizing surface area (Figure 6.1c). The thickness of the polymer-based electrolyte between the two rGO/SWCNTs composite electrodes was approximately 150 ㎛ and whole device has approximately 1 mm thickness (Figure 6.1d). All of the

electrochemical properties for the flexible PCL supercapacitor were carried out on a two-electrode configuration under fixed 180°, 120°, 60°, 30° of bending angle and 0 to 500 bending/release cycles at 30° bending angle using a Shimadzu EZ mechanical tester. In order to achieve the reproducibility of the PCL supercapacitor, we assessed the specific capacitance of 10 devices.

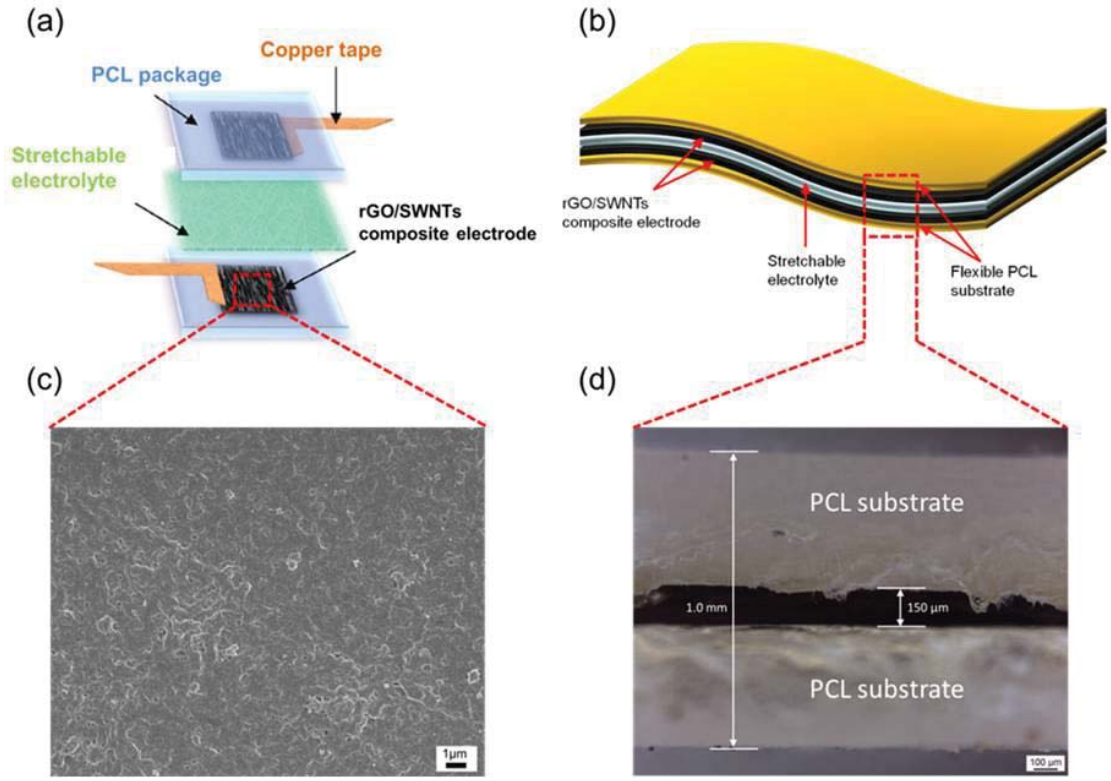

Figure 6.1 (a) and (b) Schematic of the main components for the flexible polycaprolactone (PCL) supercapacitor, (c) Surface morphology of the rGO/SWCNTs composite film on the PCL substrate, (d) Optical microscopy image (cross section) of the PCL whole device.

6.3 CHARACTERIZATION

6.3.1 Cyclic Voltammetry (CV)

Cyclic Voltammetry (CV) measurements were performed at room temperature with a two electrode system using an electrochemical analyzer (EDAQ Australia) and EChem V2 software (ADI Instruments Pty. Ltd).

CV measurements were recorded over the scan rate range 5 - 100 mV s^{-1}. All of the electrodes had bend and release cycles applied at a speed of 50 % s^{-1} using a Shimadzu EZ mechanical tester.

6.3.2 Electrochemical impedance spectroscopy (EIS)

Electrochemical impedance spectroscopy (EIS) was used to probe the electrical double layer effects at the electrode/electrolyte interface. EIS measurements were performed at room temperature using a Gamry EIS 3000^{TM} system (Gamry, USA) where the frequency range spanned 100 kHz to 0.01 Hz with an amplitude of 10mV (rms) at open circuit potential.

6.3.3 Galvanostatic charge/discharge measurement

Galvanostatic charge/discharge tests of the flexible PCL supercapacitor were performed using a battery test system (Neware electronic Co.) between 0 V and 0.8 V with constant current density as 1 A g^{-1}.

6.4 RESULTS AND DISCUSSION

The device was assembled as above and a robust structure substrate for handling was obtained.

6.4.1 Electrochemical properties

Cyclic voltammetry (CV) was used to investigate electrochemical behavior under different bending angle conditions (Figure 6.2a). The flexible PCL supercapacitor showed rectangular CV responses even at 30^{o} of bending angle (Figure 6.2a), indicating that the charge-discharge processes is highly reversible and kinetically facile. The bending of the PCL device has almost no effect on the capacitive behavior. It could be bent to 30^{o} without degrading performance.

The flexible PCL supercapacitor was also characterized by electrochemical impedance spectroscopy (EIS) under different bending conditions to obtain an insight into the electrochemical interfacial properties (Figure 6.2b). Nyquist plots exhibited a line close to 90º at low frequency even at an acute angle (30^{o}) conditions, indicating a good capacitive behavior (Figure 6.2b) [45, 46]. The internal resistance was 4.8 ohms in the unbent state (180^{o}) and increased to 5.4 ohms at 30º bending state (Figure 6.2b). There was no significant change in the internal resistance under different bending conditions.

Galvanostatic charge/discharge curves under different bending conditions with a constant current density of 1 A g^{-1} are given in Figure 6.3a. The charge/discharge curves demonstrated good capacitive behavior under various bending conditions without iR drop. The symmetrical shape of the charge/discharge curves indicated that highly conductive rGO/SWCNTs composites create a pathway for the transfer of ions and electrons, thus decreasing internal resistance (Figure 6.3a). The average specific capacitance of the flexible PCL supercapacitor at 180^{o} of bending condition was 52.5

± 0.4 (mean ± S.D., n = 10 devices) F g^{-1}, which was maintained under 120º, 60º and 30º bending conditions, respectively (Figure 6.3b).

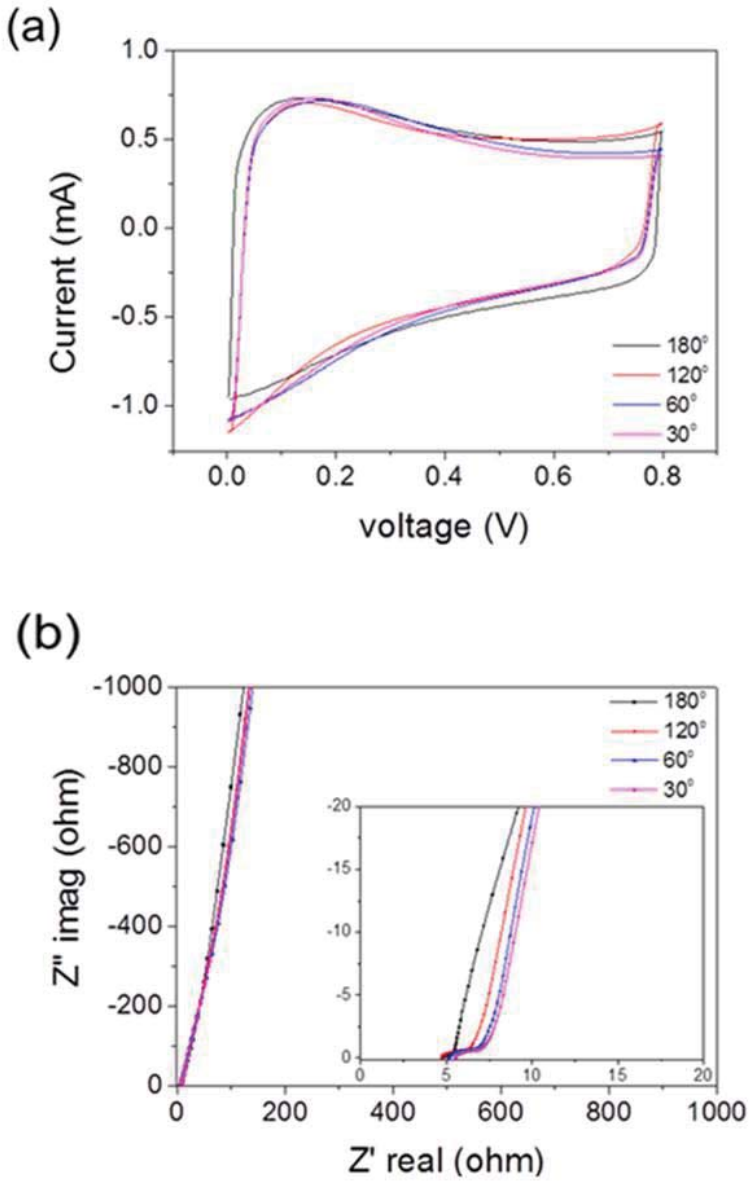

Figure 6.2 Electrochemical properties of the flexible Polycaprolactone (PCL) supercapacitor under different bending condition (180º to 30º); (a) CV of the PCL supercapacitor under different bending condition at 100 mV s^{-1}. (b) Nyquist plots of the PCL supercapacitor under different bending condition with 0.01 Hz~100 KHz frequencies.

These results agree with the surface resistance of the rGO/SWCNTs composite film on the PCL substrate under the same condition (Figure 6.3 c). The cycling stability under different bending conditions during 1000 charge/discharge cycles with constant current density of 1 A g^{-1} is given in Figure 6.3d. The flexible PCL supercapacitor still retained ≈ 99 % of its initial capacitance (52.5 F g^{-1}) under 30^{o} of bending with application of 4000 charge/discharge cycles, demonstrating high endurability and flexibility. The high stability can be attributed to the highly flexible electrodes in addition to the interpenetrating network structure between the rGO/SWCNTs composite electrodes and PVA-H_3PO_4 gelled electrolyte. The solidification of the electrolyte during the fabrication of device was able to act like a glue holding all of the components together and enhancing the mechanical integrity and stability even under extreme bending conditions [34].

Cyclic Voltammetry (CV) measurements were carried out to investigate the electrochemical properties as a function of bending cycle. The CV responses after 0 to 500 bending cycles at a scan rate of 100 mV s^{-1} are presented in Figure 6.4a. A slightly reduced current was observed after numerous bending cycles, which might be attributed to the inclusion/ejection and diffusion of counter ions being slow compared to the transfer of electrons in the rGO/SWCNTs film [47, 48]. Importantly, the CV curve after 500 bending cycles still maintained a rectangular shape, indicating the charge / discharge responses of the electric double layer were highly reversible and kinetically facile.

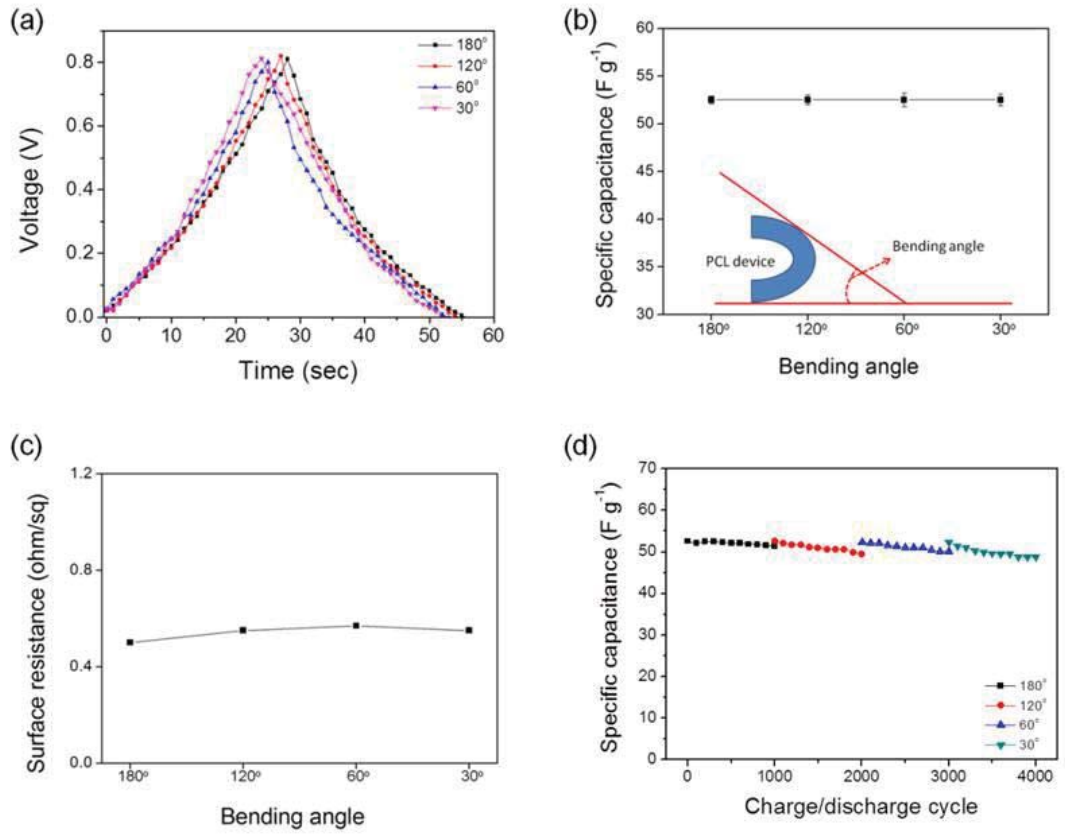

Figure 6.3 Electrochemical properties of the flexible Polycaprolactone (PCL) supercapacitor under different bending condition (180° to 30°); (a) Charge/discharge test of the PCL supercapacitor under different bending condition with 1 A g^{-1} constant current density. (b) Specific capacitance of the PCL supercapacitor under different bending condition. (c) Surface resistance of the rGO/SWCNTs composite film on the PCL under different bending condition. (d) Cycling stability of the PCL supercapacitor under different bending condition.

Nyquist plots exhibited characteristic capacitive behaviour and electrochemical interfacial properties after 0 to 500 bending cycles (Figure 6.4b). In the high frequency regime (Figure 6.4b inset), it can be seen that the semi-circles regime increased with respect to increase in number of bending cycles. This is attributed to an increase in contact impedance between the rGO/SWCNTs composite film and gold current collector as well as electrolyte resistance within the pores of the

rGO/SWCNTs composite film [49]. The internal resistance of the unbent PCL supercapacitor was 4.3 Ω, which increased to 5.8 Ω, 7 Ω, 7.2 Ω, 8.5 Ω and 9.6 Ω after 100, 200, 300, 400 and 500 bending cycles, respectively (Figure 6.4b). This was most likely due to the low electrical conductivity on the rGO/SWCNTs composite film after prolonged bending cycles (Figure 6.4c).

Galvanostatic charge/discharge curves as a function of bending cycle (Figure 6.5a) was demonstrated with a constant current density of 1 A g^{-1}. The charge/discharge curves presented good capacitive behavior and symmetrical shape without iR drop even after prolonged bending cycles up to 500 [50], indicating that the highly conductive rGO/SWCNTs composite electrode creates a pathway for the transfer of ions and electrons, thus reducing internal resistance [51]. The average specific capacitance value of the unbent PCL supercapacitor was 52.5 ± 0.6 (mean ± S.D., n = 10 devices) F g^{-1} and decreased to 37.5 ± 0.5 (mean ± S.D., n = 10 devices) F g^{-1} after 500 bending cycles (Figure 6.5b). This result also agree with the high surface resistance of the rGO/SWCNTs composite film on the PCL substrate after repetitive bending cycle up to 500 (Figure 6.4c).

The cycling stability of the PCL supercapacitor when subjected to a different number of bending cycles (Figure 6.5d) demonstrated typical galvanostatic charge/discharge profiles with a constant current density of 1 A g^{-1}. The specific capacitance retained 65% its initial capacitance (52.5 F g^{-1}) after 500 bending cycles with application of 6000 charge/discharge cycles (Figure 6.5c and 6.5d). The capacitance value might be due to the high resistance induced by the cracks on the rGO/SWCNTs film after bending cycle [34]. The cracks also cause irreversible loss of junctions between rGO/SWCNTs composite film and electrolyte [52].

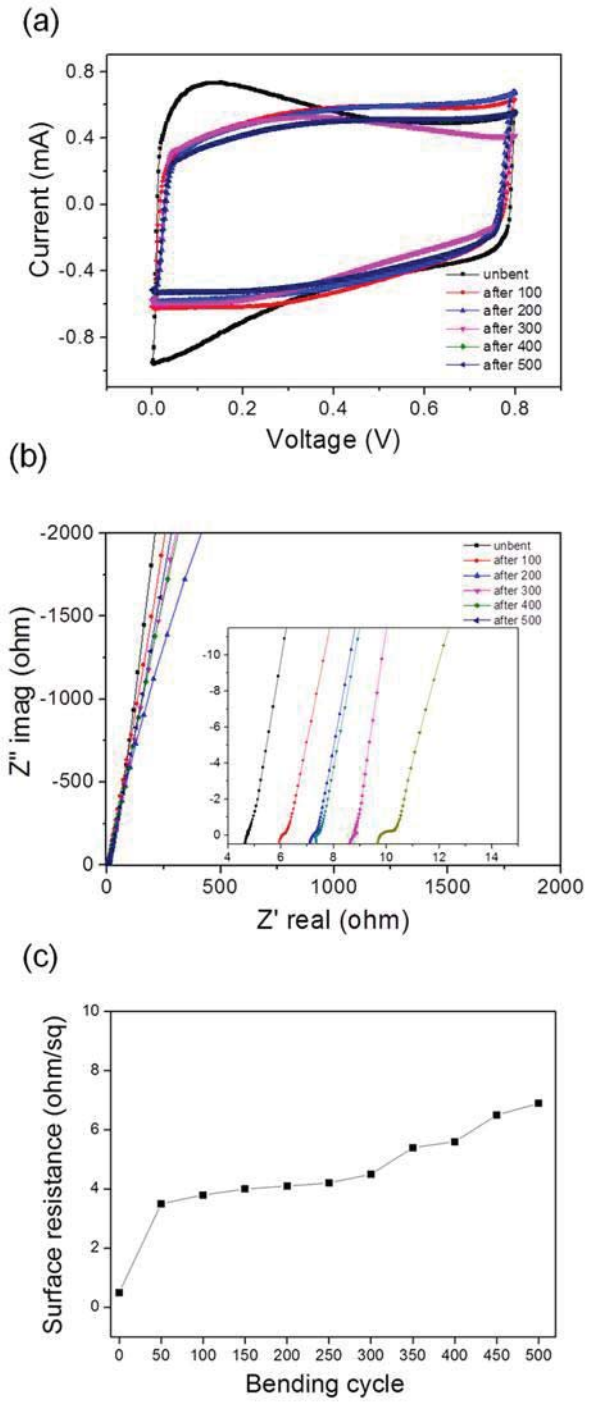

Figure 6.4 Electrochemical properties of the flexible Polycaprolactone (PCL) supercapacitor as a function of bending cycle (0 to 500 bending cycles); (a) CV of the PCL supercapacitor at different bending cycles with 100 mV s^{-1} of scan rate. (b) Nyquist plots of the PCL supercapacitor at different bending cycle with 0.01Hz ~ 100 KHz frequencies. (c) Surface resistance of the rGO/SWCNTs composite film on the PCL substrate at different bending cycles.

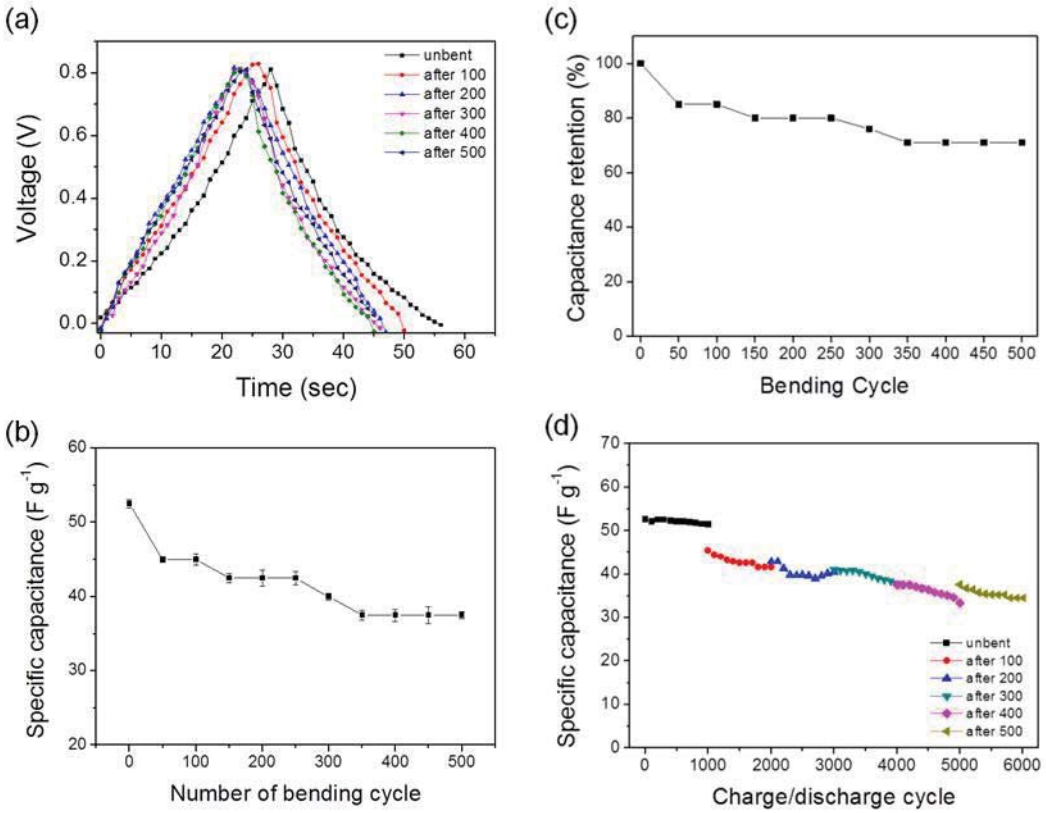

Figure 6.5 Electrochemical properties of the flexible Polycaprolactone (PCL) supercapacitor as a function of bending cycle (0 to 500 bending cycles); (a) Charge/discharge curves of the PCL supercapacitor with application of different bending cycle at 1 A g^{-1} current density. (b) Specific capacitance of the PCL supercapacitor with application of different bending cycle. (c) Capacitance retention of the PCL supercapacitor at different bending cycle. (d) Stability test of the PCL supercapacitor by charge / discharge measurement with application of different bending cycle at 1 A g^{-1} of current density.

6.5 CONCLUSIONS

In this chapter, we have fabricated a flexible polycaprolactone (PCL) supercapacitor based on the rGO/SWCNTs composite electrode with polymer electrolyte (PVA-H_3PO_4). Bending of the PCL device has almost no effect on the capacitive behaviour. The specific capacitance (unbent state) was 52.5 F g^{-1}, which was retained at the 120º,

60º and 30º bending conditions, respectively. However, the specific capacitance (unbent state) decreased to 37.5 F g^{-1} after 500 bending cycles. The specific capacitance of PCL supercapacitor retained 65% its initial capacitance after 500 bending cycle at 30^{o} bending angle with application of 6000 charge/discharge cycle. Moreover, the stability of the PCL supercapacitor was carried out via a charge/discharge test while in the bent state. Interestingly, the PCL supercapacitor showed only ~1% decrease in the capacitance under 30^{o} of bending condition with application of 4000 charge/discharge cycles, demonstrating high durability and flexibility. This was attributed to the highly flexible rGO/SWCNTs composite electrodes along with the interpenetrating network structure between the electrodes and the PVA-H_3PO_4 gelled electrolyte.

6.6 REFERENCES

[1] T. Someya, T. Sekitani, S. Iba, Y. Kato, H. Kawaguchi, and T. Sakurai, "A large-area, flexible pressure sensor matrix with organic field-effect transistors for artificial skin applications," *Proceedings of the National Academy of Sciences of the United States of America,* vol. 101, pp. 9966-9970, 2004.

[2] T. Someya, Y. Kato, T. Sekitani, S. Iba, Y. Noguchi, Y. Murase, H. Kawaguchi, and T. Sakurai, "Conformable, flexible, large-area networks of pressure and thermal sensors with organic transistor active matrixes," *Proceedings of the National Academy of Sciences of the United States of America,* vol. 102, pp. 12321-12325, 2005.

[3] M. Cheng, X. Huang, C. Ma, and Y. Yang, "A flexible capacitive tactile sensing array with floating electrodes," *Journal of Micromechanics and Microengineering,* vol. 19, p. 115001, 2009.

[4] K.-J. Cho, J.-S. Koh, S. Kim, W.-S. Chu, Y. Hong, and S.-H. Ahn, "Review of manufacturing processes for soft biomimetic robots," *International Journal of Precision Engineering and Manufacturing,* vol. 10, pp. 171-181, 2009.

[5] C. Pang, G.-Y. Lee, T.-i. Kim, S. M. Kim, H. N. Kim, S.-H. Ahn, and K.-Y. Suh, "A flexible and highly sensitive strain-gauge sensor using reversible interlocking of nanofibres," *Nature materials,* vol. 11, pp. 795-801, 2012.

[6] M. K. Kwak, H.-E. Jeong, and K. Y. Suh, "Rational Design and Enhanced Biocompatibility of a Dry Adhesive Medical Skin Patch," *Advanced Materials,* vol. 23, pp. 3949-3953, 2011.

[7] W. G. Bae, D. Kim, M. K. Kwak, L. Ha, S. M. Kang, and K. Y. Suh, "Enhanced Skin Adhesive Patch with Modulus-Tunable Composite Micropillars," *Advanced healthcare materials,* vol. 2, pp. 109-113, 2013.

[8] J. Viventi, D.-H. Kim, J. D. Moss, Y.-S. Kim, J. A. Blanco, N. Annetta, A. Hicks, J. Xiao, Y. Huang, and D. J. Callans, "A conformal, bio-interfaced class of silicon electronics for mapping cardiac electrophysiology," *Science translational medicine,* vol. 2, pp. 24ra22-24ra22, 2010.

[9] D.-H. Kim, R. Ghaffari, N. Lu, and J. A. Rogers, "Flexible and stretchable electronics for biointegrated devices," *Annual review of biomedical engineering,* vol. 14, pp. 113-128, 2012.

[10] J. J. Boland, "Flexible electronics: Within touch of artificial skin," *Nature materials,* vol. 9, pp. 790-792, 2010.

[11] T. Sekitani, U. Zschieschang, H. Klauk, and T. Someya, "Flexible organic transistors and circuits with extreme bending stability," *Nat Mater,* vol. 9, pp. 1015-1022, 2010.

[12] D. J. Lipomi, M. Vosgueritchian, B. C. K. Tee, S. L. Hellstrom, J. A. Lee, C. H. Fox, and Z. Bao, "Skin-like pressure and strain sensors based on transparent elastic films of carbon nanotubes," *Nat Nano,* vol. 6, pp. 788-792, 2011.

[13] T.-H. Han, Y. Lee, M.-R. Choi, S.-H. Woo, S.-H. Bae, B. H. Hong, J.-H. Ahn, and T.-W. Lee, "Extremely efficient flexible organic light-emitting diodes with modified graphene anode," *Nat Photon,* vol. 6, pp. 105-110, 2012.

[14] W. H. Lee, J. Park, S. H. Sim, S. B. Jo, K. S. Kim, B. H. Hong, and K. Cho, "Transparent Flexible Organic Transistors Based on Monolayer Graphene Electrodes on Plastic," *Advanced Materials,* vol. 23, pp. 1752-1756, 2011.

[15] T. Yamada, Y. Hayamizu, Y. Yamamoto, Y. Yomogida, A. Izadi-Najafabadi, D. N. Futaba, and K. Hata, "A stretchable carbon nanotube strain sensor for human-motion detection," *Nat Nano,* vol. 6, pp. 296-301, 2011.

[16] T. Takahashi, K. Takei, A. G. Gillies, R. S. Fearing, and A. Javey, "Carbon Nanotube Active-Matrix Backplanes for Conformal Electronics and Sensors," *Nano Letters,* vol. 11, pp. 5408-5413, 2011/12/14 2011.

[17] D. H. Kim, Y. S. Kim, J. Wu, Z. Liu, J. Song, H. S. Kim, Y. Y. Huang, K. C. Hwang, and J. A. Rogers, "Ultrathin Silicon Circuits With Strain-Isolation Layers and Mesh Layouts for High-Performance Electronics on Fabric, Vinyl, Leather, and Paper," *Advanced Materials,* vol. 21, pp. 3703-3707, 2009.

[18] J.-T. Yeh, M.-C. Yang, C.-J. Wu, and C.-S. Wu, "Preparation and characterization of biodegradable polycaprolactone/multiwalled carbon nanotubes nanocomposites," *Journal of Applied Polymer Science,* vol. 112, pp. 660-668, 2009.

[19] I. Janigová, F. Lednický, D. J. Mošková, and I. Chodák, "Nanocomposites with Biodegradable Polycaprolactone Matrix," *Macromolecular Symposia,* vol. 301, pp. 1-8, 2011.

[20] M. Diba, M. H. Fathi, and M. Kharaziha, "Novel forsterite/polycaprolactone nanocomposite scaffold for tissue engineering applications," *Materials Letters,* vol. 65, pp. 1931-1934, 2011.

[21] K. Saeed, S.-Y. Park, H.-J. Lee, J.-B. Baek, and W.-S. Huh, "Preparation of electrospun nanofibers of carbon nanotube/polycaprolactone nanocomposite," *Polymer,* vol. 47, pp. 8019-8025, 2006.

[22] L. Dai, D. W. Chang, J.-B. Baek, and W. Lu, "Carbon Nanomaterials for Advanced Energy Conversion and Storage," *Small,* vol. 8, pp. 1130-1166, 2012.

[23] Y. He, W. Chen, C. Gao, J. Zhou, X. Li, and E. Xie, "An overview of carbon materials for flexible electrochemical capacitors," *Nanoscale,* vol. 5, pp. 8799-8820, 2013.

[24] K. S. Novoselov, V. Fal, L. Colombo, P. Gellert, M. Schwab, and K. Kim, "A roadmap for graphene," *Nature,* vol. 490, pp. 192-200, 2012.

[25] S. Bose, T. Kuila, A. K. Mishra, R. Rajasekar, N. H. Kim, and J. H. Lee, "Carbon-based nanostructured materials and their composites as supercapacitor electrodes," *Journal of Materials Chemistry,* vol. 22, pp. 767-784, 2012.

[26] H. Jiang, P. S. Lee, and C. Li, "3D carbon based nanostructures for advanced supercapacitors," *Energy & Environmental Science,* vol. 6, pp. 41-53, 2013.

[27] M. Kaempgen, C. K. Chan, J. Ma, Y. Cui, and G. Gruner, "Printable Thin Film Supercapacitors Using Single-Walled Carbon Nanotubes," *Nano Letters,* vol. 9, pp. 1872-1876, 2009/05/13 2009.

[28] L. Hu, M. Pasta, F. L. Mantia, L. Cui, S. Jeong, H. D. Deshazer, J. W. Choi, S. M. Han, and Y. Cui, "Stretchable, Porous, and Conductive Energy Textiles," *Nano Letters,* vol. 10, pp. 708-714, 2010/02/10 2010.

[29] V. L. Pushparaj, M. M. Shaijumon, A. Kumar, S. Murugesan, L. Ci, R. Vajtai, R. J. Linhardt, O. Nalamasu, and P. M. Ajayan, "Flexible energy storage devices based on nanocomposite paper," *Proceedings of the National Academy of Sciences,* vol. 104, pp. 13574-13577, August 21, 2007 2007.

[30] C. Huang and P. S. Grant, "One-step spray processing of high power all-solid-state supercapacitors," *Scientific reports,* vol. 3, 2013.

[31] Y. J. Kang, S.-J. Chun, S.-S. Lee, B.-Y. Kim, J. H. Kim, H. Chung, S.-Y. Lee, and W. Kim, "All-Solid-State Flexible Supercapacitors Fabricated with Bacterial Nanocellulose Papers, Carbon Nanotubes, and Triblock-Copolymer Ion Gels," *ACS Nano,* vol. 6, pp. 6400-6406, 2012/07/24 2012.

[32] L. L. Zhang, R. Zhou, and X. S. Zhao, "Graphene-based materials as supercapacitor electrodes," *Journal of Materials Chemistry,* vol. 20, pp. 5983-5992, 2010.

[33] J. Hou, Y. Shao, M. W. Ellis, R. B. Moore, and B. Yi, "Graphene-based electrochemical energy conversion and storage: fuel cells, supercapacitors and lithium ion batteries," *Physical Chemistry Chemical Physics,* vol. 13, pp. 15384-15402, 2011.

[34] M. F. El-Kady, V. Strong, S. Dubin, and R. B. Kaner, "Laser Scribing of High-Performance and Flexible Graphene-Based Electrochemical Capacitors," *Science,* vol. 335, pp. 1326-1330, March 16, 2012 2012.

[35] J. Luo, H. D. Jang, T. Sun, L. Xiao, Z. He, A. P. Katsoulidis, M. G. Kanatzidis, J. M. Gibson, and J. Huang, "Compression and Aggregation-Resistant Particles of Crumpled Soft Sheets," *ACS Nano,* vol. 5, pp. 8943-8949, 2011/11/22 2011.

[36] M. D. Stoller, S. Park, Y. Zhu, J. An, and R. S. Ruoff, "Graphene-Based Ultracapacitors," *Nano Letters,* vol. 8, pp. 3498-3502, 2008/10/08 2008.

[37] Q. Cheng, J. Tang, J. Ma, H. Zhang, N. Shinya, and L.-C. Qin, "Graphene and carbon nanotube composite electrodes for supercapacitors with ultra-high energy density," *Physical Chemistry Chemical Physics,* vol. 13, pp. 17615-17624, 2011.

[38] D. Yu and L. Dai, "Self-assembled graphene/carbon nanotube hybrid films for supercapacitors," *The Journal of Physical Chemistry Letters,* vol. 1, pp. 467-470, 2009.

[39] Y. Cheng, S. Lu, H. Zhang, C. V. Varanasi, and J. Liu, "Synergistic Effects from Graphene and Carbon Nanotubes Enable Flexible and Robust Electrodes for High-Performance Supercapacitors," *Nano Letters,* vol. 12, pp. 4206-4211, 2012/08/08 2012.

[40] S.-Y. Yang, K.-H. Chang, H.-W. Tien, Y.-F. Lee, S.-M. Li, Y.-S. Wang, J.-Y. Wang, C.-C. M. Ma, and C.-C. Hu, "Design and tailoring of a hierarchical graphene-carbon nanotube architecture for supercapacitors," *Journal of Materials Chemistry,* vol. 21, pp. 2374-2380, 2011.

[41] Z.-D. Huang, B. Zhang, S.-W. Oh, Q.-B. Zheng, X.-Y. Lin, N. Yousefi, and J.-K. Kim, "Self-assembled reduced graphene oxide/carbon nanotube thin films as electrodes for supercapacitors," *Journal of Materials Chemistry,* vol. 22, pp. 3591-3599, 2012.

[42] H. Gao, F. Xiao, C. B. Ching, and H. Duan, "Flexible All-Solid-State Asymmetric Supercapacitors Based on Free-Standing Carbon Nanotube/Graphene and Mn3O4 Nanoparticle/Graphene Paper Electrodes," *ACS Applied Materials & Interfaces,* vol. 4, pp. 7020-7026, 2012/12/26 2012.

[43] B. Weng, X. Liu, M. J. Higgins, R. Shepherd, and G. Wallace, "Fabrication and Characterization of Cytocompatible Polypyrrole Films Inkjet Printed from Nanoformulations Cytocompatible, Inkjet-Printed Polypyrrole Films," *Small,* vol. 7, pp. 3434-3438, 2011.

[44] Y. Wang, L. Liu, and S. Guo, "Characterization of biodegradable and cytocompatible nano-hydroxyapatite/polycaprolactone porous scaffolds in degradation< i> in vitro</i>," *Polymer Degradation and Stability,* vol. 95, pp. 207-213, 2010.

[45] J. Gamby, P. L. Taberna, P. Simon, J. F. Fauvarque, and M. Chesneau, "Studies and characterisations of various activated carbons used for

carbon/carbon supercapacitors," *Journal of Power Sources,* vol. 101, pp. 109-116, 2001.

[46] A. Di Fabio, A. Giorgi, M. Mastragostino, and F. Soavi "Carbon-Poly(3-methylthiophene) Hybrid Supercapacitors," *Journal of The Electrochemical Society,* vol. 148, pp. A845-A850, August 1, 2001 2001.

[47] T. Chen and L. Dai, "Flexible supercapacitors based on carbon nanomaterials," *Journal of Materials Chemistry A,* 2014.

[48] C. Zhao, C. Wang, Z. Yue, K. Shu, and G. G. Wallace, "Intrinsically Stretchable Supercapacitors Composed of Polypyrrole Electrodes and Highly Stretchable Gel Electrolyte," *ACS Applied Materials & Interfaces,* vol. 5, pp. 9008-9014, 2013/09/25 2013.

[49] H. Kurig, A. Jänes, and E. Lust, "Electrochemical Characteristics of Carbide-Derived Carbon | 1 -Ethyl-3-methylimidazolium Tetrafluoroborate Supercapacitor Cells," *Journal of The Electrochemical Society,* vol. 157, pp. A272-A279, March 1, 2010 2010.

[50] K. H. An, K. K. Jeon, J. K. Heo, S. C. Lim, D. J. Bae, and Y. H. Lee, "High-Capacitance Supercapacitor Using a Nanocomposite Electrode of Single-Walled Carbon Nanotube and Polypyrrole," *Journal of The Electrochemical Society,* vol. 149, pp. A1058-A1062, August 1, 2002 2002.

[51] Y. Show and K. Imaizumi, "Decrease in equivalent series resistance of electric double-layer capacitor by addition of carbon nanotube into the activated carbon electrode," *Diamond and related materials,* vol. 15, pp. 2086-2089, 2006.

[52] S. Prabaharan, R. Vimala, and Z. Zainal, "Nanostructured mesoporous carbon as electrodes for supercapacitors," *Journal of Power Sources,* vol. 161, pp. 730-736, 2006.

CHAPTER 7

GENERAL CONCLUSIONS AND PERSPECTIVES

7.1 GENERAL CONCLUSIONS

Stretchable, biocompatible and flexible energy storage devices were fabricated by using nanocarbon based materials such as single-wall carbon nanotubes (SWCNTs), reduced graphene oxide (rGO) and rGO/SWCNTs composite. All of the stretchable and flexible electrodes were prepared via a simple and inexpensive spray coating technique, which is potentially applicable at an industrial scale. Their performance as a supercapacitor was characterized electrochemically as a function of stretching, bending and strain. As a result, the optimum performances under strain were determined for stretchable and flexible supercapacitor devices.

7.2 CAPACITIVE BEHAVIOUR OF LATEX/SINGLE-WALL CARBON NANOTUBES ELECTRODES

In chapter 3, single-wall carbon nanotubes (SWCNTs) were coated onto latex using spray coating to produce a stretchable electrode. Using a variety of electrochemical characterization techniques, the main findings showed that the SWCNTs coated latex electrodes were able to retain their electrochemical properties after 50 and 100 stretching cycles at 100% strain. In particular, the SWCNTs coated latex electrodes showed a significant energy density of 23Wh kg^{-1} compared to previously reported flexible and stretchable carbon based electrodes. The highest capacitance value obtained for the unstretched latex/SWCNTs electrode was 119 F g^{-1} in 1 M Na_2SO_4 at 5 mV s^{-1}. After 100 stretching cycles, approximately 80% of the original capacitance

value was retained. Therefore, the latex/SWCNTs electrodes were demonstrated to be potential candidates for wearable and biocompatible devices with high capacitance and stretchability.

7.3 REDUCED GRAPHENE OXIDE (rGO)/SINGLE-WALL CARBON NANOTUBES (SWCNTs) ELECTRODES ON POLYURETHANE

Reduced graphene oxide/single-wall carbon nanotubes (rGO/SWCNTs) composite electrodes were deposited onto stretchable polyurethane (PU) via spray coating. The electrochemical properties of the rGO/SWCNTs composite electrodes were assessed as a function of varying rGO/SWCNTs ratios and pure rGO and SWCNTs using cyclic voltammetry (CV), electrochemical impedance spectroscopy (EIS) and galvanostatic charge/discharge measurements. The highest capacitance value obtained for the unstretched rGO/SWCNTs (10/90) electrode was 265 F g^{-1} in 1 M H_2SO_4 at 5 mV s^{-1}. This performance decreased to 219 and 162 F g^{-1} after 50 and 100 stretching cycles, respectively. The rGO/SWCNTs composite electrode maintained 75% of its initial capacitance under 100% strain. The galvanostatic charge/discharge and electrochemical impedance spectroscopy (EIS) curves of the rGO/SWCNTs composite electrode showed well-defined capacitive behaviour after 50 and 100 stretching cycles. Overall, the rGO/SWCNTs composite electrode showed enhanced electrochemical properties in comparison to pure rGO and SWCNTs electrodes. Approximately 70% of the initial capacitance for the rGO/SWCNTs composite electrode was retained after 100 stretching cycles and 3000th CV cycles under 100 % strain, indicating that the electrodes present encouraging properties for stretchable energy storage applications.

7.4 STRETCHABLE LATEX AND POLYURETHANE (PU) SUPERCAPACITOR COMPOSED OF REDUCED GRAPHENE OXIDE (RGO)/SINGLE-WALL CARBON NANOTUBES ($SWCNT_S$) COMPOSITE ELECTRODES

Highly stretchable latex and polyurethane (PU) supercapacitors have been developed with a polymer based PVA-H_3PO_4 gelled electrolyte. The supercapacitors were fabricated a full devices by assembling two electrodes of rGO/SWCNTs on latex or PU composite electrodes and the polymer electrolyte in a sandwich conformation. The latex supercapacitor when unstretched presented a specific capacitance value of 61.3 F g^{-1}, which decreased to 41.7 F g^{-1} after 100 stretching cycles at 100% strain (70 % capacitance retention). The PU supercapacitor when unstretched gave a specific capacitance value was 42.9 F g^{-1}, which decreased to 31.1 F g^{-1} after similarly undergoing 100 stretching cycles at 100% strain (72 % capacitance retention). The stretchable latex and PU supercapacitor maintained 74 % and 89 % of the initial capacitance at 100% elongation, respectively. The latex and PU supercapacitors with high stretchability demonstrate that nanocarbon based stretchable energy storage devices have potential as supercapacitors for wearable and biocompatible devices.

7.5 FLEXIBLE POLYCAPROLACTONE (PCL) SUPERCAPACITORS

Flexible polycaprolactone (PCL) supercapacitors were fabricated as full devices by assembling rGO/SWCNTs electrodes and PVA-H_3PO_4 gelled electrolyte into a sandwich structure, as done in the previous chapter. The electrochemical properties of PCL-based supercapacitors were studied as a function of bending angle of the device, and number of charge/discharge cycles, to assess their performance under conditions

closer to practical operating requirements. The bending of the device had almost no effect on the electrochemical properties. The specific capacitance of the unbent device was 52.5 F g^{-1}, which was retained even at bending angles of 120º, 60º and 30º. However, this specific capacitance (52.5 F g^{-1}) decreased to 37.5 F g^{-1} after 500 bending cycles at 30^{o}. Interestingly, the PCL supercapacitor showed only an ~1% decline in the capacitance when the bending angle was < 30^{o} during the application of 3000 charge/discharge cycles, indicating the devices maintains high durability. This is attributed to the highly flexible rGO/SWCNTs electrodes along with the interpenetrating network structure between the electrodes and polymer gelled electrolyte [1]. The solidification of the polymer electrolyte acts like a glue which holds the components together, enhancing the mechanical integrity and improving its stability even under extreme bending conditions [1].

7.6 RECOMMENDATION AND FUTURE WORKS

In this thesis, nanocarbon materials such as single-wall carbon nanotubes (SWCNTs) and reduced graphene oxide (rGO) and their composites have been investigated for stretchable and flexible energy storage applications. First of all, in order to fabricate the stretchable and flexible supercapacitor, we needed to introduce a appropriate polymer with high stretchability and flexibility so that latex (natural rubber), biomedical grade polyurethane (PU) and polycaprolactone (PCL) were conducted for fabricating of stretchable and flexible supercapacitor by their high stretchability and flexibility. All of these materials are supposed to be a suitable for fabricating of stretchable and flexible substrate.

The nanocarbon-based materials such as, SWCNTs and rGO have introduced to use as an electrode material. They are potential candidates due to their remarkable properties including large aspect ratio, high electrical conductivity, high surface area, chemical and mechanical stability. Therefore, in this thesis, the SWCNTs and rGO were conducted to use as an electrode materials and showed promising electrochemical properties for stretchable and flexible energy storage device. However, rGO has shown low capacitance value without additive as a binder or spacer. As a result, we have introduced SWCNTs between rGO layers to improve electroactive surface area, thus leading to enhanced electrochemical performance of the supercapacitors. The nanocarbon-based materials such as, SWCNTs and rGO are also promising materials for the stretchable and flexible power sources.

The thesis contributes to a simple but novel approach for the fabrication of the stretchable and flexible supercapacitor, whilst demonstrating their ability to perform under strain. Such work could be extended to biocompatible applications such as biochemical sensors, implantable electronic robots and health monitoring devices. Despite the progress in this field, there are still limitations in achieving optimal electrochemical properties, including energy density and capacitance. For example, the electrolyte is significant factor in the performance of supercapacitors. Most of the polymer-based solid-state electrolytes are limited to an electrochemical potential window of less than 1 V. In order to overcome this issue, organic salts and/or ionic liquid-based polymer electrolytes have potential to greatly improve energy density and capacitance, and should be further explored.

The cost factor is another issue in developing supercapacitor devices. Nanocarbon-based supercapacitors with high capacity and long term stability using organic salts or ionic-liquid based polymer electrolytes should be cost effective. This could be achieved by developing simple, cheap and novel fabrication approaches such as one-step fabrication processes using 3D printing techniques.

A new generation of the stretchable and flexible supercapacitors are potential candidates to replace batteries and expected for future power and energy storage devices with high efficiency, reliability and high power. We believe that the fabrication approaches and findings in this thesis will be of significant interest in the field.

7.7 REFERENCES

[1] M. F. El-Kady, V. Strong, S. Dubin, and R. B. Kaner, "Laser Scribing of High-Performance and Flexible Graphene-Based Electrochemical Capacitors," *Science,* vol. 335, pp. 1326-1330, March 16, 2012 2012.